UNIVERSITY OF LONDON THESIS

Degree PhD Year 2007 Name of Author AABIR CHAKRABORTY

The Development of Intra-operative Ultrasound Elasticity imaging Techniques to assist during Brain Tumour Resection

Aabir Chakraborty

A thesis submitted to the University of London for the degree of Doctor of Philosophy in the Faculty of Clinical Neuroscience

Academic Department of Clinical Neuroscience,

Royal Free & University College Medical School,

Roland Hill Street,

Hampstead,

London, NW3, 2PF

February 2007

ProQuest LLC
789 East Eisenhower Parkway
P.O. Box 1346
Ann Arbor, MI 48106-1346

Abstract

Brain tumour resection requires the surgeon to evaluate mechanical properties such as tumour stiffness and adherence of tumour to the surrounding normal brain. This is a subjective assessment.

Ultrasound elasticity imaging techniques allow more objective measurement and imaging of mechanical properties such as strain, which is related to stiffness, in the case of ultrasound elastography.

This thesis describes the implementation of ultrasound elastography intra-operatively during brain tumour surgery using both an off-line processed and real-time ultrasound elastography system in 24 patients. Elastogram results on stiffness were compared to surgical findings.

Adherence of two surfaces in contact is related to slip which is a type of shear. It occurs when the frictional force binding the two surfaces is overcome.

A new imaging technique called slip elastography that images the anatomical location of a slip boundary and measures the externally applied force at which slip is first detected was developed. The technique provides a measure of the frictional force binding the two surfaces together. The theoretical basis, system development, *in vitro* testing using gelatine phantoms and the implementation of slip elastography in 22 patients intra-operatively during brain tumour resection is described.

The results indicated that ultrasound elastography is able to distinguish stiffer areas from softer areas intra-operatively during brain tumour resection. It also demonstrated the heterogeneity of brain tumour stiffness.

Slip elastography was able to identify the anatomical location of the brain tumour interface and provide a measure of adherence at the interface.

Authors Declaration and Ethical Considerations

I declare that I am the sole author of this thesis. I conducted the research at the Royal Free & University College Medical School and the Institute of Cancer Research between 1st February 2003 and 31st February 2007.

Ethical approval for the clinical studies was granted by the Royal Free Hampstead NHS Trust Local Research Ethics Committee.

Aabir Chakraborty

"The Roots of Violence:

Wealth without work,

Pleasure without conscience,

Knowledge without character,

Commerce without morality,

Science without humanity,

Worship without sacrifice,

Politics without principles"

Mahatma Gandhi

Acknowledgements

I would like to thank my 3 supervisors. Neil Dorward has been invaluable in guiding me throughout the project. Thank you for enthusiastically supporting new ideas and advising on clinical applications of the project.

I am particularly indebted to Jeff Bamber for voluntarily taking me under his wing and mentoring me. This work would not have been possible without his masterful direction. I would like to thank Robert Bradford for reminding me that the aim of research is to improve clinical practice and that my primary aim is to become a well rounded neurosurgeon.

I would like to acknowledge the diagnostic ultrasound team at the Institute of Cancer Research, in particular Gearoid Berry who always found time to spare to help me whenever I was stuck, Nigel Bush and Naomi Miller.

To the consultants, registrars and SHOs at the department of Neurosurgery at the Royal Free Hospital who allowed me to develop my neurosurgical skills whilst conducting my research and for providing me the opportunity to conduct clinical trials. I thank the patients who agreed to take part in the research despite going through desperate personal difficulty. I thank the people who generously donated to the Special Trustees of the Royal Free Fund (G90). This fund has supported equipment and conference fees.

I would like to thank my wife Emma for her patience, support, understanding and love. During the period our first child Maya was born. She has reminded me that there is more to life than just work.

I thank my father and late mother. They supported me throughout my life. I own so much to them. I would like to thank my brothers, Rana and Anjan, and all my friends and family for keeping my sanity.

Dedicated to Mrs Arati Chakraborty

2nd June 1934 – 16th July 2002

TABLE OF CONTENTS

List of Figures

List of Tables

Chapter 1

General Introduction

Chapter 1

General Introduction

Brain tumours like most tumours in the body are thought to have different mechanical properties to surrounding brain. They have different stiffness characteristics compared to brain, that are often exploited by the surgeon when resecting these tumours (Yasargil 1996). The surgeon uses a combination of visual inspection and palpation, through instruments, to determine what to resect.

Another important mechanical property that surgeons have little pre-operative information on is the adherence of tumour to brain. Pre-operative information on adherence of tumour to brain may assist the surgeon in planning resection to avoid complications, and may assist in identifying tumour pedicles where blood vessels exist.

The difference in histological structure and molecular composition are the basis of differences in stiffness and other physical properties between normal tissue and tumours.

The surgeon uses a subjective evaluation of mechanical properties such as stiffness and adherence of tumour to brain to make decisions during tumour resection. It may be advantageous to have information on these mechanical properties prior to tumour resection and in a more objective manner.

Ultrasound elastography is a relatively new imaging technique for imaging mechanical properties of a material at depth in a more objective manner. This is made possible by measuring and imaging induced strain, which is

related to stiffness, within tissue following application of an externally applied compressive force to the surface of that tissue (Ophir 1991). It has been used in a number of clinical settings in order to assist in diagnosis. For example, it has been used to demonstrate that sensitivity and specificity could be improved at detection of breast tumours when compared to ultrasound alone (see 1.1.3.1).

Adherence of tumour to brain is related to slip. If there is minimal adherence, tumour will slip over brain following application of a very small force. Thus the magnitude of force required to produce slip is related to adherence of tumour to brain. Currently, unlike conventional elastography (axial strain imaging), there is no published use of ultrasound to image and measure friction at tumour boundaries.

The aim of work reported in this thesis was to evaluate the use of current ultrasound elastography methods at imaging mechanical properties of the brain tumour interface *in vivo* during brain tumour resection. The performance of existing elastographic techniques, which have already been applied to other tissue types, is investigated. Furthermore, a new method for measuring and imaging tissue adherence at a slip boundary, based on ultrasound elastography, was developed and applied intra-operatively during brain tumour resection.

This chapter introduces key concepts in ultrasound elastography and describes clinical applications of this technique. In addition current goals in brain tumour resective surgery and the use of neuro-navigation (a technique commonly used to assist in anatomical localization of tumour intra-

operatively) are discussed. This chapter concludes by giving the aims, objectives and a brief outline of the thesis.

1.1 Background

1.1.1 Basic Physics of Ultrasound Elastography

It is important to understand a number of basic physical principles in order to appreciate ultrasound elastography.

Stress (σ) is the force applied per unit area (N/m^2). Strain (ε) is the amount of deformation a material experiences following application of a stress and has no units. Stress/strain in a linearly elastic material is a constant that defines the material's stiffness called the Young's modulus. Unfortunately

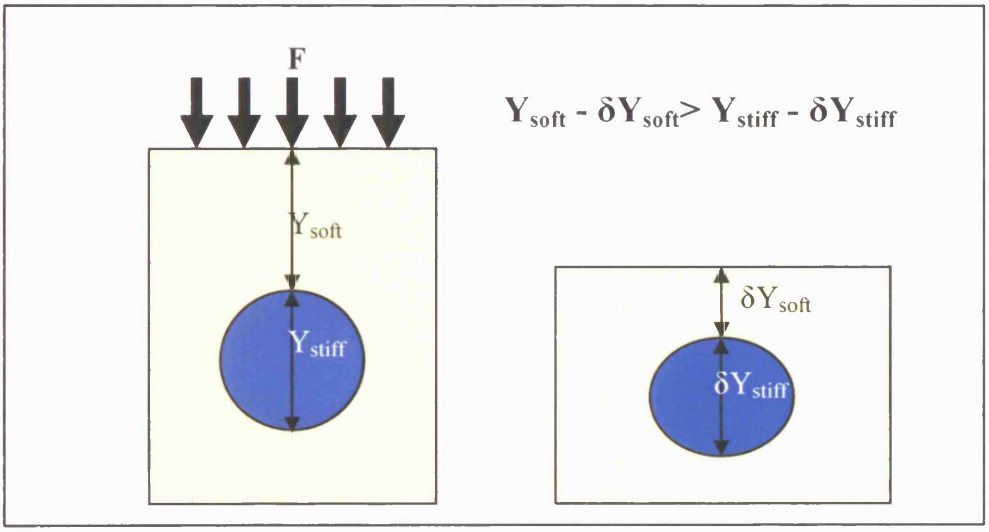

Figure 1.1 Diagram demonstrating how a stiffer inclusion strains less than its softer background. It is assumed that the top and bottom rigid boundaries are frictionless and the illustration is in 2D

most materials including brain do not exhibit such linear elastic behavior so mathematical generalizations on stress strain relationships for specific materials can be difficult to derive.

Consider 2 lengths Y_{stiff} and Y_{soft} within a material that contains a stiff inclusion (Figure 1.1). Length Y_{stiff} represents the length of the stiff inclusion and Y_{soft} represents the length of the softer surrounding background above the stiff inclusion. For convenience Y_{stiff} and Y_{soft} are the same length. Following application of an external axial compressive force F over the whole surface the object deforms as shown assuming frictionless boundaries on the top and bottom surfaces and assuming that the model is 2 dimensional. It can be seen that the change in length resulting in the stiffer inclusion is far smaller than the change in length resulting in the softer surrounding (i.e. $Y_{soft} - \delta Y_{soft} > Y_{stiff} - \delta Y_{stiff}$). Hence the stiffer inclusion strains less than the softer background ($Y_{soft}/(Y_{soft} - \delta Y_{soft}) < Y_{stiff}/(Y_{stiff} - \delta Y_{stiff})$). The stress applied (F/surface area) is assumed to be constant throughout in the example given. Stress/strain is a measure of the stiffness of a material so, assuming that the stress is constant, the stiffness would be inversely proportional to the strain in the above example. This is one of the simpler examples to demonstrate the relationship between stiffness and strain.

1.1.2 Mechanical Imaging

For any form of mechanical imaging a stress is applied and parameters related to stiffness are calculated within the image plane and represented as an anatomically accurate image. There are a number of mechanical imaging techniques that are currently being explored. They can be classified according to the imaging modality that is used. MRI applications such as MR Elastography are showing great promise in providing quantitative stiffness measurements. MR Elastography works in the following manner. A mechanical wave (shear stress) is applied to the object under study and the propagation of the mechanical wave is observed. The propagation of mechanical waves is related to elasticity hence stiffness can be calculated (Muthupillai 1996).

MR Elastography has been performed on patients with breast lesions (Sinkus 2005). The results in this paper on 15 patients demonstrated that breast malignancies were significantly stiffer than benign lesions.

Preliminary studies using MR Elastography to quantitatively assess liver fibrosis have also been performed (Rouviere 2006). In this study 12 healthy volunteers and 12 patients with a history of liver disease were recruited. They found that the mean liver shear stiffness was significantly higher in the group with liver disease when compared to the control group.

Evaluation of the use of MR Elastography on the brain has started (Hamhaber 2006). One of the difficulties however has been shear wave propagation in an intact skull.

Ultrasound techniques have been more widely used to produce mechanical images. Ultrasound based mechanical imaging is broadly divided into 2

groups. The 1st group includes techniques where a nearly continuous low frequency vibration is applied to the object under study. As a result disturbances in wavelength of the vibration wave occur as the wave moves through regions with different stiffness. This change can be imaged by reconstruction of received image data thus producing an elasticity image. This technique is called sonoelasticity imaging (Lerner 1990).

The second group is where a nearly static external deformation is applied to the object under study and the resultant internal displacements are mapped for each part of the image. By differentiating the displacement map it is possible to produce a strain image or elastogram. This technique is called ultrasound elastography. Ultrasound elastography forms the basis of the techniques used in this thesis.

1.1.3 Ultrasound Elastography

Ultrasound elastography is an objective technique for imaging mechanical properties of a material by measuring and imaging induced strain within tissue following application of an externally-applied displacement to the surface of that tissue (Ophir 1991). Its development followed from earlier studies on tissue motion assessment (Dickinson 1982, Tristam 1988, Bamber 1988). Figure 1.2 shows the first image published in the literature demonstrating mechanical properties following palpation using an ultrasound based technique (Bamber 1988). This image was obtained by

using a B mode speckle decorrelation processing method and freehand palpation of a phantom with a stiff inclusion.

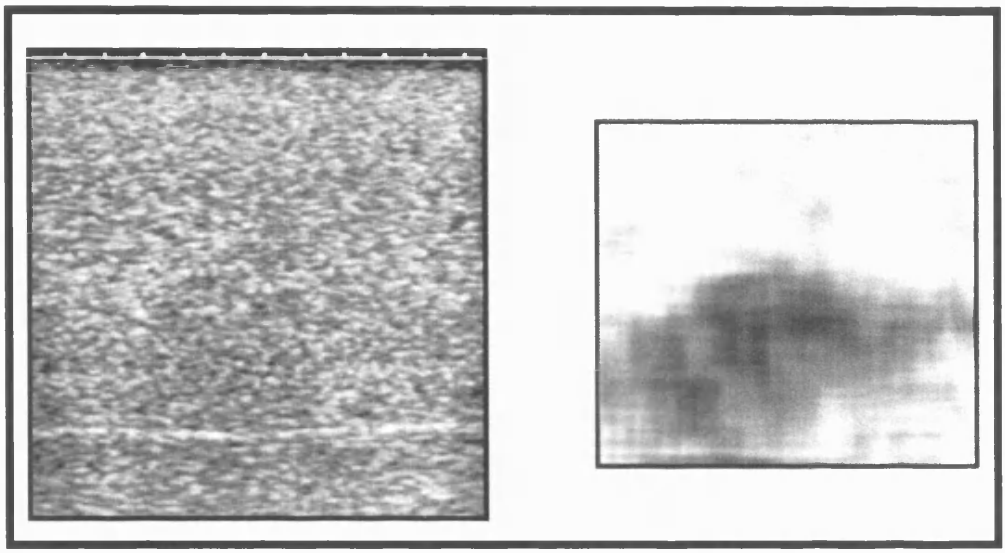

Figure 1.2 B mode ultrasound image and displacement image showing a phantom with a stiff inclusion. Reproduced with permission of J. Bamber.

Ophir made a key advance in mechanical imaging in choosing to display strain, calculated as the spatial gradient of displacement (Ophir 1991). The process of elastogram generation involves application of a stress to the material under study, usually in the form of axial compression applied by the ultrasound probe, and evaluation of the resultant strain. Relative strain images, known as elastograms, can be produced by comparison of pre- and post-compression ultrasound data.

For the purposes of this thesis conventional ultrasound elastography describes the technique by which normal axial strain is imaged. Conventional ultrasound elastography has been used in a number of clinical settings.

1.1.3.1 Clinical Studies

The most widely studied clinical application of conventional ultrasound elastography has been in the detection of malignant breast tumours. A number of studies have been performed. Garra et al examined 46 breast lesions using ultrasound elastography (Garra 1997). They initially described the elastographic appearance of normal breast tissue and then described elastographic findings in patients with fibroadenoma, cysts, fibrocystic disease and carcinoma. They found that carcinomas were statistically significantly stiffer than fibroadenomas and that their elastographic appearance was larger than the sonogram appearance. The technique used for compression of the breast involved specialized apparatus to immobilize the breast.

Hiltawsky used a freehand technique that did not require breast immobilization on 53 breast lesions (Hiltawsky 2001). They found a significant difference in stiffness between normal tissue and tumour but did not demonstrate a significant difference between carcinoma and fibroadenoma. Both groups described above concluded that ultrasound elastography may be useful for breast carcinoma detection when used in conjunction with B mode imaging.

Bamber et al examined 70 breast lesions using freehand ultrasound elastography (Bamber 2002). They found that freehand ultrasound elastography had an impact on diagnosis in 24% of cases. Combining ultrasound with ultrasound elastography increased the sensitivity and specificity at detecting carcinoma to 90% and 46% respectively, compared with 84% and 43% using ultrasound alone.

Svensson et al performed a study looking at the ratio of size of lesion seen on ultrasound compared to ultrasound elastography in 234 lesions (Svensson 2005). They found that any lesion with elasticity to B mode ratio of less than 0.75 were always benign. This ratio, it was proposed, may reduce the requirement for biopsy by half.

Itoh et al performed ultrasound elastography in 111 patients with breast tumours (Itoh 2006). 59 of the lesions were benign and 52 were malignant. An elasticity score was assigned according to the elastogram appearances. The results suggested that ultrasound elastography had a higher sensitivity and an equivalent specificity to ultrasound at detecting breast malignancy.

The use of ultrasound elastography in the detection of thyroid carcinomas have also been investigated (Lyshchik 2005). In this study 52 patients were recruited; 20 had some form of thyroid carcinoma. Real-time elastography, off-line processed ultrasound elastography and B mode ultrasonography were performed as well as *ex vivo* biomechanical testing of tissue. Malignant lesions were highly visible using ultrasound elastography when compared to benign lesions. The biomechanical estimates obtained *ex vivo* confirmed that malignant tumours were, on the whole, stiffer than benign tumours. The only parameter tested that significantly differentiated malignant tumour from benign tumour was the ratio of strain between normal tissue and tumour being greater that 4 ($P<0.001$). This parameter had 96% specificity and 82% sensitivity.

Ultrasound elastography has been used in conjunction with conventional ultrasonography to assist in the detection of prostatic carcinoma (Konig 2005). In this study, 404 patients undergoing prostatic biopsy had

ultrasonography and ultrasound elastography performed prior to biopsy. 151 of the patients had prostatic carcinoma diagnosed on biopsy. Prostatic carcinoma was suspected in 32.5% of cases using ultrasound alone, 48.3% of cases using digital rectal examination alone, 64.2% of cases using a combination of digital rectal examination and ultrasound and 84.1% of cases using ultrasound elastography alone. Thus the sensitivity was increased using ultrasound elastography compared to conventional testing.

Other applications of ultrasound elastography include the differentiation between tumour and a high intensity focused ultrasound (HIFU) ablated lesion in the prostate (Souchon 2003).

1.1.3.2 Validation of Ultrasound Elastography

There have been very few clinical studies where biomechanical stiffness measurements have been used to validate ultrasound elastogram findings. Results in this thesis and the study by Lyshchik et al have included an objective measure to compare ultrasound elastography to (Lyshchik 2005). In Lyshchik's study resected normal thyroid gland and thyroid tumour were biomechanically tested following thyroidectomy using the model of a uniformly applied load acting over the boundary of a semi-infinite elastic solid object. They found that the mean elastic modulus for normal thyroid gland tissue was 12.3kPa (range 5.8-18.7kPa), for solid benign lesions was 22.5kPa (range 11.9-37.4kPa) and for solid malignant lesions was 99.7kPa (range 15.9-590.4kPa). They noted that one of the benign lesions was not significantly stiffer than normal tissue and that one malignant lesion was in

fact softer that surrounding tissue. They suggested that the softer central core was due to tumour necrosis.

Krouskop et al described a study where normal breast tissue and breast tumour were mechanically tested following excision (Krouskop 1998). They also tested normal prostate tissue and prostatic tumour. They found that the elastic modulus of intraductal carcinoma was indistinguishable from fat at the low strain range. Furthermore they found that tissue from prostates with benign prostatic hypertrophy were significantly softer that normal tissue.

The results from the papers mentioned above put into question the validity of the assumption that benign and malignant tumours are always stiffer than normal tissue. Yet this assumption has been made in all other clinical studies using ultrasound elastography. This thesis has attempted to validate the elastogram findings with mechanical measurements.

1.1.4 The Management of Brain Tumours

Brain tumours are commonly divided into intra-axial and extra-axial. This is based on whether the tumour grows from within the brain substance or not. Extra-axial tumours are more commonly benign and cause symptoms by localized mass effect, generalized mass effect or epilepsy. Examples include meningiomas and vestibular schwannomas. Intra-axial tumours tend to be malignant and cause symptoms by a localized mass effect, generalized mass

effect, destruction of normal brain cells or epilepsy. Examples include gliomas and brain metastases.

In the majority of cases, patients with either intra-axial or extra-axial brain tumours are primarily treated by surgical resection if appropriate and if feasible (see chapter 2 for a more detailed discussion).

The surgical aim when considering resection of extra-axial tumours is slightly different to that of most intra-axial tumours. For extra-axial tumours complete excision is usually the aim. There is usually a well defined interface between tumour and brain usually with the leptomeninges sandwiched inbetween so complete excision is often possible without damage to underlying brain.

Intra-axial tumours invade brain tissue and occupy space. Complete macroscopic excision is possible but total excision is usually not possible as microscopic invasion has usually occurred. At autopsy 45% of glioblastomas extend beyond one lobe, 25% involve an entire hemisphere, and 25-30% cross over to the opposite hemisphere (Mikkelson 2004). Intra-axial tumours are more likely to be adherent to underlying brain and the brain tumour interface may be less well defined. In order to resect intra-axial tumours the surgeon must necessarily resect normal brain. Thus the aim of surgery is predominantly cytoreductive with an attempt at maximal preservation of surrounding brain.

1.1.5 Neuro-navigation and Real-time Imaging

An important consideration when resecting brain tumours is the anatomical location of the tumour. There are a number of techniques commonly used to assist in identifying the spatial position of brain tumours. Pre-operatively, CT scans and MRI scans provide excellent resolution and contrast between tumour and brain especially when contrast agents are used to identify brain tumours within the cranial vault. These scans have the added advantage of being referenced to easily identifiable landmarks on the patient such as bony structures. The position of the landmarks relative to tumour allows the surgeon to plan where to position the craniotomy flap and also where to incise the brain in order to approach an intrinsic tumour with accuracy. The accuracy of this technique is dependent on the surgeon's experience and on the site of the tumour and so can be variable.

The advent of neuro-navigation has effectively removed any variability in planning the site for the craniotomy flap. Neuro-navigation uses historically acquired imaging data, usually in the form of an MRI scan, to create a 3 dimensional model of the brain. Following co-registration of landmarks seen on the reformatted MRI scan to surface structures seen on the patient in the operating theatre it is possible to superimpose the reformatted 3 dimensional MRI scan into the co-ordinate system containing the patient's head. Furthermore, it is possible to navigate with instruments that are visible to the neuro-navigation system in real-time using the historically acquired imaging information (Barnett 2004). The surface accuracy of this technique is within 2mm (Dorward 1998).

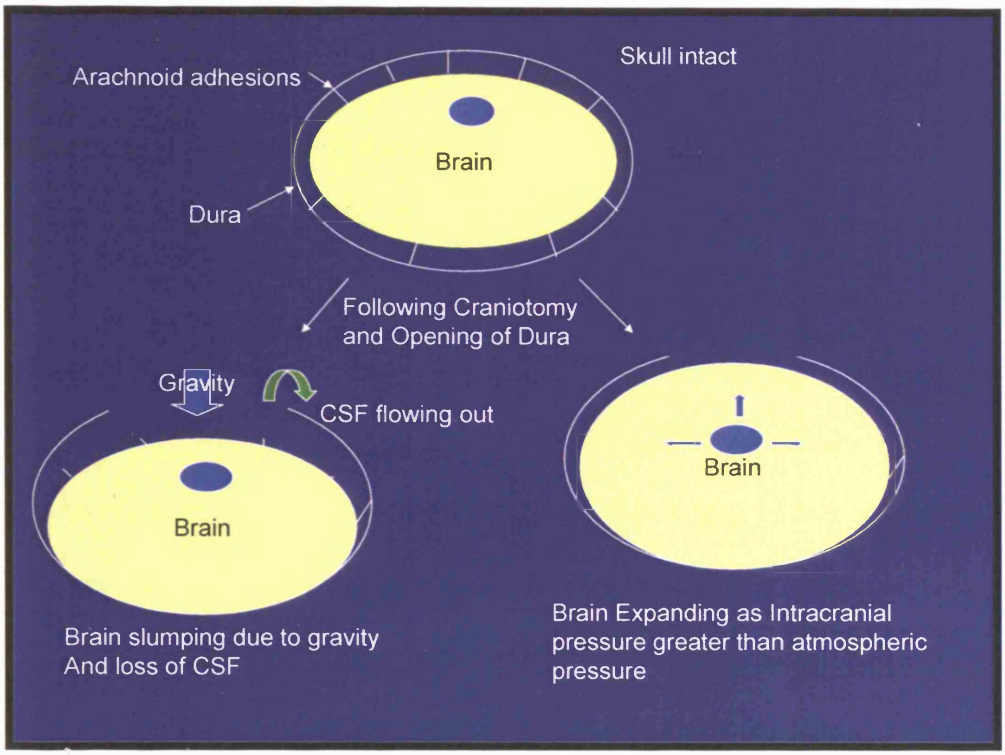

Figure 1.3 Schematic diagram demonstrating brain shifts that occur as a result of craniotomy and dural opening

One of the limitations of neuro-navigation occurs once a craniotomy has been performed. Most brain tumours occupy space thus increasing the intracranial pressure. Once the pressure has been released by performing a craniotomy the brain with tumour would tend to expand out of the craniotomy site. Furthermore, by opening the closed compartment of the subarachnoid space thus dividing arachnoid adhesions between brain and arachnoid, gravity will have a greater effect causing the brain to sink. Also cerebrospinal fluid will seep out of the craniotomy site causing further displacement of brain away from the craniotomy site. These 3 effects on brain shift as a result of performing a craniotomy and opening the dura introduce inaccuracies in neuro-navigation as the system relies on

historically acquired imaging data (figure 1.3). Thus, neuro-navigation needs to be used with caution once a craniotomy has been performed. This has been confirmed in a number of studies (see chapter 2).

Real-time imaging is a method for overcoming the problem of brain shift following craniotomy. Intra-operative CT and MRI are available in selected centres but are very expensive and intra-operative MRI requires a non ferromagnetic theatre environment. Intra-operative ultrasonography is a cost effective alternative to intra-operative CT and MRI and is widely available. It is very simple to use and the image quality continues to improve with improving technology. There are numerous ultrasound based diagnostic techniques such as colour-flow Doppler Ultrasonography which can provide vascular information that may be clinically relevant. Intra-operative ultrasonography has a number of drawbacks. The image quality and contrast between tumour and brain is not as good as is seen on contrast-enhanced MRI however this may change with improved ultrasound visualisation techniques such as the use of microbubble contrast agents in conjunction with ultrasound. Another drawback is the lack of reference using ultrasonography. However, systems are now commercially available that are able to track the position of the ultrasound probe and its image and reference this data to historically acquired MRI scans (Gronningsaeter 2000).

1.2 Aims, Objectives and Outline of Thesis

1.2.1 Aims

The aim of this project was to evaluate the use of freehand ultrasound elastography based techniques to assist in resection of brain tumours. This was with a view to ultimately providing more accurate and complete resection margins with minimal sacrifice of normal brain. This was based on the hypothesis that brain tumours had different stiffness characteristics to normal brain and that brain tumours had variable adherence to underlying brain.

Specifically, ultrasound elastography was evaluated to determine whether it could differentiate stiffer tissue from less stiff tissue *in vivo* during brain tumour resection. Furthermore a new technique was developed to image the anatomical location of a slip boundary and provide a measure of adherence between the two surfaces comprising that slip boundary. This technique, called slip elastography, was then applied intra-operatively during brain tumour resection to evaluate adherence between tumour and brain.

Freehand ultrasound elastography is at an early stage of development. It is likely that image quality and robustness of the technique will improve over the next few years. Thus the work described is aimed at evaluation of the use of current freehand elastography methods and also to judge the potential of the method if the quality of the data were to improve.

1.2.2 Objectives

The methods used to reach the aim were divided into 3 stages;

1) Ultrasound elastography with off-line processing was applied intra-operatively during brain tumour resection and compared to surgical findings on relative stiffness of brain compared to tumour. In a number of cases tumour specimen and brain specimen were obtained and mechanically tested *ex vivo* to obtain stress versus strain plots. This part of the thesis determined whether it was feasible to perform ultrasound elastography intra-operatively during brain tumour resection. In addition it evaluated whether ultrasound elastography was able to differentiate stiff tissue from softer tissue.
2) A commercial ultrasound elastography system with real-time capability was used in a similar manner. A comparison was made between images obtained using the real-time and surgical findings. This part of the thesis determined whether the real-time system was a suitable alternative to the off-line system thus making ultrasound elastography a clinically feasible imaging modality for use intra-operatively where images are required at the time of surgery.
3) Currently there are no investigations that provide information on mechanical properties at the brain tumour interface, specifically the adherence of tumour to brain. Thus, a new imaging technique called slip elastography was developed and tested *in vitro*. It was then implemented *in vivo* during brain tumour resection to identify the anatomical location of the brain tumour interface and to measure the adherence of tumour to brain at this interface.

Many of these cases were performed with the assistance of neuro-navigation to assist in referencing ultrasound data to MRI scans.

This work is important because in current clinical practice there are no imaging modalities that provide information on both brain and tumour stiffness. Yet surgeons often resect areas of tissue based on personal, rather subjective evaluations of stiffness. Ultrasound elastography may provide a more objective measure of stiffness of these areas and be able to provide stiffness information in areas not accessible to the surgeon. This may assist in affording a more complete tumour resection with sparing of normal brain. The timing of this project is ideal with the introduction of commercial real-time ultrasound elastography scanners in the past few years thus making clinical intra-operative applications a possibility.

The concept of slip elastography came from this author's observation of surgeons resecting brain tumours. Prior to resection there appeared to be no reliable method of determining how hazardous or how difficult resection was going to be. Another observation was that, at surgery, the development of the brain tumour interface as a plane of cleavage is routinely advocated. Slip elastography may reduce risk and assist in planning dissection along the brain tumour interface by providing the surgeon with a preoperative tool to objectively measure how difficult it would be to develop the brain tumour interface. To date, this will be the first study to attempt to image mechanical properties at the brain tumour interface *in vivo* or for that matter any tumour interface.

1.2.3 Outline of Thesis

The thesis is divided into 8 chapters

Chapter 2 provides a literature review to assess whether brain tumours should be resected. It also looks at the literature relating to how completeness of resection affects prognosis. Following from this a review on current surgical and imaging methods for ensuring safe and complete resection is discussed. The chapter concludes by generating the hypothesis for this thesis.

Chapter 3 discusses the ultrasound scanner used for the majority of experiments and how the machine was optimized for data acquisition.

Chapter 4 describes the ultrasound elastography technique used in more detail and describes its implementation intra-operatively during brain tumour resection. The technique of co-registration of ultrasonography with MRI using neuro-navigation to aid image interpretation is reported. The comparison with surgical findings is reported. The results following *ex vivo* testing are also discussed.

Chapter 5 describes the implementation of the real-time ultrasound elastography system during brain tumour resection.

Chapter 6 describes the theoretical basis for slip elastography. This follows with the methods by which slip elastography was developed and the *in vitro* experiments performed to test the system. The results are reported.

Chapter 7 describes the implementation of slip elastography during brain tumour resection. Comparisons to surgical findings are reported.

Chapter 8 summarizes the conclusions that can be made from the work performed and discusses how mechanical imaging may enhance neurosurgery in the future.

Chapter 2

Literature Review and Hypothesis

Chapter 2

Literature Review and Hypothesis

This chapter discusses the literature pertaining to brain tumour resection. It concentrates primarily on intrinsic high grade gliomas where most of the controversy exists. It then reviews the evidence on how completeness of resection affects prognosis. Following on from this it discusses current surgical and imaging techniques available to assist in safe and complete surgical resection and then discusses information that the surgeon may wish to have prior to resection that may reduce the risk of complication or incomplete resection. This leads on to the hypothesis for this thesis.

2.1 Should Brain Tumours be Resected?

2.1.1 Introduction

Brain tumours account of 1.6% of all cancers in England and Wales with an incidence of 4.5 to 6.5 cases per 100000 (Quinn 2001). Brain tumours can be categorized into intrinsic or extrinsic. Intrinsic tumours invade and grow within the brain substance whereas extrinsic tumours grow from structures surrounding the brain substance. Table 2.1 summarizes the common types of intrinsic brain tumours. It is important to note that there is a great deal of variation in the survival statistics for patients with brain tumours. The data

Tumour	Tumour Subgroup	Survival Data
Primary Gliomas	Grade 1	>90% 5 yr survival (Kehler 1990)
	Grade 2	72% 5yr survival (Leighton 1997)
	Anaplastic Astrocytoma	73 weeks median survival (Laws 2003)
	Glioblastoma Multiforme	40 weeks median survival (Laws 2003)
Secondary (Lang 2005)	Lung	<6 – 20 months
	Breast	6-16 months
	Melanoma	5-11 months
	Renal	8-21 months
	Colon	8-10months

Table 2.1 Table of Types of Intrinsic Brain Tumours and Survival Data (Kehler, 1990, Leighton 1997, Laws 2003, Lang 2005)

provided is from larger studies.

There are a large variety of extrinsic tumours but many types are quite rare. The most common types include meningiomas and vestibular schwannomas. Extrinsic tumours tend be benign and rarely invade brain parenchyma. They cause symptoms by 1) localised pressure on cranial nerves or on brain, 2) generalized mass effect causing the symptoms of raised intracranial pressure, 3) blocking cerebrospinal fluid pathways causing either obstructive or communicating hydrocephalus or 3) causing epilepsy. The aim of surgery is complete excision as this is likely to reduce the symptoms attributable to localized or generalized mass effect and prevent recurrence. Complete surgical excision is often seen as curative.

In contrast intrinsic tumours tend to be malignant. They cause symptoms by generalized mass effect, localised mass effect and epilepsy but also by destroying and invading normal brain. This invasive potential of intrinsic tumours means that complete excision of a high grade glioma is not usually possible. Studies have shown that despite maximal resection malignant gliomas recur at the site of resection (Demuth 2004). In fact studies where hemispherectomy has been performed have shown recurrence of the tumour not long after resection. Thus the aim of surgical resection is cytoreductive for symptom control. Resection is usually not seen as curative however. In fact there is still some controversy as to the appropriate management of high grade gliomas.

Other prognostic factors that have been show to influence survival include age, histopathology (anaplastic astrocytoma versus glioblastoma multiforme), pre-operative performance status (Lacroix 2001), and the

administration of radiotherapy (Walker 1980). These factors will no longer be discussed.

2.1.2 Surgical management of high grade Gliomas

There is a great deal of literature pertaining to the prognosis following resection of high grade gliomas however there is just 1 randomized controlled study on the topic (Vuorinen 2003). 30 patients over the age of 65 were randomized into a diagnostic stereotactic biopsy group or an open surgery and resection group. Only 23 patients were eligible for the study however. There was one patient requiring re-operation for post operative haematoma in the resection group. The median survival time for the biopsy group was 85 days (95% confidence interval of 55-157) and for the tumour resection group was 171 days (95% confidence interval of 146-278). This survival difference was statistically significant ($p=0.0346$). The time to deterioration was not statistically significant between the 2 groups however ($p=0.0566$). The results show a clear advantage in surgical resection and it is encouraging that statistical significance was achieved with such a small cohort of patients. It must be emphasized that the sample size is very small and so one needs to use caution when generating conclusions.

Authors	Date	Number of Cases	Histology	Retrospective/ prospective	Extent of Resection	Survival in Months	Surgery improves survival
Kreth	1993	115	GBM	Retrospective	Biopsy	32	No
					Resection	39.5	
Devaux	1993	263	AA & GBM treated separately	Retrospective	Biopsy of AA	98.2	Yes, in GBM
					Resection of AA	135.4	
					Biopsy of GBM	19	
					Resection of GBM	44	
Simpson	1993	645	GBM	Prospective from 3 trials	Biopsy	6.6	Yes
					Partial Resection	10.4	
					Total Resection	11.3	
Jeremic	1994	86	GBM	Prospective, GBM	Biopsy	29	Yes
					Resection	56	
Kelly	1994	128 (age> 65)	GBM	Retrospective	Biopsy	15.4	Yes
					Resection	27	
Nitta	1995	101	AA & GBM	Retrospective	Biopsy	11	Yes
					Partial	12	
					Subtotal	20	
					Complete	41.7	
Kreth	1999	225	GBM	Retrospective	Biopsy	33	Yes
					Resection	37	
Lacroix	2001	416	GBM	Prospective database	<98%	40.5	Yes
					>98%	52	
Whittle	2002	80 (age> 60)	AA & GBM	Retrospective	Biopsy	23	Yes
					Resection	41	
Laws	2003	565	AA & GBM treated separately	Prospective database	Biopsy of AA	52.1	Yes
					Resection of AA	87	
					Biopsy of GBM	21	
					Resection of GBM	45.3	

Table 2.2 Table summarizing main non randomized studies on survival following resection of high grade glioma

(Kreth 1993, Devaux 1993, Simpson 1993, Jeremec 1994, Kelly 1994, Nitta 1995, Kreth 1999, Lacroix 2001, Whittle 2002, Laws 2003)
(post 1993)

There are a many more studies where data has been prospectively or retrospectively acquired but where randomization has not occurred. Table 2.2 summarizes many of the recent studies after 1993 that have looked into the question of whether surgical resection affords a survival advantage to the patient. An important paper written by Quigley et al in 1991 (Quigley 1991) summarized the available literature in the preceding 30 years pertaining to surgical treatment of supratentorial malignant glioma. This encompassed 5691 patients over 20 identified series. He concluded that there may be some subgroups such as younger patients with favourable histology that may benefit from surgical resection. It is important to recognise that this paper includes work prior to CT and MRI, prior to neuro-navigation and prior to the use of the operating microscope. These advances in modern neurosurgical practice, undoubtedly, will have a positive impact on the safety of surgical resection and the extent of surgical resection. However, it is likely that controversy on whether surgical resection should be contemplated is born from this paper.

The studies following this paper initially show conflicting results with regard to a significant survival benefit as a result of surgical resection. However, the later studies using large prospective databases all show a definite survival advantage with resective surgery. It is important to reiterate that none of these studies refer to randomized controlled trials and so selection bias is inevitable.

The one randomized controlled study does show a survival advantage by surgical resection as mentioned earlier but the cohort of patients is so small that caution is warranted when concluding from this paper.

It is interesting to note that within the subgroup population of elderly patients with malignant gliomas, surgical resection appears to confer a survival benefit compared to biopsy alone.

In summary the available evidence suggests that surgical resection confers a survival advantage to the patient.

2.1.3 Surgical Management of Low grade Gliomas

The surgical management of intrinsic low grade gliomas is also controversial. There have been no randomized controlled studies or case control studies looking into the survival benefit of surgical resection. This is likely to be due to the long follow up time that would be required. In addition the tumours are quite heterogeneous in nature and presentation. An excellent review of 30 series of patients with low grade glioma has been reported (Keles 2001). A summary table from the paper showing all the publications used is shown in table 2.3. There were no randomized controlled studies. There appeared to be a trend with time towards the literature supporting more extensive resections. The authors concluded that the prognostic effect of extent of surgical resection for cerebral hemispheric

*Studies in which the prognostic effect of GTR on survival was assessed using statistical analysis**

Authors & Year	No. of Patients	Extent of Resection (no. of patients)	Estimated 5-Year Survival Rate (%)	UV p Value	MV p Value
studies w/ 5-yr survival estimates					
Laws Jr, et al., 1984	461	GTR (57)	61	<0.0001	S†
		RST (48)	44		
		STR/Bx (356)	32		
Philippon, et al., 1993	179	GTR (45)	80	0.00022	<0.01
		STR (95)	50		
		Bx (39)	45		
Scerrati, et al., 1996	131	GTR (76)	100	0.0005	0.001‡
		STR (31)	93.7		
		PR (24)	91.7		
Soffietti, et al., 1989	81§	GTR (19)	51	0.0009	<0.01
		STR (49)	24		
		PR <50% (13)	0		
Rajan, et al., 1994	82	GTR (11)	90	<0.05	NS
		STR (30)	52		
		PR (22)	50		
		Bx (19)	42		
North, et al., 1990	77	GTR (8)	85		0.002‖
		STR (43)	64	NS**	
		Bx (26)	43	0.013**	
Nicolato, et al., 1995	74	GTR (16)	87	0.0001	S†
		PR (58)	26		
Shaw, et al., 1994	71	GTR (10)	80	NS?	0.0065
		STR/Bx (61)	55		
Piepmeier, et al., 1996	55	GTR (31)	100	0.0013	S†
		STR/Bx (24)	77		
Medberry, et al., 1988	50	GTR (8)	57	NS	NS
		<GTR (42)	43		
studies w/o 5-yr survival estimates					
Whitton & Bloom, 1990	88	GTR (6)	NA	NS	NA
		STR (33)	NA		
		PR (28)	NA		
		Bx (21)	NA		
Ito, et al., 1994	87	GTR (19)	NA	NA	0.0011
		STR (51)	NA		
		Bx (17)	NA		
Peraud, et al., 1998	75	GTR (40)	96††	0.01	NA
		STR (35)	64††		
Bahary, et al., 1996	63	GTR (14)	NA	NA	0.002‖
		PR (34)	NA		
		Bx (15)	NA		
Piepmeier, 1987	60	GTR (23)	8 yrs‡‡	NS	NA
		STR (22)	7 yrs‡‡		
		Bx (15)	6 yrs‡‡		
Miralbell, et al., 1993	49	GTR (6)	NA	NS	NS
		STR (10)	NA		
		PR (24)	NA		
		Bx (9)	NA		

* Studies with 5-year survival estimates are presented by sample size in decreasing order, followed by studies without 5-year survival data. Abbreviations: Bx = biopsy; MV = multivariate; NA = not available; NS = not significant; PR = partial resection; RST = radical subtotal resection; S = significant; UV = univariate; ? = possibly.

† Significant according to multivariate analysis; probability value not provided.

‡ Partial resection compared with all others.

§ In this study 81 of 85 cases (Table 1) were analyzed.

‖ Biopsy only compared with others.

** Compared with GTR.

†† Four-year survival rate.

‡‡ Mean survival duration in group.

Table 2.3 Table summarizing survival following resection of low grade glioma (From Keles 2001)

low-grade gliomas, as it relates to clinical outcome, has not been specifically evaluated and that all available management strategies are acceptable treatment options, but none are supported by enough high-quality evidence.

2.1.4 The Extent of tumour resection

It appears that surgical resection is justified in a number of clinical settings. The next step is to decide how much tumour should be resected. This has been addressed in a number of publications however there were no randomized controlled studies looking at this potential prognostic factor.

Quigley et al (1991) discussed some of the issues that arise when attempting to assess whether extent of tumour resection was an independent prognostic factor. Most of the studies in his review used the surgeon's estimate rather than a quantitative measure of tumour residual. Albert et al in 1994 performed a prospective study where patients with glioblastoma multiforme had contrast enhanced MRI 1-5 days following gross tumour resection (Albert 1994). Their results suggested that there was a 3 fold improvement in accuracy at determining extent of tumour resection when compared to the surgeon's findings. Furthermore, and more significantly, he found that the presence of enhancement in the post operative MRI scan conferred a 6.595 times higher risk of death in comparison to patients with no enhancement.

The effect of radiotherapy had been accounted for in this study.

Author	Date	Number of cases	Histology	Prospective/ retrospective	Radiological correlate	Median survival/Months
Simpson	1993	645	GBM	Prospective	No	Complete11.3 Partial 10.4 Biopsy 6.6
Nitta	1995	101	GBM & AA	Retrospective	Yes, volumetric	100% 20 75-100% 12 <75% 11
Albert	1994	60	GBM	Prospective	Yes, but no size analysis	6.595 x increased risk of death if residual left
Keles	1999	55	GBM	Retrospective	Yes, volumetric	100% 93 66.8% 68.7 43.9% 49 32.1% 50.8
Lacroix	2001	416	GBM & AA	Prospective	Yes, Volumetric	100% 13.1 >98% 13.0 >96% 12.6 >94% 11.3 >90% 10..9 >85% 10.9
Keles	2006	67	AA	Retrospective	Yes	Reduced if post resection residual seen*

Table 2.4 Table summarizing studies evaluating extent of tumour resection on survival for high grade gliomas

(Simpson 1993, Nitta 1995, Albert 1994, Keles 1999, Lacroix 2001, Keles 2006)
*** The T2W MRI amount of residual was a predictor of survival**

Keles et al performed a volumetric analysis on 55 patients with glioblastoma multiforme (Keles 1999). This was based on a comparison of the pre- and post-operative CT or MRI scan with the assumption that tumour size was related to the volume of contrast enhancement. The data was also adjusted to performance status, chemotherapy and age. This paper provides the strongest evidence that complete resection confers a better prognosis compared to partial resection but there is a chance of selection bias as this was not a randomized study.

Lacroix's study also clearly demonstrated a survival advantage from aggressive surgical resection taking into account age and performance status (Lacroix 2001). The data was retrospectively analysed from a prospectively run database.

Sawaya's data also showed a clear survival advantage from more aggressive resections (Sawaya 2002).

2.1.5 Conclusions

It is clear that symptomatically apparent extrinsic tumours should be resected. Complete excision should be the aim as this may be curative.

High grade intrinsic tumours should be resected providing patients have good preoperative functional status, are not too elderly and if the tumour is surgically accessible. Low grade tumours could be resected although there is

no good evidence that this improves survival. This means that the decision should be individualised to the patient at present.

There is some evidence to suggest that complete surgical resection confers a survival advantage to patients with high grade glioma when compared with partial resection. Extent of resection should be evaluated with imaging obtained following resection. These conclusions need to be taken with caution as these results may be as a result of selection bias.

2.2 Current Surgical Techniques to Ensure Safe and Accurate Surgical Resection

As described above surgical resection is usually appropriate and complete macroscopic excision of tumours is probably the optimal treatment strategy. This section discusses the methods by which safe and complete surgical resection is achieved. Management of extrinsic tumours and intrinsic tumours differ in this respect but many principles hold true for both instances.

The key stages in resection of any tumour are as follows;

1) Exposure

2) Tumour dissection and removal

2.2.1 Exposure

This almost always requires removal of bone in order to gain access to the cranial compartment. The surgeon must decide the amount of bone to remove in order to provide adequate access to the tumour. Exposure may need to be increased to provide vascular control, for example it is sometimes appropriate to expose part of the superior saggital sinus when resecting convexity meningiomas near the midline. Determination of the size of exposure and the position of the exposure has been facilitated by neuro-navigation techniques (Barnett 2004) whereby historically acquired imaging data (such as MRI) are reformatted and co-registered with surface landmarks on the patient. Navigation with pointing devices within the 3 dimensional space around the patient's head using the reformatted imaging is possible. *In vitro* accuracy has been measured at 1.1mm for CT directed navigation and 1.4mm for MRI directed navigation (Dorward 1999). This is comparable to the surface accuracy on the patient. Thus neuro-navigation is useful in determining the site and size of exposure required.

2.2.2 Neuro-navigation and intra-operative imaging

The amount of brain shift as a result of craniotomy and opening of the dura has been calculated in a number of studies. Dorward et al calculated the average shift of the cortex following dural opening to be 4.6mm into the

cranial cavity using neuro-navigation (Dorward 1998). Nimsky utilised intra-operative MRI to measure the amount of cortical brain shift into the cranial cavity following dural opening (Nimsky 2000). This was up to 24mm. Brain shift has also been measured using ultrasound co-registered with MRI (Keles 2003). In this report cortical shift was 3.5mm into the cranial cavity but this may have been an overestimate as compression with the ultrasound probe was required in order to produce an ultrasound image. It can be seen from the studies described that neuro-navigation is useful in planning the approach and extent of bone work required to provide adequate access to the tumour. However, neuro-navigation cannot be relied upon to accurately navigate to critical structures once craniotomy has been performed and dura is open.

There is a requirement for real-time imaging in order to navigate safely during tumour resection. There are 2 main real-time imaging systems that are used.

1) Intra-operative MRI is becoming more widely available but, at the time of writing, there were no intra-operative MRI suites available in the UK. The cost of this technology is still great and there is a requirement for a non-ferromagnetic operating theatre. Intra-operative MRI has been used to assess extent of tumour resection for intrinsic gliomas (Nimsky 2004). This group found that its use altered surgical decisions on extent of resection 36.2% of the time reducing the final tumour volume significantly. Furthermore, there was no increase in the amount of postoperative deficit as a result of the more radical resection.

2) Intra-operative ultrasound has been used for many years (Makuuchi 1998). It is relatively inexpensive, portable and easy to use. It can be incorporated with other imaging modalities such as MRI using neuro-navigation (Gronningsaeter 2000). Vascular imaging is possible using colour flow Doppler (Shinoura 2005). A study has demonstrated that intra-operative ultrasound is as effective as post operative CT at determining whether residual tumour is present (Chacko 2003). This was compared to the gold standard of biopsy of the residual cavity bed. Ultrasound does suffer from drawbacks in that image signal-to-noise ratio is poor compared to MRI. With improving technology this is likely to improve (Keles 2003). Also the contrast between tumour and brain is not as great as with contrast enhanced MRI. The use of ultrasound contrast agents that exploit breaches in the blood brain barrier, as occurs in association with many intrinsic brain tumours, may improve this contrast differential however. Finally, the lack of recognisable landmarks that can be used as reference points on images makes image interpretation difficult however the incorporation of ultrasound with neuro-navigation effectively removes this problem.

2.2.3 The process of tumour removal

This will be divided into 2 components depending on pathology.

2.2.3.1 Extrinsic Lesions such as Meningiomas and Vestibular Schwannomas

Once access is adequate, with retraction of brain kept to a minimum, the tumour can be approached. The usual manner of removal is to develop the plane between the capsule of the tumour and the arachnoid or pial membrane usually using dissection with sponges (Yasargil 1996). The tumour-arachnoid plane is commonly bloodless with minimal adherence between the 2 surfaces. During subpial dissection, however, adherence of tumour to brain is more evident. There is also a much greater risk of cortical damage. In a study investigating the planes of cleavage in meningiomas it was found that in 43% of patients, a cleavage plane between tumour and brain could be achieved by passing in the extrapial plane over more than two thirds of the total brain tumour interface (Alvernia 2004). In 46% of cases, a subpial plane was found in more that two thirds of the dissection and 11% of cases were a mixture between the two. Furthermore this paper could find no preoperative MRI evidence to predict mechanical properties or the anatomical site of plane of cleavage. To date there have been no methods for determination of adherence between tumour and brain prior to resection although this information may assist the surgeon in planning his approach. For other extrinsic tumours these surgical principles hold true.

Vascular structures supplying the tumour may be the cause of the adherence in a number of cases. Thus, when approaching an area of tumour adherence to brain care is usually taken to prevent haemorrhagic complications. Again prior knowledge of the adherence of tumour to brain may assist in this process.

Following dissection along the plane of cleavage the tumour is often entered and internally debulked (Yasargil 1996). The consistency of these tumours is subjectively variable and a range of techniques are required depending on the stiffness of the tumour (Weingart 2004). If the plane of cleavage between tumour and brain is subpial and the tumour is soft then it can become difficult to distinguish tumour from brain. Currently the surgeon evaluates what to resect based on visual inspection of the operative field and palpation through instrumentation. Palpation assesses mechanical properties such as stiffness and adherence. There are no imaging techniques used in everyday clinical practice that objectively assess the stiffness of tumours intra-operatively during brain tumour resection.

Following internal debulking the tumour capsule is excised with the dural base.

2.2.3.2 Intrinsic Tumours such as gliomas and metastases

Surgical resection of intrinsic tumours utilises slightly different techniques when compared to extrinsic tumours.

1) Intrinsic High grade Gliomas

The aim of surgery is to remove the enhancing portion of the tumour. It is safe to assume that almost all of the cells within the contrast enhancing area are tumour cells (Weingart 2004). However tumour cells and brain cells are likely to be found beyond these boundaries. This has been confirmed on post mortem correlates with MRI (Van Den Hauwe 1995). If the tumour is not apparent on the cortical surface a common technique is to split a sulcus (Yasargil 1996). Alternatively a transgyral approach can be taken. The tumour should be approached with minimal sacrifice of normal brain where possible. An internal debulking is then commenced. Despite the invasiveness of high grade gliomas these tumours often respect pial borders at tumour boundaries (Toms 1999, Yasargil 1996). Thus, following partial debulking the tumour wall is dissected away from the brain and the cleavage plane developed. Of course there are usually multiple adherent areas and tumours extending into white matter tracts often do not have any discernable interface with brain. The surgeon again uses visual inspection and palpation to determine what to resect. Specifically the surgeon evaluates colour changes, relative stiffness and adherence. The surgeon has stereoscopic vision with an operating microscope to assist in the evaluation of colour changes. There are no objective methods used in routine surgical practice for determination of the stiffness or adherence however.

2) Metastatic tumours

The approach to a metastatic tumour is very similar to that used for resection of high grade gliomas except that sulcal dissection is preferable (Weingart 2004). The difference occurs when the metastasis is exposed. Metastatic tumours often have a well-defined capsule and are located

subcortically. Once the tumour has been approached the tumour brain interface should be developed. It is important to note that metastatic deposits are variable in their degree of adherence to brain and the vascular supply is also variable. Once there has been adequate dissection of the plane of cleavage the tumour can often be removed in one piece. Sometimes an internal debulking is required however. Due to the variability of adherence it would be optimal to determine the adherence preoperatively. Furthermore objective information on the stiffness of tumour may also assist in affording a safe and complete resection.

2.3 Literature Review of the Use of Mechanical Imaging intra-operatively during brain tumour resection

At the outset of this project the author was aware of no other group working on mechanical imaging intra-operatively during brain tumour resection. However, during the course of the present work, 2 groups that were also attempting to do this made their work known. This work and that of the 2 other groups appear to have begun at similar times, and have occurred

completely independently of each other. All have used ultrasound based techniques.

The first group (Scholz 2005) used a previously described technique called vibrography (Pesavento 2000). This technique is based on ultrasound elastography (Ophir 1991). It differs from other forms of ultrasound elastography in 2 ways. Differential displacement (from which strain is calculated) between successively acquired RF frames is estimated using a so called "phase root seeking" algorithm as opposed to the cross correlation technique (Pesavento 1999). This displacement estimation technique is computationally less expensive when compared to the cross correlation technique and so enables real-time imaging with modest computing hardware. The second major difference was that static compression was replaced with low frequency vibrations by using a stepper motor vibrating at approximately 5-10Hz. This was necessary to reduce the magnitude of strain required to produce stable strain images.

The clinical results using this method have been documented in the paper by Scholz et al (Scholz 2005). They initially performed experiments on swine brains performing vibrography and measuring intracranial pressure (Scholz 2004). No rise in intracranial pressure was observed. The RF data were digitized for off-line and real-time processing. A special applicator equipped with a stepping motor was required to generate low frequency vibration of the probe with amplitude of 0.3mm. It was possible to produce 30 strain images every second. 19 patients had vibrography performed intra-operatively. Tumour was visualized in 18 of these 19 patients. 3 major groups of tumour were identified as follows;

1) Tumours with identical strain to surrounding brain centrally but with peripheral high strain. All these cases were metastatic deposits.
2) Tumours with higher strain than brain tissue
3) Tumours with lower strain than brain tissue.

Unfortunately there was no comparison to surgical findings in this paper so it is difficult to draw conclusions as to what was being imaged in terms of stiffness. The authors suggested that patients with elastographic appearances of group 1 had a peripheral zone of enhancement due to a zone of oedema. However I propose that an alternative explanation may be that this peripheral area of high strain may represent shearing strain artefact due to the tumour slipping against the brain (see chapter 7) as observed during the studies reported in this thesis. Another drawback in drawing conclusions from the study by Scholz et al is that the imaging shown in the publication has not been referenced to an MRI image in the correct plane although the authors do suggest that this technique could be applied in conjunction with neuro-navigation. Another criticism is that the device used seems somewhat cumbersome with a number of working parts. It is unclear how sterilization issues were overcome.

Selbekk et al also used mechanical imaging during brain tumour resection (Selbekk 2004). Strain was measured by a correlation technique for time shift estimation described by Simon et al (Simon 1998). This technique was initially designed for thermal imaging and the Selbekk group have altered it for the purposes of performing ultrasound elastography. Data was also synchronized with ECG pulsations. The probe was held as stationary as

possible, to determine whether elastograms could be created using strain generated by the natural variation of blood pressure during the heart cycle. They concluded that the internal pulsation as a result of systole was sufficient to drive elastogram generation and that external compression was not required. They also noted that the quality of the strain images produced deteriorated when compression was applied. Ultrasound elastography was performed on just 2 patients.

Again, in this paper, there has been no attempt to correlate findings to the surgical findings so it is not possible to draw conclusions on what the strain images show. The technique used is relatively straightforward to use but data analysis was performed postoperatively. Correlative MRI scans were not included in their images.

This thesis describes in greater detail the findings from an extension of first clinical study to have been published on this topic (Chakraborty 2004, Chakraborty 2006). The findings are presented in the following chapters and so will not be discussed here.

There have been no other mechanical imaging techniques that have been applied intra-operatively during brain tumour resection.

2.4 Hypothesis

Relative tumour stiffness and adherence of tumour to brain can be imaged using ultrasound elasticity imaging techniques intra-operatively during brain tumour resection.

This would be the first question to answer before determining whether ultrasound elasticity imaging techniques can assist in improving completeness of resection during brain tumour resection.

Chapter 3

Ultrasound Optimization

Chapter 3

Ultrasound Optimization

This chapter discusses how RF ultrasound data were obtained from the ultrasound system used for off-line creation of elastograms (as opposed to the commercial real-time elastography system also employed). In addition it describes how the scanner was optimized, in conjunction with the computing hardware to optimize data capture. This step was fundamental prior to acquiring any data for elastogram generation.

3.1 Introduction

The Acuson 128XP (Acuson, CA, USA) ultrasound scanner was used with the 7.5MHz L7 ultrasound probe in all experiments involving off-line data analysis. This included the off-line conventional ultrasound elastography experiments (chapter 4), the *in vitro* slip elastography experiments (Chapter 6) and the *in vivo* slip elastography experiments (Chapter 7). This particular scanner was used as it contained an interface allowing access to intermediate frequency data thus allowing raw data manipulation away from the scanner. It was therefore important to optimize data capture from the machine to provide optimal data.

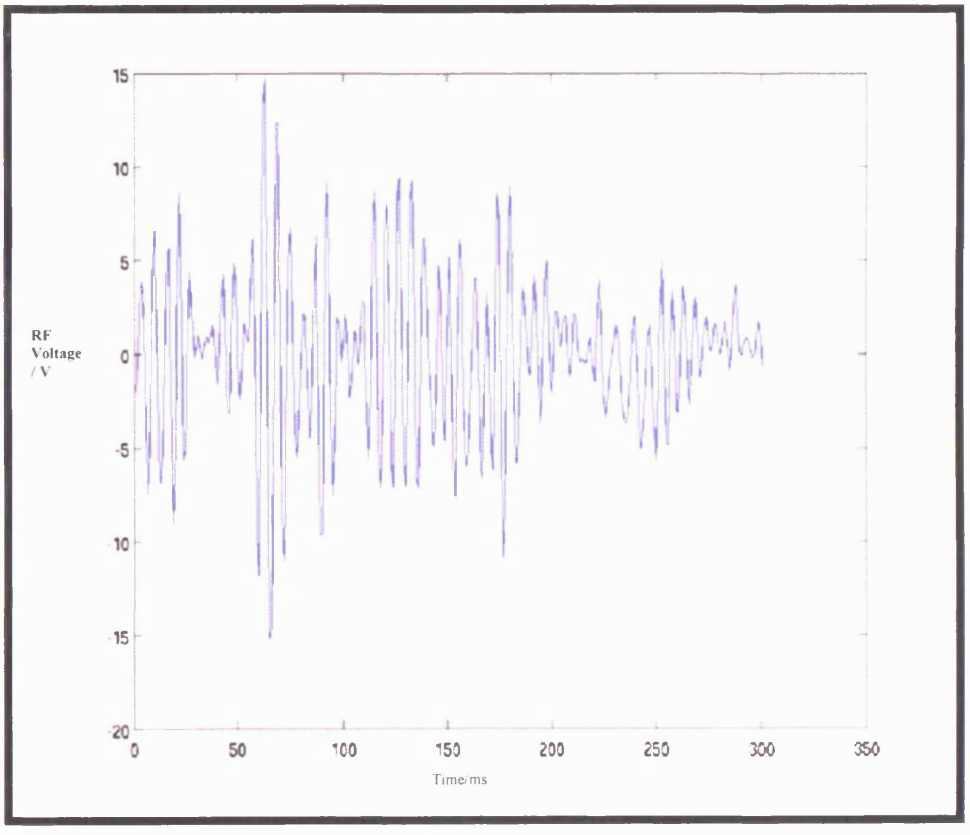

Figure 3.1 An RF voltage signal or A line

In order to understand optimization it is worthwhile explaining how raw ultrasound data is produced and processed within the Acuson 128XP. The L7 is a linear ultrasound probe that contains 256 paired piezoelectric elements which are uniformly distributed along its length. Following excitation of the ultrasound probe by returning acoustic waves the piezoelectric material of each element generates a voltage. This voltage emanating from the piezoelectric material is termed radiofrequency (RF) data and is related to the acoustic reflectivity of the object that has been insonated. There is one RF signal for each of the 256 elements but not all of these can be observed simultaneously by the receive electronics, which comprises only 128 voltage channels. A switching circuit controls which group of 128 elements is directed into the 128 receive channels at any moment, forming a 128 element-wide window that can be swept along the array under electronic control. The 128 channels of RF voltage signals are then combined into a single RF signal by adding them together after each signal is passed through its own time delay, in a circuit known as the beamformer. The distribution of time delays across the 128 channels is under system control, allowing the acoustic spatial sensitivity pattern of the probe to be focused at any desired depth in the tissue. The output of the beamformer is also an RF voltage signal, and is a timeline relating the amplitude of received echoes to depth along a line in the tissue that is centered on a chosen group of consecutive elements. Such a signal is called an A-line, an example of which is shown in figure 3.1. By switching the 128 receive channels so that they are connected, a new group of 128 (or less) elements along the centre line of the direction from which echoes are being

received may be swept along the array with the successful sound pulses that were used to elicit the echoes. Each pulse, and each corresponding switch to a new group of elements, creates a new RF A-line. A conventional echographic image is formed from multiple RF A-lines, after each has been processed to detect the magnitude of the voltage. When the L7 probe is connected the Acuson 128XP forms images by producing 256 adjacent A-lines.

In order to simplify the electronics in the beamformer many older scanners including the one described modify the raw RF voltage signals. This technique is called heterodyning and involves rescaling of voltage frequencies to so called intermediate frequency (IF) data. The output from the beamformer is then also an IF signal. This beamformed IF signal can be converted to the equivalent beamformed RF signal if the components of the heterodyning process are known. However, the specific details of conversion of IF signals to RF signals are beyond the scope of this discussion; a description of the method may be found in Doyley et al (2000).

This particular ultrasound machine was equipped with an inbuilt interface providing access only to the analogue IF signal produced by the beamformer. Thus it was necessary to extract the IF signal from the ultrasound scanner, digitize this signal and convert it to RF data.

Furthermore it was important to optimize ultrasound parameters that could affect the analogue IF signal. It was clear that the gain and time gain compression (TGC) controls had an effect on the amplitude of the analogue IF signal hence this aspect was optimized for the current study as very small

gain and TGC values would lead to poor echographic signal-to-noise ratio of the object under investigation and too high a value would saturate the signal for the given digitization range.

3.2 Methods

The analogue IF signal was digitized using the Mutech MV-1000® analogue to digital conversion PC card (Mutech corporation, MA, USA). This analogue to digital converter digitized signals to 10bits at a sampling rate of 20MHz. The sampling rate was considered adequate for digitizing the IF signal, which is centered around a frequency of 2MHz, and the bit range was considered adequate for a signal that is post-TGC and has therefore been corrected for depth dependent attenuation. This card was configured so that the full dynamic voltage range of the analogue IF signal was digitized. The upper and lower bounds of the digitization range were determined by insonating a flat metal plate in a water-bath as a water-metal interface is intensely reflective to acoustic waves. The maximum voltage detected using this method was 2.96V using an oscilloscope.

The next stage was to obtain optimal gain and TGC parameters. Gain modulates the amplitude of RF voltage throughout the entire echo image whereas TGC allows modulation at different time instances i.e. at different depths seen on the ultrasound B mode image.

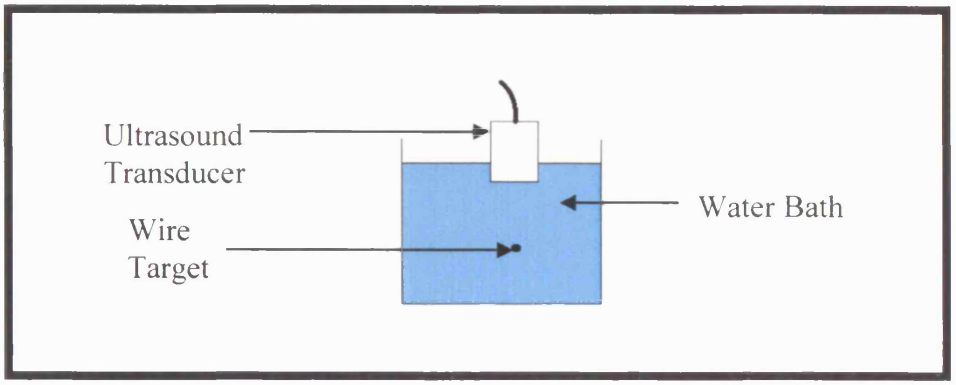

Figure 3.2 Experimental setup used to optimize gain and TGC controls

Thus an experiment was required for each TGC setting.

A very thin nylon wire was submerged in a water bath. The wire was parallel to the base of the water bath and kept stretched. An ultrasound probe was placed submerged above the wire target at different depths. The wire target was insonated to provide a cross-sectional B mode image.

IF signals were digitized and converted to RF data using programs developed at the Institute of Cancer Research Physics Department written in Matlab®. A-lines for an ultrasound RF frame were plotted.

The A-line with the largest amplitude IF voltage on an oscilloscope was selected and the magnitude of the maximum amplitude noted.

This was repeated for each TGC setting as the gain was altered through its dynamic range. The maximum RF voltage amplitude for each gain setting was plotted as a function of gain, as read in decibels (dB) from the machine's display. This was then repeated for each TGC setting.

Thus one graph for a fixed TGC setting was created. It was found that these graphs could be combined into one cumulative graph incorporating the effects of both controls. From this graph it was possible to determine the point at which signal saturation was occurring.

The Acuson 128XP has an inbuilt echo signal amplitude detector that highlights areas where a desired voltage amplitude exceeds a specified threshold. This feature of the Acuson 128XP was subsequently programmed to show green on the B mode display if the voltage amplitude exceeded the point at which signal saturation was found to occur.

3.3 Results

Figure 3.3 shows the graph of the voltage amplitude against the gain values for three TGC settings, labeled TCG 1, TGC 2, and TGC 3. Figure 3.4 shows the composite graph. It is clear from this graph that the point of saturation occurs at a scanner IF output voltage of 2.7V.

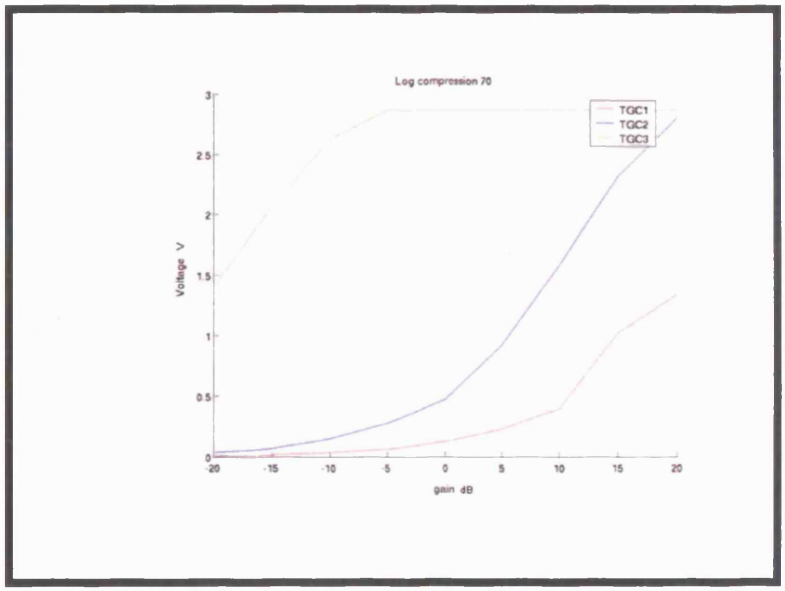

Figure 3.3 Voltage versus gain plots for 3 different TGC settings

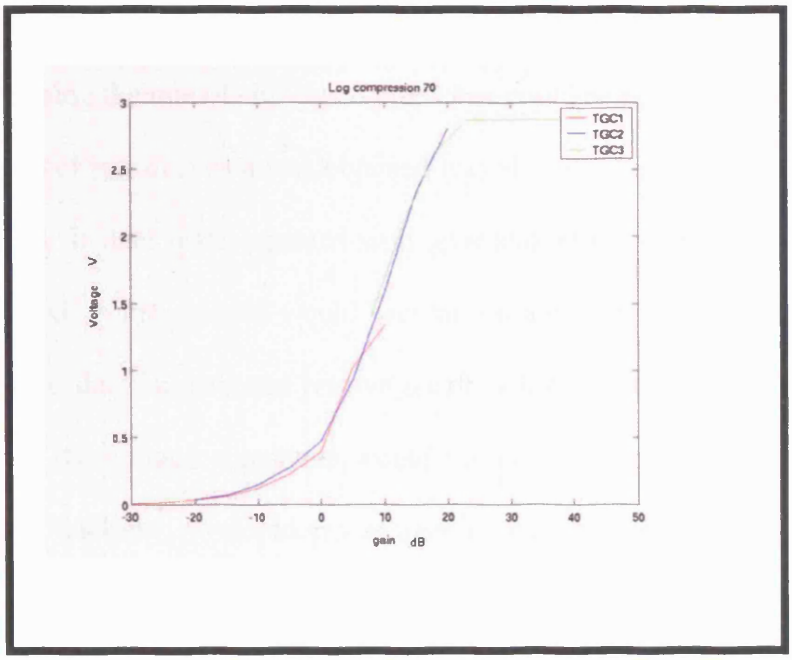

Figure 3.4 Cumulative curve for TGCs.

Note the point of signal saturation is at 2.7V

3.4 Discussion

This chapter describes how analogue IF data from the scanner were converted to digitized RF data. This step was essential as it provided the raw data that was used for subsequent image processing described later in this thesis. It was possible to digitise 20 ultrasound IF frames per second at a scan depth of 70mm using the Mutech MV-1000. Hence it was possible to produce up to 19 elastogram images per second retrospectively. This frame capture rate was at least halved when using the external trigger mode on the

Mutech MV 1000 card, needed for the work described in chapters 6 and 7, thus determining the rate of slip elastograms that could be produced.

Optimisation of raw data as it was obtained was also an essential component of this thesis. If data were captured with gain and TCG settings too high, parts of the RF voltage signal would become saturated. Thus, it would not be possible to discriminate and resolve areas of high acoustic reflectivity. Furthermore RF voltage signatures would become less specific hindering displacement tracking As displacement tracking was essential in the type of ultrasound elastography used in this thesis poor tracking would significantly affect the performance of the algorithms used to create ultrasound elastograms. If the gain and TGC settings were too low on the other hand then RF voltage signatures would be dampened also hindering displacement tracking.

For all experiments following this, the echo signal amplitude detector was switched on, providing a real-time B-mode image where echoes were displayed in green, rather than grey scale, if they corresponded to an IF voltage amplitude greater than 2.7V. In all the experiments performed, the TGC was always set to produce as uniform a B-mode image throughout the depth chosen, and the gain set for a comfortably bright echo image. At no time were the scanner gain or TGC increased to the point where IF signal saturation would have been evident.

This simple method of calibrating the gain characteristic of the scanner helped to ensure that the digitized echo signals were amplified as linearly as possible.

Chapter 4

Conventional Off-Line Processed Ultrasound Elastography with Co-registered MRI during Brain Tumour Resection

Chapter 4

Conventional Off-Line Processed Ultrasound Elastography with Co-registered MRI during Brain Tumour Resection

This chapter introduces the technical aspects of conventional off-line processed ultrasound elastography used in this thesis. A brief discussion of the mechanical properties of brain and tumour is also included. The method by which this technique was implemented intra-operatively during brain tumour resection in combination with neuro-navigation is then described with a description of the methodology for data capture and palpation. The results from 24 patients where ultrasound elastography was performed intra-operatively during brain tumour resection are then presented with a comparison to surgical findings on stiffness. The results of *ex vivo* mechanical testing are also presented and the implications of these results discussed. The chapter concludes with a summary of the findings.

4.1 Introduction

4.1.1 Ultrasound Elastography

This chapter introduces some of the more technical aspects of ultrasound elastography. Some details on ultrasound elastography mentioned previously have been repeated for the purposes of continuity.

Ultrasound elastography is a technique for imaging mechanical properties of a material by measuring and imaging induced strain within tissue following the application of an externally-applied displacement to the surface of that tissue (Ophir 1991). The process of elastogram generation involves application of a stress to the material under study, usually in the form of axial compression applied by the ultrasound probe, and evaluation of the resultant strain. Relative strain images, known as elastograms, can be produced by comparison of pre- and post-compression ultrasound echos.

4.1.1.1 Technical Details of Ultrasound Elastogram Generation

As described in Chapter 3 an ultrasound radiofrequency (RF) echo waveform is a plot of the time evolution of voltage produced following excitation of a piezoelectric material within an ultrasound probe by returning ultrasound echos. The time of return for a given echo is dependent on the depth of the material that reflected the incident wave, assuming speed of sound is constant throughout the scan plane. Conventional B mode ultrasound echographic imaging displays an image derived by calculating

the magnitude of the RF echo signal. Hence, a B mode ultrasound image depicts the acoustic reflectivity of a scanned area. Fine structure in ultrasound echo images may be dominated by an acoustic interference pattern known as speckle that can be tracked from one echographic frame to the next (Bamber 1986). A region of interest within a scan plane, or window, will have a unique RF voltage signature or echo signal relating to the speckle pattern and resolved tissue structure.

Following compression by the ultrasound probe, the basic shape of the post-compression echo signal from the tissue, for a given window, at a specific depth, for small deformations, will not have changed significantly compared to the pre-compression echo signal, i.e. the RF voltage signature for that specific window will be present regardless of compression. However, the time for the echo to return to the probe will be reduced due to a reduction in

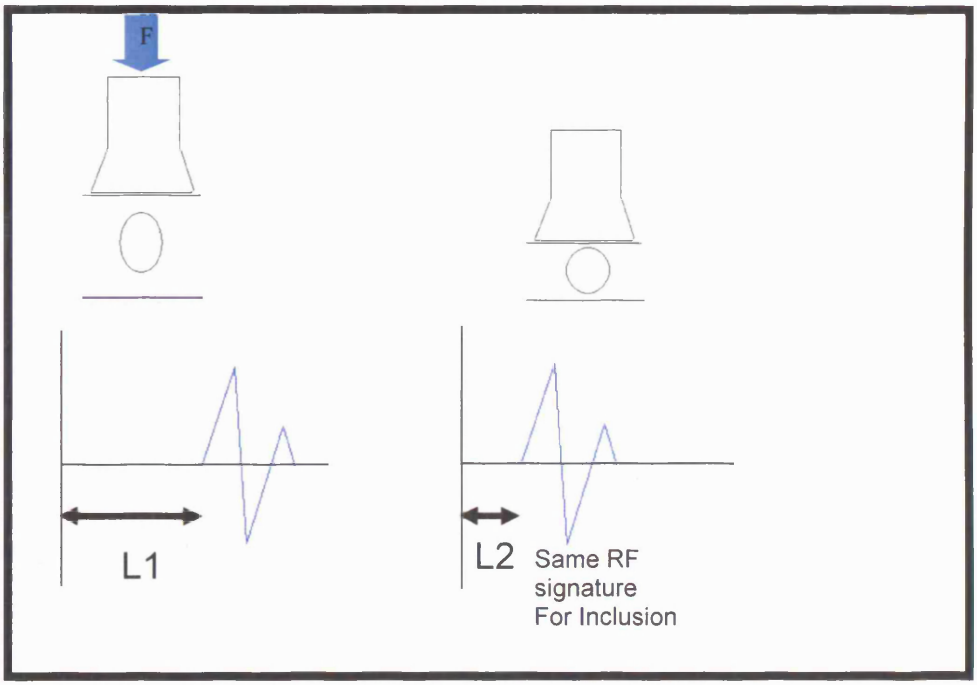

Figure 4.1 Diagram illustrating the theory behind displacement tracking.

The RF voltage signature shown represents the inclusion. Note that the RF signature is assumed not to change significantly but the distance travelled is far less than softer areas. L1 – L2 is the measure of displacement that is calculated using a cross correlation tracking method

distance brought about by compression. A computerized cross correlation tracking algorithm searches selected post-compression RF echo signal signatures for the best fit to the chosen pre-compression RF echo signal signature (also known as the pre-compression reference window). The difference between the position of the pre-compression reference window and that of the post-compression RF echo signal signature that best fits the shape of the echo signal signature in the reference window provides the magnitude and direction of displacement for that reference window. By showing the magnitude and direction of displacement for each reference window a displacement image is thus produced. For a homogeneously solid material that is evenly axially compressed the displacement image will show a gradient of gradually increasing displacements with depth. Thus, it is important to investigate where there are changes in this gradient indicating tissue with different stiffness characteristics. This is possible by obtaining the spatial derivative of the displacement data. This provides the normal axial strain and is the basis of a strain image or elastogram. The technique used to obtain the derivative uses a least squares strain estimator (Kallel 1997). The least squares strain estimator fits a straight line to the points chosen on a short section of the displacement data. The best fit line is chosen by a least squares method. The slope of the line or the gradient is calculated thus providing a strain value for a short window surrounding each displacement value. The least squares strain estimator has been shown to perform with improved signal to noise ratio when compared to the finite difference method which detects only differences between adjacent displacement values (Kallel 1997).

Elastograms can be produced using a freehand palpation technique (Bamber 1996, Doyley 2001, Bamber 2002). Free hand palpation involves the operator holding the ultrasound probe and applying an axially compressive force to the material under study. This avoids the necessity for cumbersome devices for holding ultrasound probes when applying compression and is ideally suited for the operative environment where time and sterilization considerations are important. However there is a greater risk that the scan plane will alter with compression. Out of plane motion prevents accurate displacement tracking as reference window RF voltage signatures would no longer be visible within the scan plane.

This chapter describes the use of a freehand ultrasound elastography technique intra-operatively during brain tumour resection. In many of the cases ultrasound elastography was co-registered with MRI to aid interpretability of the images.

4.1.2 Mechanical Properties of Brain and tumours

There have been some biomechanical experiments on brain tissue, primarily in animals on *ex vivo* brain tissue, aiming to elucidate repeatable stress strain relationships of brain. The stress strain relationship has been shown to be non-linear. Observations have been made on how the brain reacts in certain conditions to help understand this stress strain relationship. The

brain has been shown to have elastic (Estes 1970), viscoelastic (Galford 1970), poroelastic (Pena 1999), anisotropic (Velardi 2006) and hyperelastic (Sahay 1992) properties under various conditions. This makes it impossible to objectively comment on absolute stiffness and compare to other materials in different conditions.

To date there have been few studies looking at stiffness characteristics of brain in humans and no studies looking at stiffness characteristics of human brain tumours and comparing them to normal brain. There has been some work looking at mechanical properties of breast tumours, prostatic tumours and thyroid tumours in humans however (see chapter 1).

Rather unsurprisingly there is currently no model that is able to provide an exact and repeatable prediction of the behavior of brain tissue when tumour is present.

Despite this lack of accurate data on the mechanical properties of brain and brain tumours there is a large and continually growing interest in developing biomechanical models (Carter 2005). These models are being used to identify pathophysiological mechanisms involved during head injury, modeling brain deformation occurring as a result of surgery or even as a result of tumour growth (Kyriacou 2002). The accuracy of a model will be reflected by the accuracy of the mechanical properties inputted into the software.

This chapter describes a method for providing a more objective measure of the mechanical properties of tumour compared to brain by mechanically testing *ex vivo* samples of brain and brain tumour.

4.2 Methods

Approval from the Local Research Ethics Committee was obtained. Patient recruitment was from the Neurosurgical Department at the Royal Free Hospital, London. Twenty four patients who were due to undergo craniotomy for excision of brain tumour were recruited for this study. Inclusion criteria into this study were all patients undergoing craniotomy and debulking of presumed brain tumour and the patient's ability to provide informed consent. All consecutive cases that fulfilled these criteria were included. Intrinsic and extrinsic tumours were included. Data were captured intra-operatively and analysis, including elastogram generation, was performed by the author retrospectively using computing facilities at the Institute of Cancer Research Physics Department.

A freehand ultrasound scanning technique was adopted for data capture. The ultrasound probe was housed in a sterile sheath manufactured for this purpose (Mana-Tech, England).

All patients were placed in 3 pin skull immobilization. For patients with extrinsic tumours, data were obtained prior to dural opening and, for patients with intrinsic tumours, following dural opening. Neuro-navigation was set up in the manner described in 4.2.1. Following craniotomy, data were obtained for elastogram production by the method described in 4.2.2.

4.2.1 Co-registration of Ultrasound and MRI data intra-operatively

The probe was co-registered with the StealthStation™ neuro-navigation system using the SureTrack™ system (Medtronic, USA) in a number of cases. This enabled visualization of the MRI image in the identical plane as the ultrasound image plane (Figure 4.2). This assisted image interpretation.

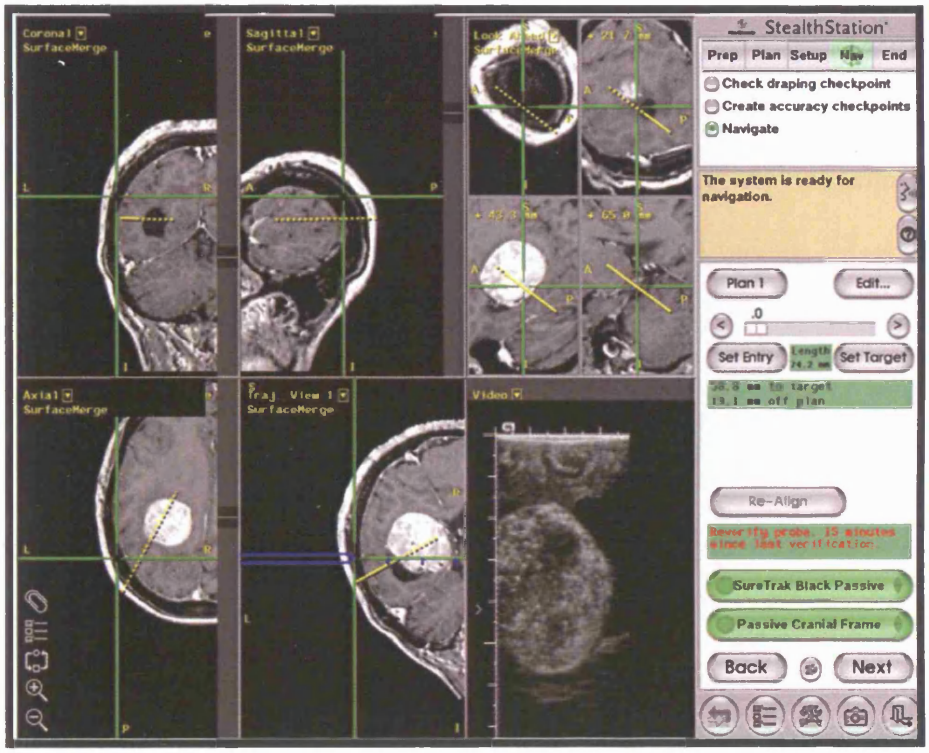

Figure 4.2 Screenshot from the StealthStation Neuro-navigation system

The area representing tumour on the B mode ultrasound image was compared to the area representing tumour on the MRI image. The distance from the probe's surface to the brain surface depicted on the StealthStation™ trajectory view image was calculated. This gave an

indication of the magnitude of apparent brain displacement as a result of craniotomy and application of the ultrasound probe on the brain's surface. A visual assessment of co-registration accuracy by evaluation of tumour extent was also made. Figure 4.3 shows the ultrasound probe on the surface of the brain with the SureTrack^{TM} device attached.

4.2.2 Technique of Palpation

Two cycles of axial displacement by the ultrasound probe were applied manually to the surface of the brain or dura for each ultrasound echo data capture sequence (Figure 4.3). Each dataset lasted about 2 seconds providing 30 IF echo frames. Axial displacements of no more than 5mm were applied to the surface of the brain. Compression was only applied to areas where resection would occur.

Care was taken by visual observation of the real-time B mode ultrasound image during all acquisitions to minimize lateral and elevational displacements caused by undesired transducer motion, thus aiming to maximize correlation between pre and post compression RF images. The effect of altering the amplitude of axial compression on quality and information obtained on elastograms was evaluated.

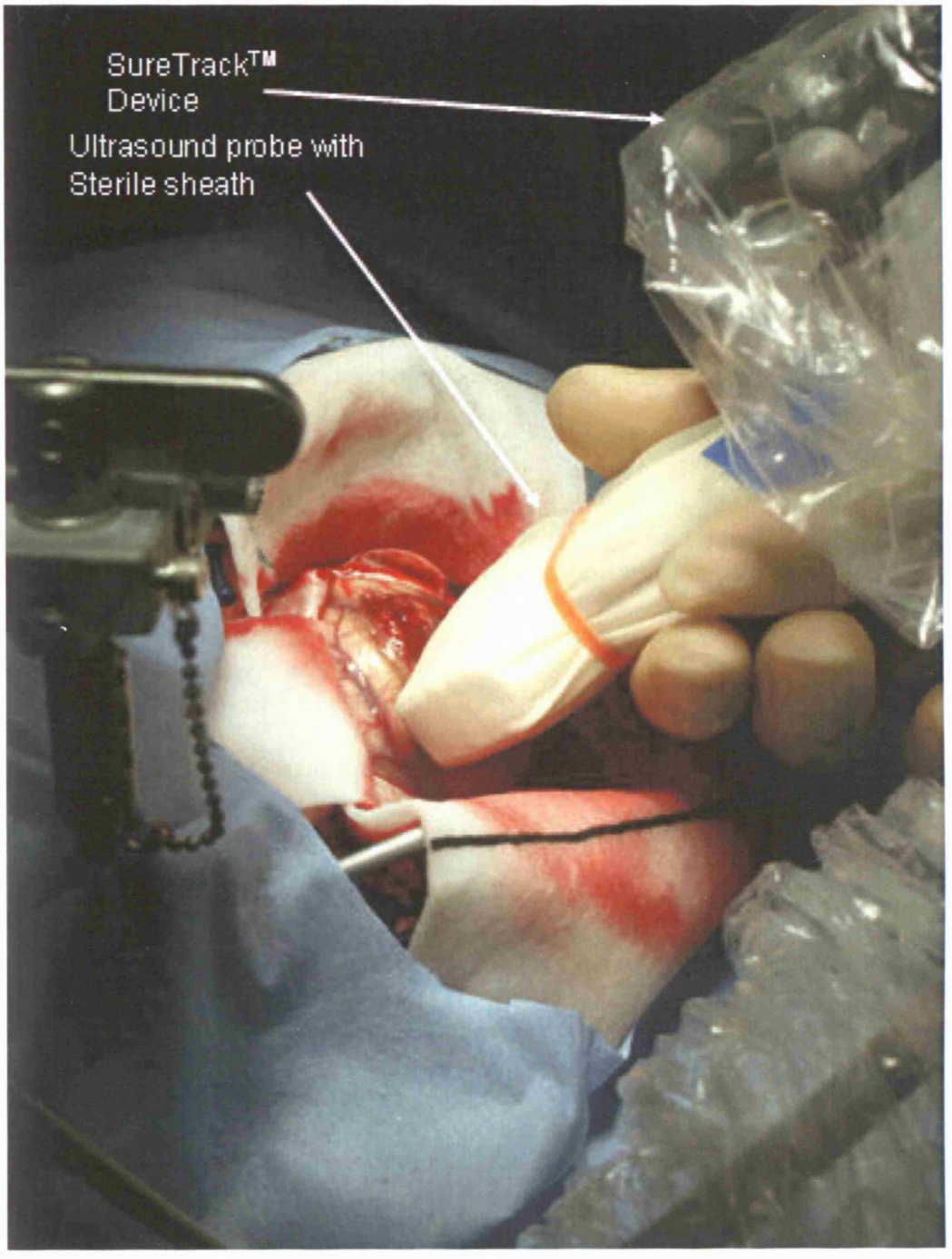

Figure 4.3 Image of freehand palpation applied intra-operatively during brain tumour resection

Note the sterile covering and the Suretrack™ system allowing tracking of the surface of the probe using the StealthStation™ system

4.2.3 Data and Image Processing

Ultrasound elastograms were created using equipment and software described below.

Analogue IF data acquired from the Acuson 128XP (Acuson, CA, USA), were converted to RF data after digitization as described in chapter 3. The digitized RF echo data were interpolated up to 40 MHz to improve tracking precision.

A cross correlation based tracking algorithm was applied to pre- and post-compressed RF data, producing displacement images. For all possible windows in the pre-compression RF data, the cross correlation algorithm detected the X-Y position of the best-fit RF window in the post-compression RF data. Thus, displacement images comprising tissue displacement values for X (or lateral displacement) and Y (or axial displacement), were created. Axial and lateral displacement images were optimized for visualization by altering size of the reference window, reference window overlap and search window size. These 3 parameters had significant consequences on the quality of the displacement images produced. The use of a small reference window improves the spatial resolution of the elastogram but at the expense of the signal to noise ratio. The reference window overlap refers to the progression along the A line to the next calculation. A progression of a very small distance would result in a large number of points improving overall resolution but at the expense of spatial resolution at areas where there is a marked change in stiffness. Also computational expense is far greater. The final parameter refers to the extent to which the post compression image is searched. Larger search areas result in greater computational expense.

Smaller values could result in the too small a search area being analyzed thus reducing the chance the correct window being found in the post compression image. Values for these parameters were chosen so that there was adequate contrast between stiff areas and soft areas with a reasonably high resolution. This was an iterative process and was dependent on the quality of the raw data, the method of palpation and the acoustic characteristics of the area under investigation.

Occasionally a technique called companding, where the post compression A-line is stretched so that RF peaks correlate in the time domain, was employed to improve displacement tracking thus improving quality of the elastograms.

Correlation images were also obtained by determining correlation coefficients between pre- and post-compression RF data for each window. Axial displacements, lateral displacements and correlation coefficients were used to determine the nature of movement within the scan field, and the confidence with which displacement, hence relative strain image data could be relied upon.

A least squares strain estimator was applied to displacement data to produce elastograms. The least squares strain estimator measured the relative strain from a displacement image. The number of points over which the estimator was calculated over (i.e. the window size) was 3. Figure 4.4 summarizes the process of elastogram generation used.

For a set of 30 echographic images in a dataset 29 elastograms were produced. It was possible to identify contiguous frames that were produced during compression or extension of the probe by visualizing the axial

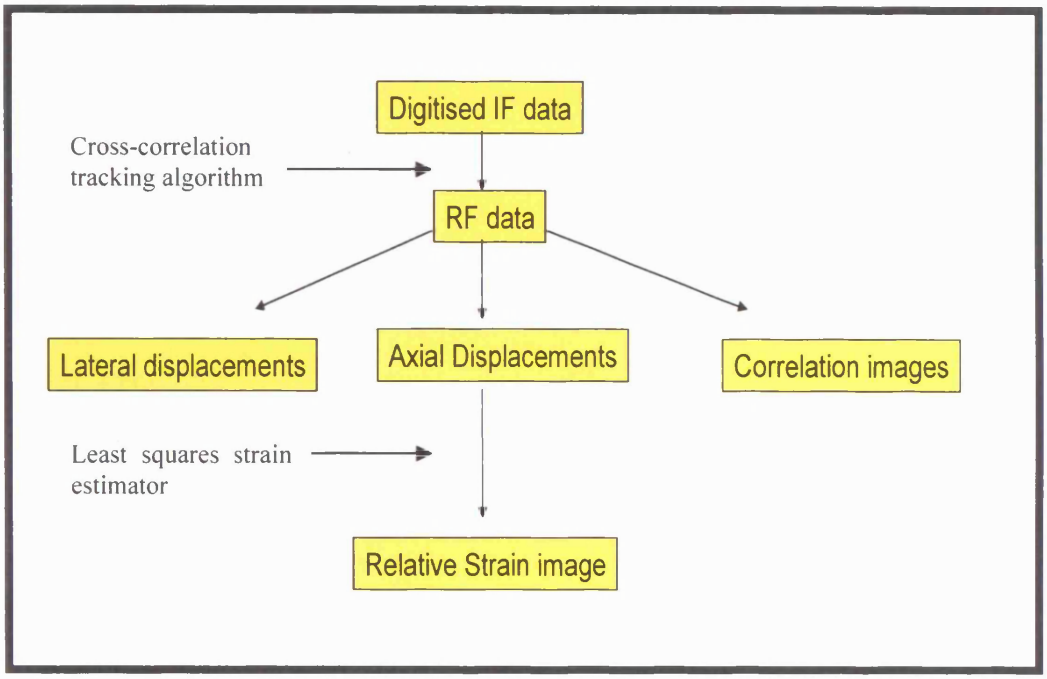

Figure 4.4 Summary of the steps taken to create an elastogram

displacement images. Composite elastograms were produced by obtaining the average strain value for each pixel within the elastogram image over a cycle of compression or extension and plotting this value.

4.2.4 Comparison of Surgical Findings with Ultrasound Elastogram Findings

Information provided by the surgeon was not available when elastograms were produced in order to limit bias.

Elastograms were processed and evaluated with the B mode ultrasound movie by the author only. Relative strain of tumour compared to brain was assessed, as was the presence of fluid and tumour strain heterogeneity.

The elastogram data were compared to surgical findings as follows. Patients were divided into 4 groups depending on surgical findings on stiffness. The groups were;

1) Control subjects

   Patients with no pathologically demonstrable tumour, patients in whom elastogram data was obtained following complete macroscopic excision and patients with tumour cyst where the cyst wall was of a similar stiffness to brain,

2) Patients with solid tumours where the surgeon felt that the tumour had stiffness homogeneity,
3) Patients with solid tumours where the surgeon felt that the tumour had stiffness heterogeneity,
4) Patients with cystic tumours where the cyst wall was found to be stiffer than normal brain.

The demarcation of the interface between brain and tumour was assessed on ultrasound echography, and compared to ultrasound elastography.

Following the surgical procedure, the surgeon was asked to compare stiffness within the operative field to normal brain. Furthermore he was asked to describe the composition and the stiffness heterogeneity of the tumour.

Brain tumour interface identification on the ultrasound echogram was compared to elastogram images. An assessment of the demarcation of brain

compared to tumour at the interface was made using B mode ultrasonography and compared to elastography by visual inspection of the images. This assessment was not made in patients belonging to group 1.

4.2.5 *Ex vivo* Stress Strain Measurements on Brain and Tissue

In 4 patients, it was possible to obtain 4 *ex vivo* tumour and one *ex vivo* brain sample. These samples were mechanically tested using the Inspec 2200 portable mechanical testing device (Instron, USA) in the operating theatre. As soon as the samples were removed from the patient, they were cut to a cuboid shape using a scalpel and its dimensions measured. The time from resection to mechanical testing was less than 10 minutes in all cases. The sample was placed, unconstrained, on a glass slide and a compressive force applied by the Inspec 2200. The rate of compression was 0.25mm/s. The graph of stress against strain was plotted for each of the samples tested.

4.3 Results

Table 4.1 summarizes surgical and elastogram findings on stiffness for all 24 patients. In general ultrasound echography was superior to elastography at demonstrating the tumour brain interface.

4.3.1 Co-registration of Ultrasound and MRI data intra-operatively

9 patients out of 24 had ultrasound echography and elastography co-registered with MRI using the StealthStation^{TM} and the SureTrack^{TM} adaptor. In 2 cases there was no measurable brain displacement as a result of craniotomy and application of the probe to the brain's surface. The other 7 cases demonstrated brain shift indicating that the brain surface had displaced into the cranial cavity. The average measured brain shift into the cranial cavity for all 9 cases was 1.6mm with a range of 0 to 3mm. The 2 cases where no shift was observed were intra-ventricular tumours. Figure 4.2 (about 9 pages back) shows a screenshot from the StealthStation^{TM}. The imported ultrasound echographic video and corresponding trajectory view MRI are shown. The ultrasound image correlated perfectly once the image was rotated 90^0 and flipped 180^0 along the vertical axis. In all cases, features seen on the ultrasound images correlated with features seen on the trajectory

Patient Number	Diagnosis	Group	Surgical Tumour Stiffness comparison to brain	Elastogram Tumour Stiffness comparison to brain	Correlation in surgical and elastogram findings	Demarcation of brain tumour interface using echography vs elastography
7	L frontal GBM	1	Cystic, not much tumour, tumour wall same stiffness as brain	Cystic, tumour wall same as normal brain, plane of cleavage through for potential cyst expansion	Yes	N/A
13	R frontoparietal GBM, post op images	1	Cystic, no stiffened wall (post op so no tumour)	No stiffened wall	Yes	N/A
16	L frontal arachnoid cyst, normal brain	1	Cystic, no stiffened wall	No difference in strain, no grey white differentiation	Yes	N/A
20	R occipital cystic GBM	1	Cystic, No stiffened wall	Cystic, No stiffened wall	Yes	N/A
23	Occipital cystic GBM	1	Cystic, No stiffened wall	Cystic, No stiffened wall, bending artefact seen	Yes	N/A
1	Intraventricular Meningioma	2	Solid, homogeneous, tumour much stiffer than brain, floating in ventricle	Homogeneous, tumour stiffer than brain	Yes	Similar performance
5	L parietal Convexity Meningioma	2	Solid, homogeneous, tumour stiffer than brain	Homogeneous, stiffer than brain, dural tail of stiffness	Yes	Similar performance
8	L Parafalcine meningioma	2	Solid, homogeneous, tumour same stiffness as brain	Homogeneous, tumour stiffer than brain	No, elastogram stiffer	elastography superior to U/S
10	CP angle Meningioma	2	Solid, homogeneous, tumour stiffer than brain	Homogeneous, tumour stiffer than brain	Yes	Similar performance
11	Parafalcine GBM	2	Solid, homogeneous, tumour same stiffness as brain	Homogeneous, tumour stiffer than brain	No, elastogram stiffer	U/S superior to elastography
15	R temporal low grade intrinsic glioma	2	Solid, homogeneous, tumour softer than brain	Homogeneous, tumour softer than brain	Yes	U/S superior to elastography
19	L sphenoid ridge meningioma	2	Solid, homogeneous, tumour same stiffness as brain	Homogeneous, same stiffness as brain	Yes	elastography superior to U/S
21	CP angle acoustic Neuroma	2	Solid, homogeneous, tumour stiffer than brain	Homogeneous, stiffer than brain	Yes	elastography superior to U/S
3	L parietal GBM	3	Solid, heterogeneous, tumour mainly same stiffness as brain, sometimes softer	Solid, heterogeneous, sometimes softer than brain	Yes	U/S superior to elastography
4	L parietal Gliosarcoma	3	Solid, heterogeneous, stiffer than brain with some areas similar to brain	Solid, heterogeneous, slightly stiffer than brain	Yes	U/S superior to elastography
6	L posterior frontal metastasis	3	Solid, heterogeneous, tumour mainly softer than brain, gelatinous	Heterogeneous, softer than brain	Yes	U/S superior to elastography
9	Recurrent R frontal GBM	3	Solid, heterogeneous, tumour mainly stiffer than brain	Heterogeneous, tumour stiffer than brain	Yes	U/S superior to elastography
17	L parietal GBM	3	Solid, heterogeneous, tumour same as brain with stiffer areas	Heterogeneous, tumour the same stiffness as brain	No, elastogram never stiffer than brain	U/S superior to elastography
18	L frontal low grade glioma	3	Solid, heterogeneous, softer and stiffer than brain	Heterogeneous, solid	Yes	elastography superior to U/S
22	L parietofrontal GBM	3	Solid, heterogeneous, tumour mainly softer than brain	Heterogeneous, tumour softer than brain	Yes	U/S superior to elastography
2	L Parietal multicystic metastasis	4	Multicystic tumour, parts of tumour wall stiffer than brain	Multicystic, parts of wall stiffer than brain, clot similar stiffness to brain, septae stiffer than brain	Yes	U/S superior to elastography
12	Intraventricular GBM	4	Cystic, heterogeneous and multicystic, wall stiffer than brain	Multicystic, Excellent heterogeneity seen in tumour stiffness, stiffer than brain, wall stiffer	Yes	U/S superior to elastography
24	Occipital Cystic GBM	4	Cystic, stiffened wall, looked like abscess	Cystic, stiffened wall	Yes	U/S superior to elastography
14	L frontal GBM (biopsy only)	N/A	-	Tumour same stiffness as brain	-	U/S superior to elastography

Table 4.1 Table summarizing histological, surgical and elastogram findings in 24 patients who had Intra-operative ultrasound elastography

Patients were categorized according to the scheme described in section 4.24.
***Note GBM stands for glioblastoma multiforme.**

view MRI. The area of tumour depicted on echography was identical to the area of tumour depicted on MRI.

4.3.2 Surgical Details

17 out of the 24 patients had intrinsic tumours, (one of which was located primarily in the intra-ventricular area), 1 patient had an intrinsic arachnoid cyst, 5 had extrinsic tumours and one had an intra-ventricular meningioma. 1 patient underwent craniotomy and biopsy only so surgical stiffness assessment was not possible for this case. One patient had elastography performed following complete macroscopic tumour resection so the surgical assessment was that no stiff component was present in the imaging field.

4.3.3 Examples of displacement images, correlation images and elastograms

Patient 1

For a given acquisition sequence, 30 RF frames were captured over 2 seconds. This produced a total of 29 axial displacement images with corresponding lateral displacement images and correlation images. Figure 4.5 shows a B mode image (figure 4.5a) and appropriate StealthStation^{TM}

screenshot (figure 4.5b) with corresponding correlation image (figure 4.5c), axial displacement image (figure 4.5d), lateral displacement image (figure 4.5e) and elastograms (figures 4.5f & 4.5g).

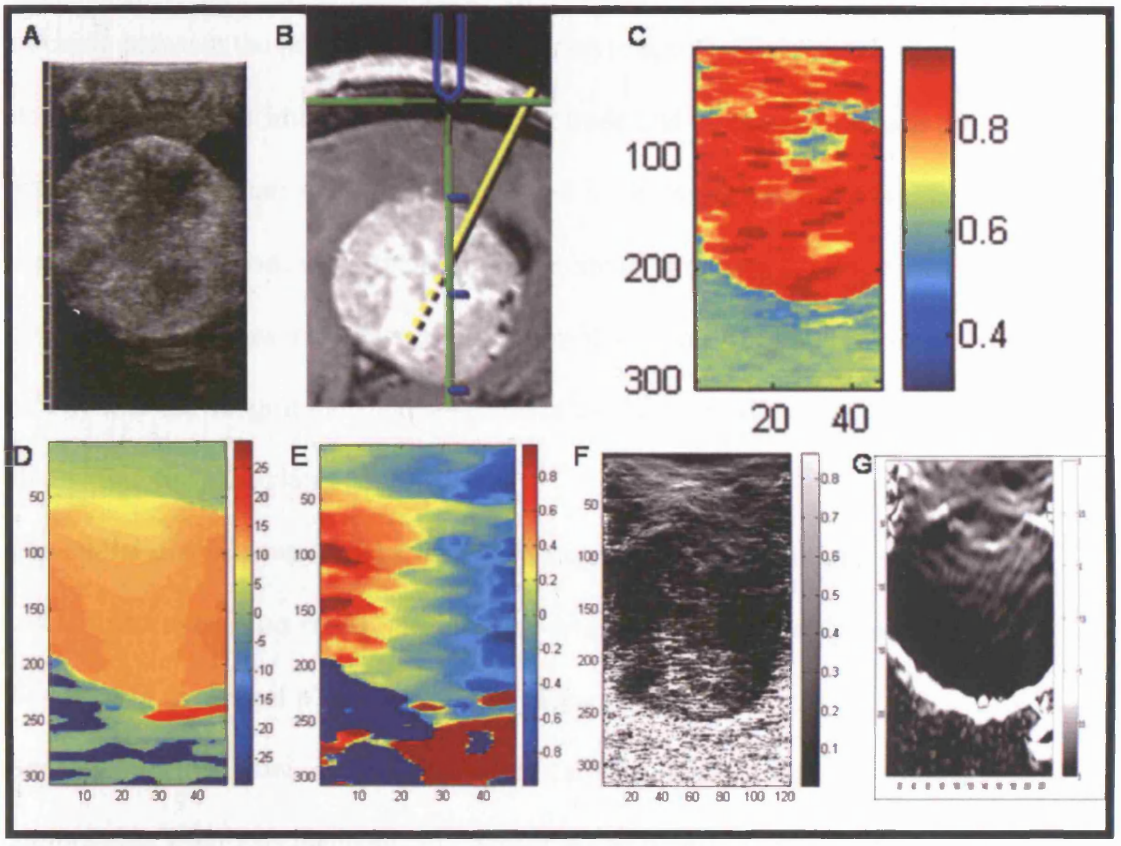

Figure 4.5 Figure showing images used for elastogram generation in patient 1

a) B mode ultrasound image, b) StealthStation™ screen-shot in the trajectory analogous to a). The blue overlay near the brain surface is a representation of the position of the ultrasound probe (at the centre of its front face) and its direction. The blue blue tick marks along the green line indicate the scale that was used to measure the magnitude of brain shift at the brain surface as a result of craniotomy, c) correlation image. The red areas represent areas where correlation is high (see the colourbar to the right of the image), d) axial displacement image. The colourbar demonstrates the magnitude and direction of axial displacement for each area within the scanplane producing the displacement image, e) lateral displacement image, f) and g) elastograms for patient 1. The colourbar shows magnitude and direction of normal axial strain, f) was produced when no axial compression was applied. The strain was thus generated from the intrinsic pulsations of the brain. It can be seen that tumour was stiffer than brain as tumour was darker that brain in this representation, g) was produced following pre-compression at the surface. Tumour brain stiffness heterogeneity is not as obvious compared to f). The tumour contained a slip boundary as described by the surgeon. The slip boundary is represented by the white area at the tumour periphery as a very high strain region. Areas deep to the tumour had poor correlation coefficient values so elastogram images could not be relied upon in these areas.

The correlation image was depicted on a colour-scale as shown. Values varied between 0 and 1; red areas accounted for high correlation values. Note that the magnification of the different images is different for each image.

The areas with high correlation values indicated where there was good tracking between the pre and post compression images.

Axial displacement images identified magnitude and direction in which the areas within the scan plane were displaced in the axial plane during data capture. The colour-scale to the right of the image indicates the direction of displacement (yellow-red towards and cyan-blue away from the ultrasound probe) and the magnitude of displacement in the axial direction for each area within the scan plane.

The lateral displacement image identified magnitude and direction (yellow-red left and cyan-blue right) in which the areas within the scan plane were displaced in the lateral plane during data capture.

Analysis of the axial and lateral displacement images together helped demonstrate what was mechanically happening to particular areas within the scan field following application of stress by the probe. For example, tumour compression could be discriminated from tumour movement without compression.

Lateral displacement images were of poorer quality when compared to axial displacement images, but nevertheless indicate clearly in this example that there was on average an approximately symmetrical lateral expansion (due to the tendency for tissue to be incompressible) with little or no net lateral translation of the tissue during axial compression with the ultrasound probe.

High correlation coefficients (>0.95) were found superficial to tumour, and within the tumour itself, whereas deeper areas beyond tumour had poor correlation values (<0.8) (figure 4.5c). Fluid within the ventricular system produced areas with poor correlation coefficients during application of the stress with the probe.

Axial and lateral displacement images demonstrated the free movement of tumour within the lateral ventricle. Discrimination between displacement and compression was possible by analyzing lateral displacement images. The tumour expanded in the lateral direction when a compressive force was applied.

An elastogram obtained by application of the stress with the ultrasound probe is shown in figure 4.5g. The elastogram image plots the magnitude of strain with spatial position within the ultrasound scan plane. The grey-scale to the right of the image depicts the scale used for plotting the strain value for each given spatial position within the scan plane. Areas with low strain (i.e. stiffer areas) on this scale were a darker grey than high strain (softer) areas. This elastogram is a cumulative image averaging all frames involved on compression. The most apparent feature was the boundary between brain and tumour. This area was clearly evident on the MRI scan, the ultrasound echo image and the elastogram, and was confirmed as the boundary between brain and tumour by the surgeon. The relative strain was so high at this presumed slip boundary that artifact was produced obscuring surrounding structures. Furthermore slip most likely dissipated stress transmission into and beyond the tumour. The B mode movie confirmed that tumour was slipping relative to brain at the points where high strain was demonstrated.

Contrast in strain between tumour and brain was not obvious in this sequence. Low strain values were also noted deep to the tumour on the elastograms. Correlation images showed this area to have poor correlation coefficients so strain data from these areas could not be relied upon.

Figures 4.5f & g shows elastograms produced following application of different magnitudes of pre-compression. It is interesting to note that it was possible to produce elastograms by holding the probe absolutely stationary relative to the skull (figure 4.5f). The intrinsic pulsations of the brain as a result of the cardiac output are the most likely mechanism for stress generation in this instance. Relative strain contrast of brain to tumour was more evident when smaller amounts of pre-compression were applied. Conversely slip boundaries appeared to be more evident following application of greater amounts of pre-compression.

4.3.4 Elastogram and Surgical Findings According to Group

4.3.4.1 Group 1

Cystic tumours with no stiffed areas-control group

There were 7 patients who had cystic lesions. Of those, four demonstrated no increased stiffness within the cyst wall according to the surgeon. These 4 cases and the case where images were obtained following resection

comprised the control group. Figure 4.6 shows a B mode image with corresponding elastogram for a patient in this group (patient 16). Predominantly normal brain has been imaged here. The elastogram demonstrates relative homogeneity, for the given scan field, in terms of strain. This is as one would expect. At the base of the ultrasound image the edge of the cyst can be seen. This elastography technique assigned high strain values and poor correlation values for fluid as fluid cannot be tracked. Fluid cannot be tracked because it is dynamic in nature and has poor ultrasound scattering properties. This demonstrates the importance of elastographic visualization in conjunction with conventional ultrasonography. In all 5 cases where no stiff component was evident surgical findings accurately corresponded with the elastogram findings.

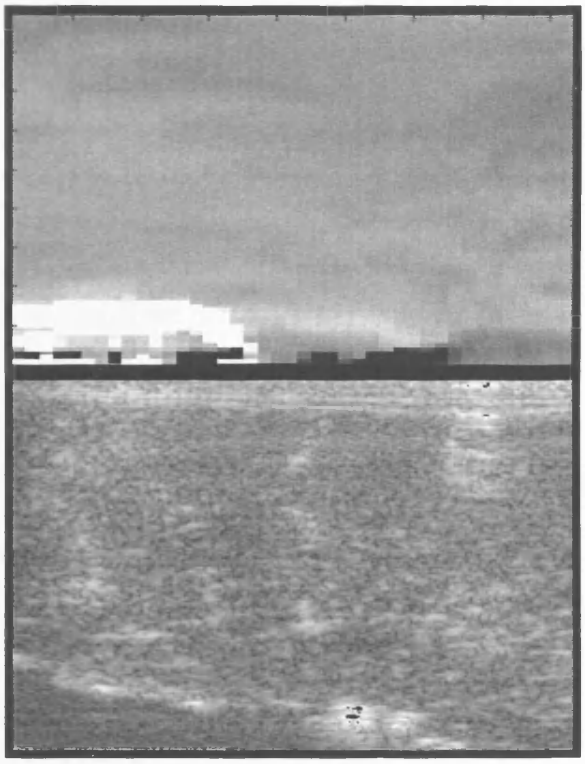

Figure 4.6 B mode image and elastogram for a patient with no stiffened region of tumour

Note how the elastogram demonstrates relative stiffness homogeneity. This is essentially an image of normal brain

4.3.4.2 Group 2

Solid homogeneous tumours

There were 8 patients where the surgeon felt tumour was homogeneous in terms of stiffness (group 2). This accounted for all the extrinsic tumours.

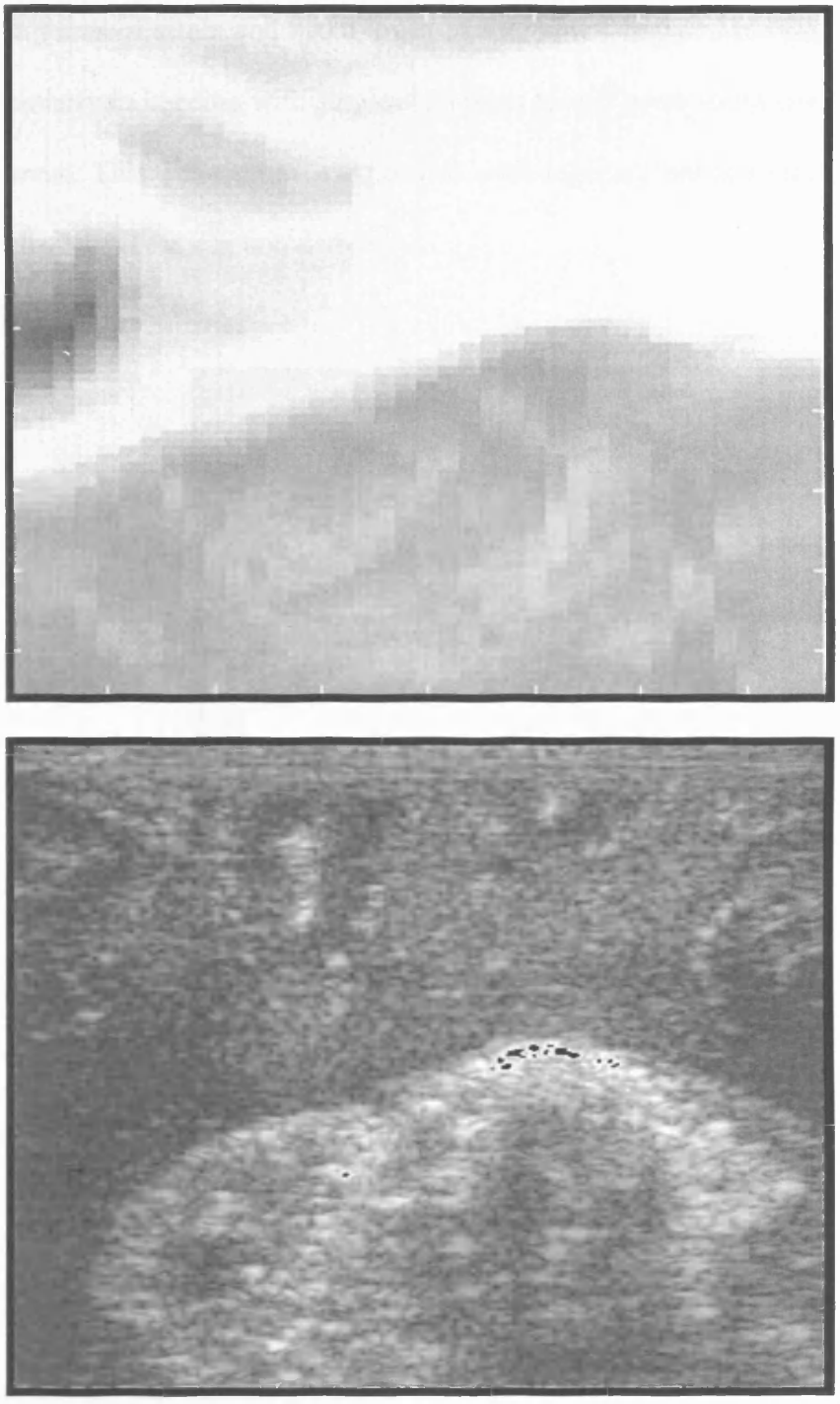

Figure 4.7 B mode image and elastogram for a patient with a homogenously stiff tumour

Figure 4.7 shows a B mode image with corresponding elastogram for patient 1. Patient 1 had an intra-ventricular meningioma that was described by the surgeon as being homogeneous in terms of stiffness and very stiff compared to brain. The elastogram image clearly shows that tumour was homogeneous in terms of strain and had a lower strain value compared to brain. This was entirely in keeping with surgical findings as stiff areas strain less than softer areas. This elastogram was formed with minimal pre-compression so the slip boundary was not visible.

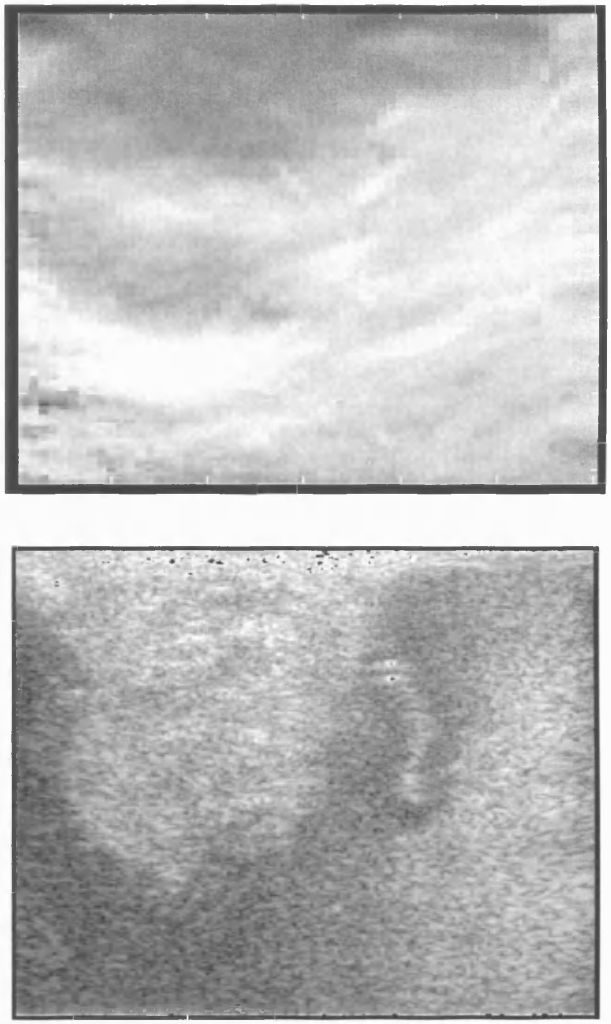

Figure 4.8 B mode image and elastogram for patient 5

Note that the tumour is darker than brain indicating that it was stiffer. Also note the high strain at the brain tumour interface inferiorly.

Figure 4.8 shows a B mode image with corresponding elastogram for patient 5. This patient had a convexity meningioma. The surgeon felt that this tumour was slightly stiffer than brain but homogeneous. Also he identified a very clear plane of cleavage between brain and tumour. The image demonstrates that the tumour was stiffer than brain. It is interesting to note that the dural tail associated with the tumour can also be identified on the elastogram. This was confirmed by the surgeon as well. Furthermore the area of high strain at the brain tumour interface on the elastogram may be indicative of a slip boundary. These findings were compatible with the surgical findings.

Within this group, there was agreement between elastogram findings and surgical findings in 6 of the 8 cases. There were 2 cases where elastography findings suggested that tumour was stiffer than the surgical findings. In both these cases the tumours were found to be parafalcine. They were both described as being of a similar stiffness compared to brain whereas the elastogram suggested that tumour was stiffer than brain.

In general, brain tumour demarcation was more apparent on B mode ultrasonography for solid homogeneous tumours, however.

4.3.4.3 Group 3

Solid Heterogeneous Tumours

There were 7 patients where the surgeon felt tumour was solid but had a heterogeneous consistency (group 3). All these cases were intrinsic tumours. There was only 1 case where there was disparity between surgical findings

and elastogram findings. In this case, the surgeon felt tumour, in certain areas, was stiffer compared to brain. There was no evidence of tumour having a greater stiffness than brain on any elastograms generated for patients in this group. This may be because the appropriate scan plane containing stiffer components was not imaged. Figure 4.9 shows the B mode image and elastogram for patient 22.

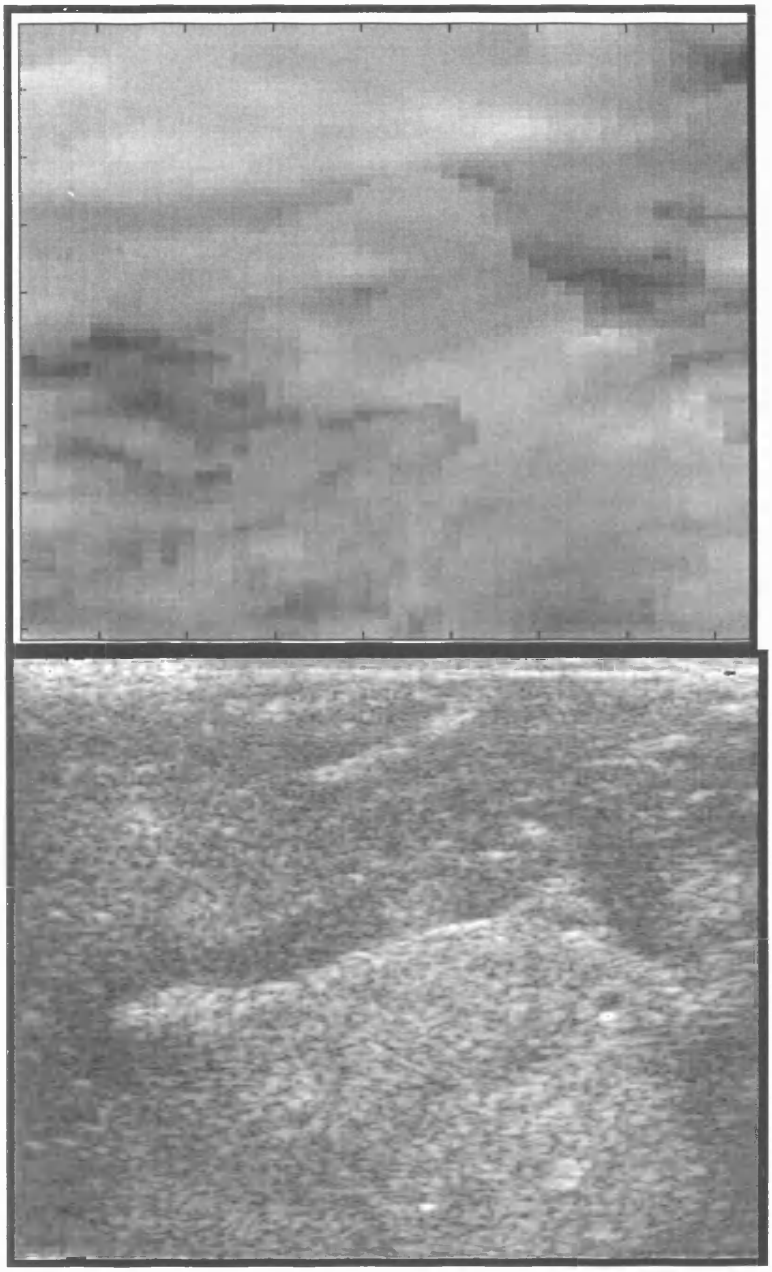

Figure 4.9 B mode image and elastogram in a patient with a solid tumour with heterogeneous stiffness

The surgeon felt this tumour was on the whole softer than brain with areas that were of a similar stiffness to brain. The elastogram also demonstrated these findings.

4.3.4.4 Group 4

Cystic Tumours with a Solid Component

There were 3 patients where the surgeon found cystic tumour with tumour wall stiffer than brain. In all 3 cases elastograms demonstrated this stiffer wall in the presence of the cyst.

Figure 4.10 shows a B mode image and elastogram from patient 24. There was an area of low strain just below the cystic area.

The elastograms produced in this group were of poor quality probably because stress propagation diminishing as a result of the presence of the cyst.

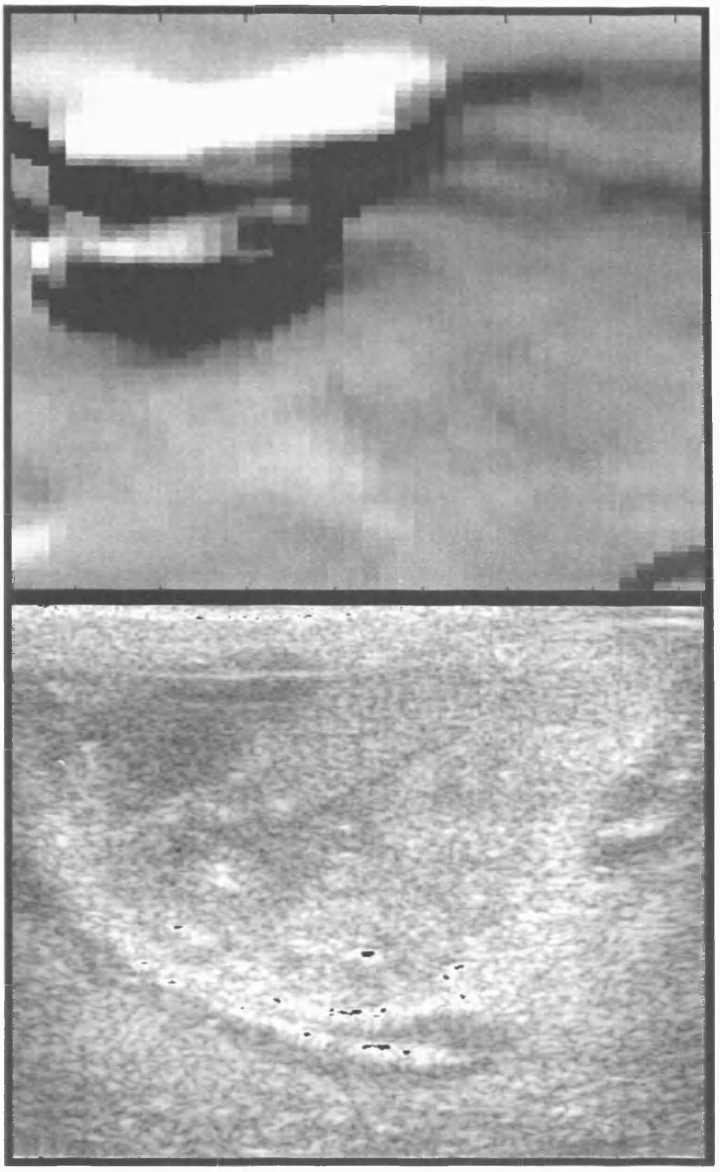

Figure 4.10 B mode image and elastogram in a patient with a cystic tumour where the wall of the cyst was stiffer than normal brain

4.3.5 *Ex vivo* Stress Strain Measurements on Brain and Tissue

Data on 4 tumour specimens and one brain sample were obtained. The data including displacement and force were exported into matlab^{TM}. Table 4.2 shows the details of the dimensions of the samples tested.

Patient	Surface area	Thick-ness	Histology	Surgical findings	Elastogram Findings
Patient 12 Brain	89	8	-	-	-
Patient 4	56	4	Gliosarcoma	Heterogeneous, stiffer than brain	Solid, heterogeneous, slightly stiffer than brain
Patient 7	255	5	Glioblastoma	Cystic, tumour wall same stiffness as brain	Cystic, tumour wall same as normal brain,
Patient 8	44	7.5	Meningioma	Solid, homogeneous, tumour same stiffness as brain	Homogeneous, tumour stiffer than brain
Patient 12	38	3	Glioblastoma	Cystic, heterogeneous and multicystic, wall stiffer than brain	Multicystic, stiffer than brain, wall stiffer

Table 4.2 Table demonstrating subjectively assessed stiffness characteristics of patients where tissue was mechanically tested *ex vivo*

The stress/strain curves for the samples are shown in figure 4.11. The graph demonstrates the non linearity of all samples, both tumour and brain. It was not possible to obtain a value for the Young's modulus given this non-linearity.

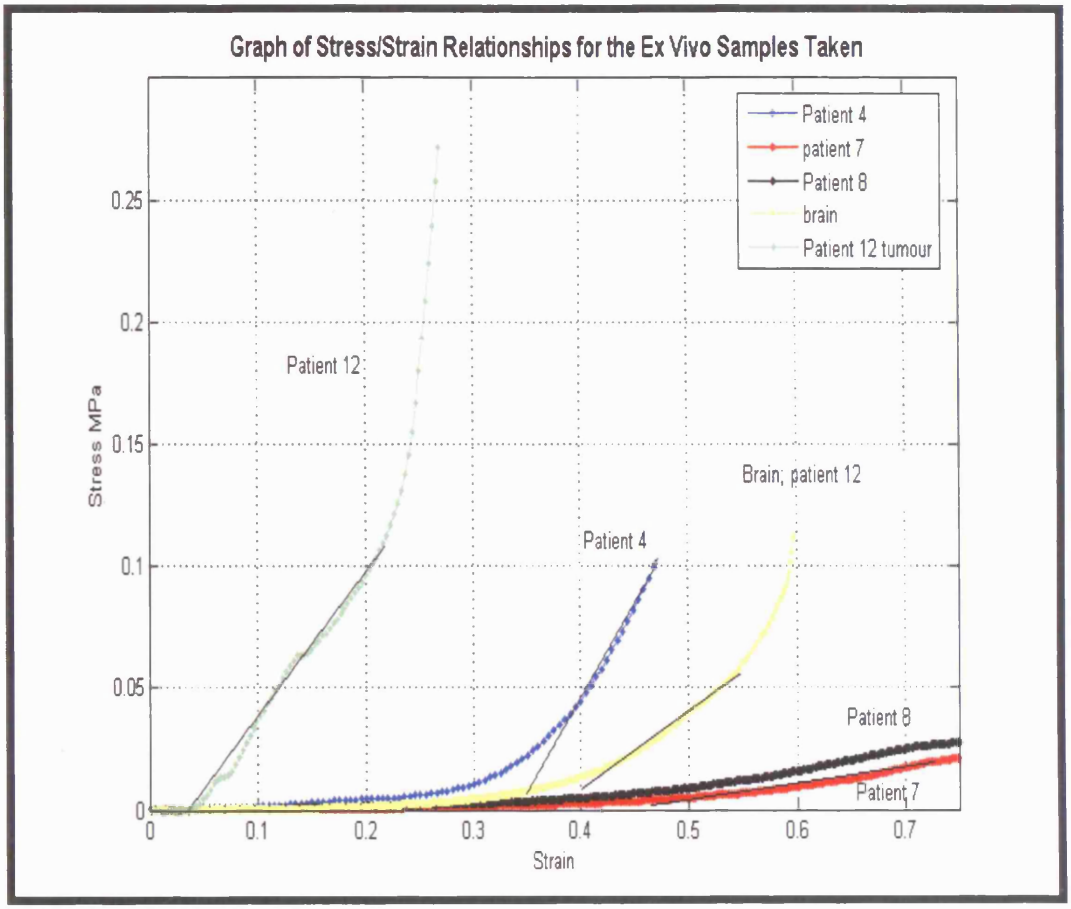

Figure 4.11 Stress strain graphs of *ex vivo* mechanically tested samples of brain tumour and brain

4.4 Discussion

4.4.1 Co-registration of Ultrasound and MRI data intra-operatively

Conventional B mode ultrasonography has been used intra-operatively to assist resection of brain tumours for decades (Makuuchi 1998). Its use has been limited by the interpretability of images (Keles 2003). Contrast between brain and tumour is not as marked when compared to alternative imaging modalities such as MRI. Combining real-time ultrasonography with neuro-navigation techniques using historically acquired MRI may overcome some of these limitations of ultrasonography. Co-registration of ultrasound with historically acquired MRI using neuro-navigation provides a means for quantifying brain shift produced as a result of craniotomy prior to tumour resection (Keles 2003). In our study the average value for brain shift at the surface following craniotomy using ultrasonography was 1.6mm into the cranial vault. This was within the range quoted by Keles et al (2003). It is important to note that this value represents the sum of brain displacement as a result of craniotomy and compression applied to the surface of the brain by the ultrasound probe in order to obtain good contact, and so may overestimate the degree of displacement of brain into the cavity as a result of gravity and loss of CSF. In addition, when considering this type of imaging technique during resection, the simple surface correction calculation is unlikely to result in an image that truly represents the intra-operative situation as the loss of volume as a result of tumour resection

would not have been accounted for on the MRI. Furthermore, brain is unlikely to simply displace en mass following dural opening but would have undergone some form of deformation.

Despite these inaccuracies the technique of co-registration of historically acquired MRI with ultrasound potentially provides a cost effective method for enhancing real-time ultrasound image interpretability. The calculated shift of the cortical surface as a result of craniotomy could be used to assess reliability of neuro-navigation using historically acquired MRI data. Furthermore, correction of the representation of the probe's surface on the MRI using this calculation may improve neuro-navigation accuracy during tumour resection. There are a number of commercially available neuro-navigation systems such as SonoNav^{TM} (Medtronic, USA) that provide this functionality.

A number of studies have suggested that conventional ultrasonography may be inferior to pre operative CT or MRI at visualizing extent of tumour (Van Velthoven 2003). Hence, for the purposes of this study, in a selected group of patients, co-registration of ultrasound with MRI was performed to ensure representation of tumour on MRI as opposed to ultrasound, was used when evaluating tumour extent. Our findings suggested that the representation of tumour using conventional ultrasonography was similar to the representation of tumour on MRI within the same imaging field. This gave us confidence that tumour was accurately portrayed on ultrasound echographic data used to produce ultrasound elastograms. It is important to note however that MRI does not necessarily visualize the full extent of tumour infiltration (Van Den Hauwe 1995).

4.4.2 Ultrasound Elastography

There have been three groups to date including data from this thesis (Chakraborty 2004, Chakraborty 2006) that have published results on imaging strain intra-operatively during brain tumour surgery. Selbekk et al (2005) described 2 cases where ultrasound elastography was performed intra-operatively prior to surgical resection. Scholz et al (2005) described 20 cases where a technique called vibrography was used intra-operatively. In both these cases observational elastographic findings were presented primarily.

Our study aimed to determine whether elastographic findings correlated well with surgical findings. It was the first to compare elastographic findings with surgical findings in this manner. It was also the first study to score elastogram features of stiffness heterogeneity and visibility of the brain tumour interface, and to observe the variation of both tumour-brain strain contrast and visibility of the interface with applied stress, as described. The results show that, broadly speaking, the described technique of ultrasound elastography correlated with surgical findings on stiffness.

There have been no adverse outcomes as a result of elastography suggesting this to be a safe method of imaging.

The manner in which palpation was performed influenced the quality of the elastograms. Too fast a palpation cycle resulted in poor image quality. A cycle of compression over 0.5s appeared optimal. Elastogram quality appeared to improve with experience suggesting a learning curve for the procedure. It was important to ensure that the region of interest within the scan plane was in view throughout the palpation cycle. Thus the operator

needed to look at the ultrasound screen rather than the operative field once the probe was in place on the surface of the brain.

The amplitude of compression was another important consideration. Large amplitude compressions appeared to produce elastograms demonstrating less strain contrast between brain and tumour but more strain at the brain-tumour boundary. It was hypothesized that this was due to the tumour slipping over the brain at the brain tumour interface manifesting as shear strain. It is interesting to note that shear was less apparent in patients with intrinsic tumours where tumour would be expected to be more adherent to brain compared to extrinsic tumours. These observations led to the development of a novel modification of conventional ultrasound elastography to detect slip, called slip elastography and is discussed in chapters 6 and 7. Lower amplitude compressions resulted in images showing improved stiffness contrast. In fact, it was possible to produce elastograms by holding the probe still and allowing the brain's intrinsic pulsations to drive strain generation. This is consistent with the observations of Selbekk et al (2005).

Patients in the control group provided an opportunity to evaluate relative stiffness of normal components of brain. It was encouraging that stiffness homogeneity was seen when analyzing the appropriate elastograms. However, many studies suggest that grey matter may have different stiffness characteristics compared to white matter (Prange 2002, Kyriacou 2002). Conversely there are a number of studies that did not demonstrate stiffness heterogeneity when the stiffness of white matter was compared to grey matter (Bilston 1997). There is sparse literature addressing this apparent

conflict. Furthermore a recent study has shown that grey matter has different stiffness in different parts of the brain (Coats 2006). Another complicating factor is that brain tissue has been shown to be anisotropic (Prange 2002).

There is some *in vivo* data looking at this stiffness heterogeneity. McCracken et al used MR Elastography on the brain and found that white matter was stiffer that grey matter *in vivo*; this is contrary to results from most publications using *ex vivo* mechanically tested data (McCracken 2005).

It was not possible to differentiate grey matter from white matter with our ultrasound elastography technique. This suggests that the current sensitivity of the technique presented was not adequate to differentiate grey matter from white matter. Furthermore the literature does not unequivocally assist in determining what one would expect to see even if contrast and spatial resolution were good enough. Resolution is likely to improve in the near future with improvements in ultrasound probe design, the development of more efficient computer algorithms and techniques for creating elastograms and improved processing power.

A particularly interesting case within the control group was the patient who had elastography performed following complete macroscopic excision. One of the drawbacks of conventional B mode intra-operative ultrasonography for tumour resection is the difficulty in interpretation of images obtained immediately following resection. This is, in part, due to the inability of conventional B mode ultrasonography to distinguish bloody products from tissue. Currently, there are few intra-operative techniques that can differentiate tumour from post-operative changes. Intra-operative MRI or

intra-operative CT currently have limited availability and are very expensive. Imaging relative stiffness using ultrasound elastography may assist in differentiation of post-operative changes from tumour provided the leading edge of tumour is solid. Ultrasound elastography would not suffer from the drawbacks of conventional ultrasound.

This study has shown that extrinsic tumours tended to be more homogeneous in terms of stiffness compared to intrinsic tumours. This was reflected in the surgical and elastographic findings. Elastogram quality was enhanced when slip between tumour and brain did not occur following compression.

Quality of elastograms was not degraded by tumour stiffness heterogeneity. The technique described was able to resolve different areas of tumour stiffness within the same scan plane.

Tumour cysts were a common feature observed in this study. According to the data presented, cystic areas appear to degrade quality of elastograms. This may be because cyst fluid cannot be tracked from one ultrasound frame to the next following application of a stress as fluid is has poor echogenic properties and is in a dynamic state (i.e. the echo pattern that it produces does not remain correlated to the degree necessary for tracking), and because fluid is unable to support a shear stress (i.e. it flows instead of straining). In addition stress applied over a cyst did not appear to propagate efficiently beyond the cyst cavity thus limiting quality of elastogram data deep to the cyst. This problem may be overcome by using radiation force elastography (Nightingale 2002) where strain is generated within the scan plane by the ultrasound wave focusing on a specified area thus producing

focused stress at depth. It has recently been shown that this technique also produces a focused and transient strain at depth (Melodelima 2006), allowing high quality elastograms to be created even beyond slip boundaries (Melodelima et al, 2006a). This compares to conventional elastography where strain is created by propagation of externally applied compression, usually using the ultrasound probe, to deeper tissues.

It is important to note that ultrasound elastography correlated very well with surgical findings irrespective of tumour stiffness heterogeneity or the presence of cysts. Scholz et al (2005) also noted this heterogeneity in tumour stiffness. This inherent heterogeneity in stiffness that brain tumours possess is not surprising as many intrinsic tumours undergo necrosis in certain areas (Ribalta 2004). This stiffness heterogeneity may limit the sensitivity of ultrasound elastography at detecting tumours however.

In the present study demarcation of the brain tumour interface using conventional B mode echography and ultrasound elastography was compared. In general, the distinction between brain and tumour was more evident using ultrasonography although ultrasound elastography was comparable in patients with solid homogeneous tumours. There are a number of reasons for this. Ultrasound echo images will contain information than is not present on elastograms (and vice versa). This is true both in the nature of the information (echo strength versus strain) and in the spatial detail shown (echograms tending to be higher spatial resolution). Information present in echographic images not utilized in elastogram generation may be useful for identifying the brain tumour interface. Furthermore strain generation when creating ultrasound elastograms is

dependant on the propagation of an externally applied compressive force down the scan plane. Boundary conditions, unpredictable mechanical behaviour of tissue and poor ultrasound tracking characteristics of tissue may result in strain dissipation at depth. These effects may adversely affect elastogram generation. Combining ultrasound echography with ultrasound elastography may enhance visualization of the brain tumour interface. Certainly, in the context of breast tumours, ultrasound elastography used in conjunction with conventional B-mode ultrasonography has been shown to improve sensitivity and specificity at detecting breast malignancy (Bamber 2002).

4.4.3 *Ex vivo* Stress Strain Measurements on Brain and Tissue

The results demonstrate the non linear mechanical behavior of brain samples *ex vivo*. For the first time it also demonstrates that samples of brain tumours also demonstrate non-linear biomechanical behaviour. It was impossible to draw any conclusions on comparison of stiffness as a result.

These were a number of drawbacks that are important to highlight. It is important to note that despite the specimens being analyzed immediately following resection the mechanical properties may well be substantially different to what is encountered *in vivo*. This could be due to the lack of blood supply, desiccation of the sample, the cellular and molecular

cytotoxic response to resection or from changes that may occur as a result of surgical technique.

An equally important consideration was the technical aspects of mechanical testing. The tumour samples were very small and so cutting them without specific equipment may have been inaccurate. It is likely that the surfaces in contact with the glass slide and the compression platen were not perfectly flat and perfectly parallel to the platen. This imperfection could cause non-linear behaviour. This is because, as the platen compresses the test material, the surface area in contact with the platen will change so the stress will be unpredictable.

Another possible technical problem was whether the test sample was adherent to the glass slide or the compression platen. Brain and brain tumour appeared adherent but this may have varied with applied stress. Furthermore, compression when a sample is adherent to the compression platen and/or glass slide would cause the shape of the test sample to bulge in the central portion as it was being compressed assuming that the Poisson's ratio was greater that 0. This would affect the stress-strain curves.

It would be difficult to draw any more conclusions based on these limitations on the technique described for *ex vivo* mechanical testing.

4.5 Summary

Ultrasound echography co-registered with MRI is a simple method for checking co-registration accuracy once a craniotomy has been performed. Pre-operative MRI greatly assists the interpretation of intra-operative echography and elastography, which in turn assist the use of the preoperative MRI in guiding surgery.

Ultrasound elastography, when used in the context of brain tumour resection, is safe and is able to distinguish stiffer areas from less stiff areas. Ultrasound elastography used in conjunction with conventional B mode ultrasonography may assist in identifying the brain tumour interface.

It has not been possible to objectively measure mechanical properties on *ex vivo* brain and tumour samples and compare to ultrasound elastogram results however.

Chapter 5

A Comparison between Surgical Findings on Stiffness and Real-Time Conventional Ultrasound Elastography during Brain Tumour Resection

Chapter 5

A Comparison between Surgical Findings on Stiffness and Real-Time Conventional Ultrasound Elastography during Brain Tumour Resection

This chapter discusses the use of a commercial real-time ultrasound elastography system intra-operatively during brain tumour resection. Elastogram strain information is compared to surgical findings.

5.1 Introduction

The majority of non commercial ultrasound elastography systems produce images following data acquisition i.e. off-line. One of the reasons for this has been computational expense at producing ultrasound elastograms which is considerably greater when compared to B mode ultrasound images. The computational expense is dependent on the efficiency of the computer algorithm and the speed of computer processing hardware.

Another reason is that there has been little requirement for real-time scanning. Most systems have been used in a research capacity with a view to improving quality of data and images rather than to improve speed of data production. In addition, the majority of clinical applications do not necessarily require ultrasound elastogram imaging data at the time of ultrasound data acquisition as most of these applications are to assist in diagnosis rather than to guide management at the time of imaging.

There are a number of clinical situations where it would be essential to have ultrasound elastogram data at the time of imaging. An example would be the intra-operative use of ultrasound elastography to assist brain tumour resection. Currently, it is not possible to perform ultrasound elastography pre-operatively as the skull acts as a barrier to insonating the brain and axial compression of the brain surface is not possible. Furthermore post-operative ultrasound elastograms using data obtained at the time of operation would not be of use for obvious reasons. Thus real-time elastography would be essential in order to alter management intra-operatively.

As mentioned previously, ultrasound elastography may be of use at distinguishing tumour from brain based on the assumption that tumour has

different stiffness characteristics when compared to brain at the brain tumour interface. Thus this technique could assist the surgeon in planning extent of tumour resection.

In this study surgical findings on stiffness have been compared with relative strain findings from a real-time ultrasound elastography system on patients undergoing brain tumour resection.

5.2 Methods

22 patients were recruited into this study. These were the last 22 patients recruited for the study investigating the use of an off-line processed ultrasound elastography system as described in the previous chapter. Local research ethics committee approval was obtained. Inclusion criteria for this trial included patients undergoing craniotomy for presumed tumour. This included both intrinsic and extrinsic tumours. Patients with intrinsic tumours had ultrasound elastography performed following dural opening whereas patients with extrinsic tumours had ultrasound elastography performed prior to dural opening.

5.2.1 Real-time Ultrasound Elastography

The Acuvix XQ® ultrasound scanner (Medison, Korea) (figure 5.1) with the L5-12LM probe was used for real-time ultrasound elastography data acquisition. This commercial scanner had an inbuilt real-time elastography capability named Elastoscan®. The technique of palpation was identical to the technique used to produce off-line elastograms (see chapter 4).

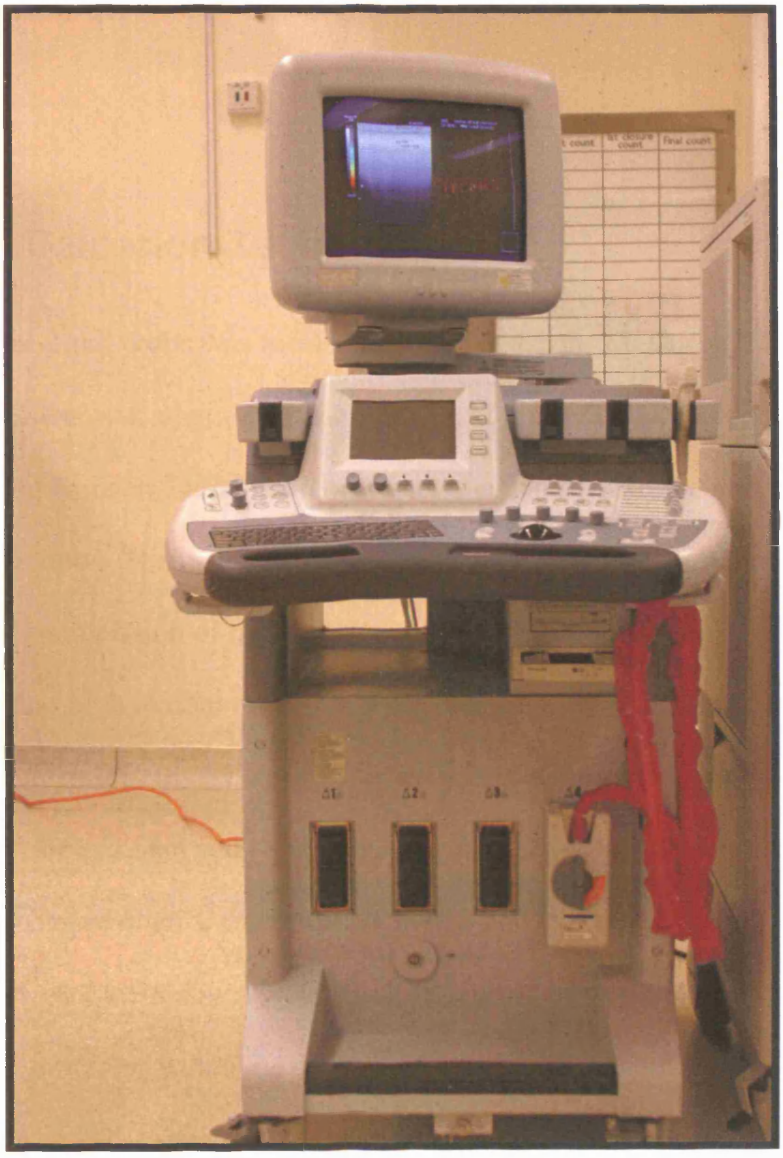

Figure 5.1The Acuvix XQ® Ultrasound Scanner

This system was capable of producing more than 10 ultrasound elastogram frames per second. The algorithm used to produce these images is not known. The B mode image and elastogram were displayed side by side. The elastogram images had a colour scale with black and red representing stiffer areas and yellow and blue representing softer areas. Data were saved onto the machine's computer as an AVI movie. Data could be transferred using USB ports or using the inbuilt CD rewriter.

5.2.2 Palpation Technique

The ultrasound probe was housed in a sterile sheath (Manatech, UK). Axial compression was applied to the surface of the brain or the dura in the following manner. Initially, contact was established with the surface of the brain or dura. Then a small displacement (less than 5mm) was applied causing compression of the underlying brain and tumour. Care was taken to ensure that both tumour and brain were present within the same scan plane. The compression was followed by relaxation back to the original position. A cycle of compression and relaxation took about 2 seconds to complete.

Whilst compressing, the ultrasound image and elastogram were observed. The aim was to minimize rotational, lateral or elevational movements by keeping structures within the scan plane in view throughout the cycle.

Different types of compression were attempted. A faster compression cycle with smaller amplitude displacements was attempted to see how this affected image quality.

5.2.3 Comparison of Surgical Findings for Ultrasound Elastogram Findings

The surgeon was asked a number of questions with regard to mechanical properties that he encountered during each resection. He was asked to evaluate whether the tumour was cystic or solid. For cystic tumours he was asked whether the cyst wall was stiffer than brain or the same consistency as brain. Tumours that were cystic, with no discernible difference in stiffness within the wall compared to brain, were treated as a control group.

For solid tumours he was asked to determine whether tumour was heterogeneous or homogeneous in terms of stiffness. For homogeneous tumours he was then asked to comment as to whether tumour was stiffer, the same or softer than brain. These groupings are summarized in figure 5.2.

Thus patients were divided into 4 groups depending on surgical findings on stiffness. The groups were;

1) Control subjects

   Patients with no pathologically demonstrable tumour, patients in whom elastogram data was obtained following complete

macroscopic excision and patients with tumour cyst where the cyst wall was of a similar stiffness to brain,

2) Patients with solid tumours where the surgeon felt that the tumour had stiffness homogeneity,
3) Patients with solid tumours where the surgeon felt that the tumour had stiffness heterogeneity,
4) Patients with cystic tumours where the cyst wall was found to be stiffer than normal brain.

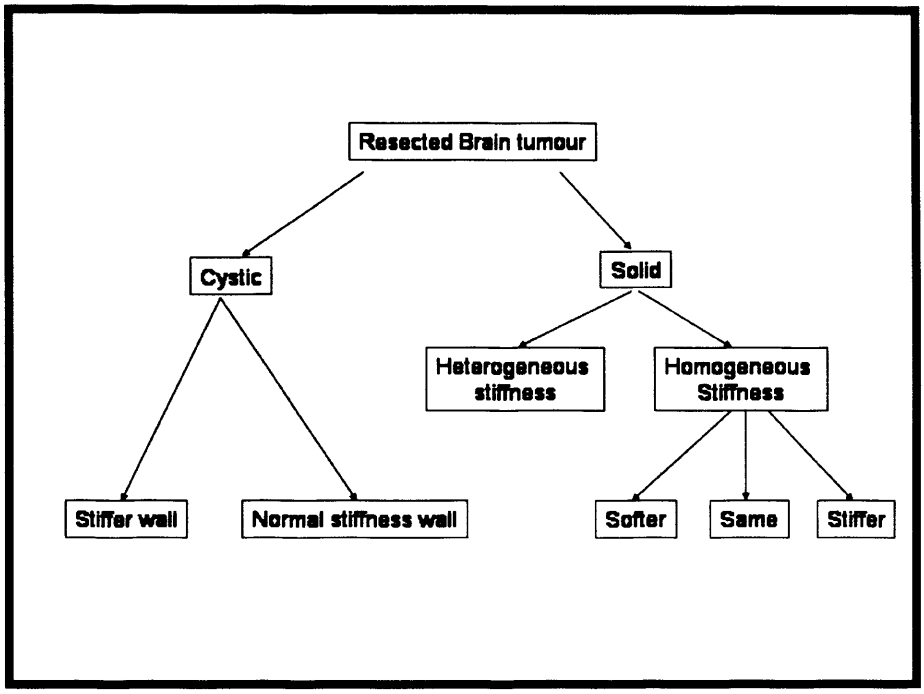

Figure 5.2 Diagram showing the categorization of tumours according to morphologic and stiffness characteristics

The demarcation of the interface between brain and tumour was assessed on ultrasonography, and compared to ultrasound elastography.

Brain tumour interface identification on ultrasound was compared to elastogram images. An assessment of the demarcation of brain compared to tumour at the interface was made using B mode ultrasonography and

compared to elastography by visual inspection. This assessment was not made in patients belonging to group 1.

5.3 Results

Table 5.1 shows diagnosis, surgical stiffness characteristics and real-time elastogram stiffness evaluations for all 22 patients.

17 out of the 22 patients had intrinsic space occupying intracranial lesions, (one of which was primarily intraventricular) and 5 had extrinsic tumours.

1 patient underwent craniotomy and biopsy only so surgical stiffness assessment was not assessed. One patient had elastography performed following complete macroscopic tumour resection so the surgical assessment was that no stiff component was present in the imaging field. This patient's data was treated as a control. 1 patient had a biopsy only so surgical comparison was not possible.

Of the 21 patients 16 had good correlation between surgical findings and real-time elastogram findings. Of the 5 cases where elastogram findings differed from surgical findings 2 were due to the poor quality of the elastograms. One case was where the elastogram was unable to resolve tumour stiffness heterogeneity. The remaining 2 cases demonstrated tumour or brain stiffness heterogeneity when the surgical findings did not suggest any stiffness heterogeneity.

Patient Number	Diagnosis	Group	Surgical findings	Real-time Elastogram findings	Correlation in Surgical and Elastogram Findings	Identification of Brain tumour interface using ultrasound vs elastography
7	L frontal GBM	1	Cystic, not much tumour, tumour wall same stiffness as brain	Cystic, wall heterogeneous stiffness	No, elastogram stiffer	N/A
13	R frontoparietal GBM, post op images	1	Cystic, no stiffened wall (post op so no tumour)	Cystic, no stiffened wall	Yes	N/A
16	L frontal arachnoid cyst, normal brain	1	Cystic, no stiffened wall	Cystic, no stiffened wall	Yes	N/A
20	R occipital cystic GBM	1	Cystic, No stiffened wall	Cystic, No stiffened wall	Yes	N/A
23	Occipital cystic GBM	1	Cystic, No stiffened wall	Cystic, No stiffened wall	Yes	N/A
5	L parietal Convexity Meningioma	2	Solid, homogeneous, tumour stiffer than brain	Solid, homogeneous, tumour stiffer than brain	Yes	Similar performance
8	L Parafalcine meningioma	2	Solid, homogeneous, tumour same stiffness as brain	Solid, homogeneous, tumour same stiffness as brain	Yes	Similar performance
10	CP angle Meningioma	2	Solid, homogeneous, tumour stiffer than brain	Solid, homogeneous, tumour stiffer than brain	Yes	Elastography superior to U/S
11	Parafalcine GBM	2	Solid, homogeneous, tumour same stiffness as brain	Solid, heterogeneous, cannot see brain	No, elastogram stiffer	Similar performance
15	R temporal low grade intrinsic glioma	2	Solid, homogeneous, tumour softer than brain	Solid, homogeneous, tumour softer than brain	Yes	U/S superior to elastography
19	L sphenoid ridge meningioma	2	Solid, homogeneous, tumour same stiffness as brain	Solid, homogeneous, tumour same stiffness as brain	Yes	Similar performance
21	CP angle acoustic neuroma	2	Solid, homogeneous, tumour stiffer than brain	Solid, homogeneous, tumour stiffer than brain	Yes	Similar performance
3	L parietal GBM	3	Solid, heterogeneous, tumour mainly same stiffness as brain, sometimes softer	Solid, heterogeneous, similar stiffness to brain	Yes	Similar performance
4	L parietal Gliosarcoma	3	Solid, heterogeneous, stiffer than brain with some areas similar to brain	Solid, heterogeneous, tumour stiffer than brain	Yes	U/S superior to elastography
6	L posterior frontal metastasis	3	Solid, Heterogeneous, tumour mainly softer than brain, gelatinous	Solid, heterogeneous, tumour softer than brain	Yes	U/S superior to elastography
9	Recurrent R frontal GBM	3	Solid, heterogeneous, tumour mainly stiffer than brain	Poor quality	No, poor quality	Similar performance
17	L parietal GBM	3	Solid, heterogeneous, tumour same as brain with stiffer areas	Solid, homogeneous, stiffer than brain	No, elastogram homogeneous	U/S superior to elastography
18	L frontal low grade glioma	3	Solid, heterogeneous, softer and stiffer than brain	Solid, heterogeneous	Yes	Elastography superior to U/s
22	L parietofrontal GBM	3	Solid, heterogeneous, tumour mainly softer than brain	Solid, heterogeneous, tumour mainly softer than brain	Yes	Similar performance
12	Intraventricular GBM	4	Cystic, heterogeneous and multicystic, wall stiffer than brain	Poor Quality	No, poor quality	U/S superior to elastography
24	Occipital Cystic GBM	4	Cystic, stiffened wall, looked like abscess	Cystic, stiffened wall	Yes	Similar performance
14	L frontal GBM (biopsy only)	4	-	Solid, heterogeneous	-	-

Table 5.1 Comparison of surgical findings to Real-time Elastogram findings

GBM stands for glioblastoma multiforme

Table 5.1 also shows how the real-time elastogram compared to B mode ultrasound imaging at defining the brain tumour interface. On the whole ultrasound echographic imaging was superior to elastography at defining the brain tumour interface. Of the 16 patients assessed in this manner (group 1 was not analysed for obvious reasons) 10 real-time elastograms demonstrated the brain tumour interface as clearly as the echographic image, if not more clearly. Of the 6 cases where the brain tumour interface was not apparent on elastography the majority were from the group of tumours where the tumour had stiffness heterogeneity.

5.3.1 Elastogram and Surgical Findings According to Group

5.3.1.1 Group 1

Cystic tumours with no stiffened areas-control group

Within the control group real-time elastogram findings corresponded to surgical findings in 4 out of the 5 cases. Figure 5.3 shows the real-time elastogram screenshot for the patient whose elastogram findings did not corroborate with surgical findings (patient 7).

To the left of the screenshot of the real-time ultrasound scan (Figure 5.3a) is the conventional B mode image and to the right is the elastogram appropriately scaled to the B mode image. The colour-scale used for elastograms is shown to the left of the ultrasound image. Black and red

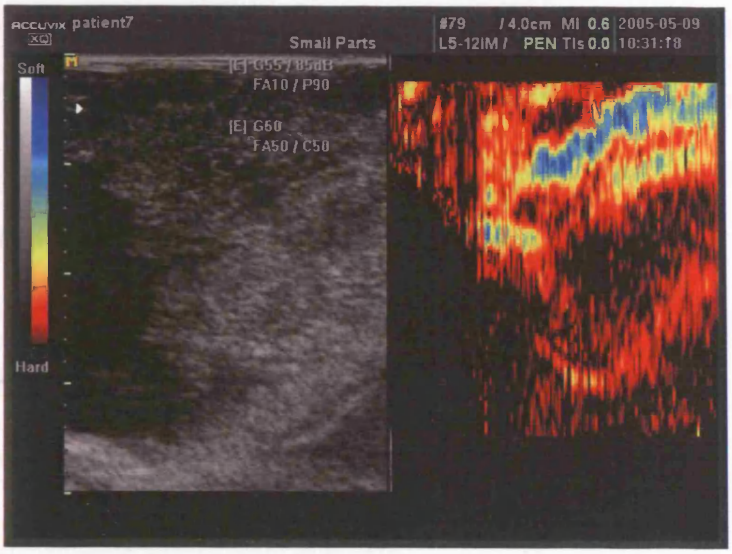

5.3a

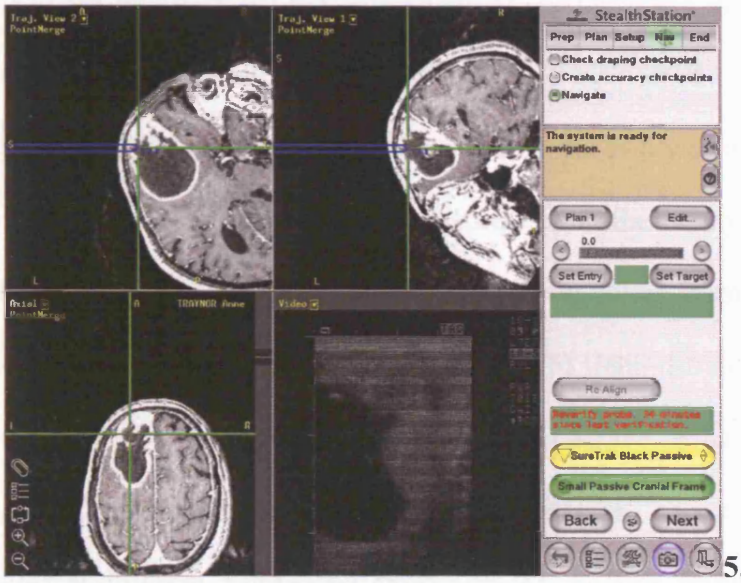

5.3b

Figure 5.3 a) Real-time elastogram and b) Stealthstation™ screenshot for patient 7 where surgical findings did not corroborate elastogram findings

a) The surgical findings were that the wall of the tumour was not stiffer than normal brain however the elastogram demonstrates an area of stiffness below an area of high strain. This high strain area was due to shear strain, b) note that the screenshot does not correspond to the ultrasound image as it was taken with a different ultrasound probe

depict low strain or stiffer areas whereas blue represents softer areas. It is important to note that the stiffness measures are relative within the scan field. It is interesting to note the area of high strain (soft area) that is seen almost splitting the brain. This is most likely due to development of a

cleavage plane that was not apparent on the B mode image. This cleavage plane would result in one surface slipping against the other surface creating shear strain. It is likely that the cyst pressure would have created this cleavage plane. The ultrasound movie clearly demonstrates slip at this area.

The part of the elastogram representing cystic fluid is black. This is an artefact and does not represent low strain as the colour scale suggests. This elastography technique assigns the colour black for areas where tracking of ultrasonic signals is not possible such as fluid. Fluid cannot be tracked because it is dynamic in nature and has poor ultrasound scattering properties. This demonstrates the importance of elastographic visualization in conjunction with conventional echography.

The surgeon felt that the surrounding tissue around the cyst was of a similar stiffness to brain but the elastogram demonstrates that the pericystic areas, especially around the cleavage plane, are stiffer than normal brain. However, the co-registered MRI scan (figure 5.3b) demonstrates that the pericystic area around the cleavage plane contained an area enhancing with contrast. It is important to note that the StealthStation^{TM} screenshot was taken using a different ultrasound probe so the images shown do not correspond to the ultrasound image shown in figure 5.3a. The screenshot was reviewed only as a guide so care was taken when making conclusions based on the image.

5.3.1.2 Group 2

Solid homogeneous tumours

There were 7 patients where the surgeon felt tumour was homogeneous in terms of stiffness. This accounted for all extrinsic tumours.

Of these 7 patients, 6 had similar real-time elastogram findings. Patient 11 showed a difference. This patient's elastogram image suggested that tumour was stiffer than brain however the surgeon felt tumour was of a similar stiffness to brain.

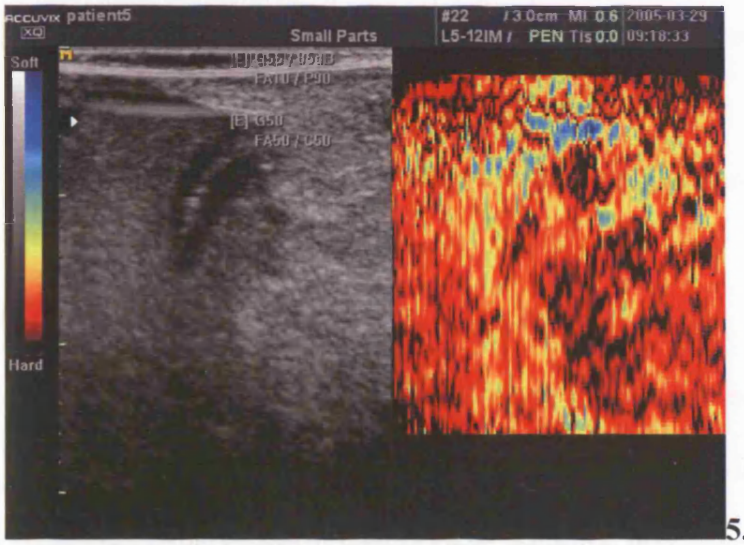

5.4a

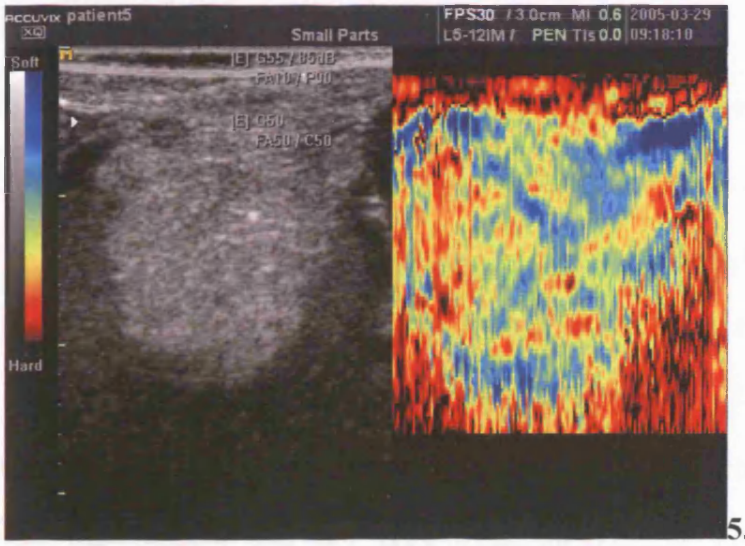

5.4b

Figure 5.4 2 real-time elastograms on patient 5 showing the effect of different palpation techniques

a) shows an elastogram produced with minimal pre-compression, b) shows an elastogram produced with moderate pre-compression

Figure 5.4 shows 2 real-time elastography system screenshots for patient 5, who also was part of group 2. This patient had a convexity meningioma. The surgeon felt this tumour was solid, homogeneous and slightly stiffer than brain and there was a good plane around the tumour which made dissection easy. The B mode image with the elastogram (figure 5.4a) showed the tumour to be well demarcated from the brain, and to be stiffer than brain.

Figure 5.4b shows the real-time elastogram where palpation was altered. This image was taken at the end of the compression cycle. It demonstrates an area of high strain around the tumour indicative of a slip boundary between tumour and brain. The strain values are so high here that it makes the tumour look softer than brain which was not the case. This is a good demonstration of the potential drawbacks of the shearing artefact. However this image does demonstrate mechanical properties that are potentially useful to the surgeon. The reason why shearing effects are most evident with maximal compression is possibly that it takes some compressive force to initiate slip between 2 surfaces.

Figure 5.5 shows the 2 real-time elastogram images taken at different times within the same palpation cycle for patient 21 who had an acoustic neuroma. This tumour was found to be very stiff. Figure 5.5a demonstrates this quite nicely with a homogeneous low strain area for the area where tumour was situated. Figure 5.5b was taken following axial compression. Note how, once again, the slip boundary was evident in figure 5.5b where pre-compression was evident and not present in figure 5.5a where pre-compression was minimal.

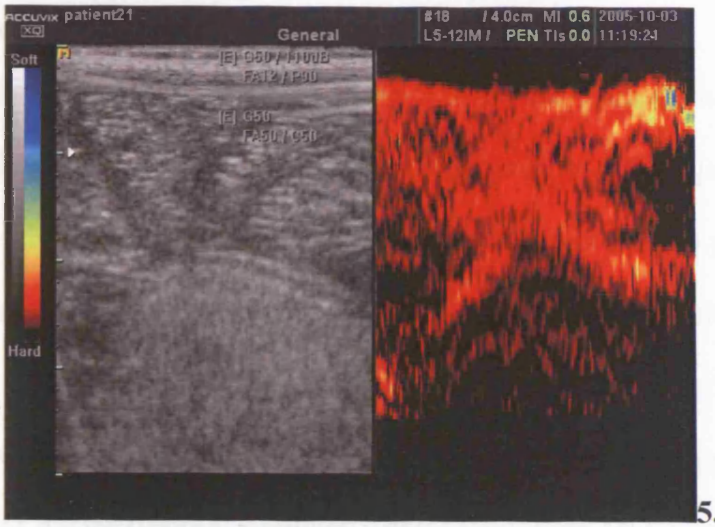

5.5a

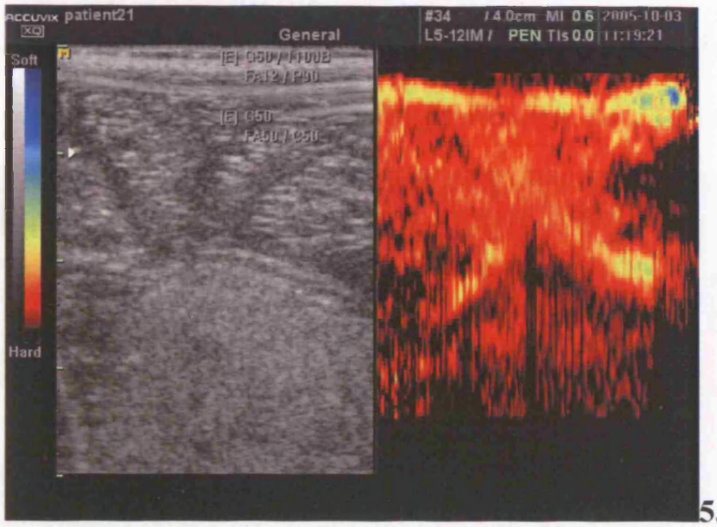

5.5b

Figure 5.5 2 Real-time elastograms for patient 21 taken from the same palpation Cycle

a) elastogram produced with minimal pre-compression, b) elastogram produced with moderate pre-compression. Note the artefact.

Figure 5.5b also demonstrates an artefact where a black vertical line is shown near the centre of the image. This artefact was seen in a number of elastograms and most likely demonstrates a tracking problem within the software.

5.3.1.3 Group 3

Solid Heterogeneous Tumours

There were 7 patients where the surgeon felt the tumour was solid but heterogeneous. Of the 7 patients, 5 had elastogram findings similar to surgical findings. One patient had elastograms that were of too poor quality to evaluate (patient 9). One patient with a glioblastoma multiforme had surgical findings of a solid heterogeneous tumour. The elastogram was not able to resolve this stiffness heterogeneity. Figure 5.6 shows an elastogram screenshot demonstrating a patient with a low grade glioma (patient 18). The surgeon felt that the deeper part of the tumour was stiffer than the more superficial part. The elastogram demonstrated exactly these features.

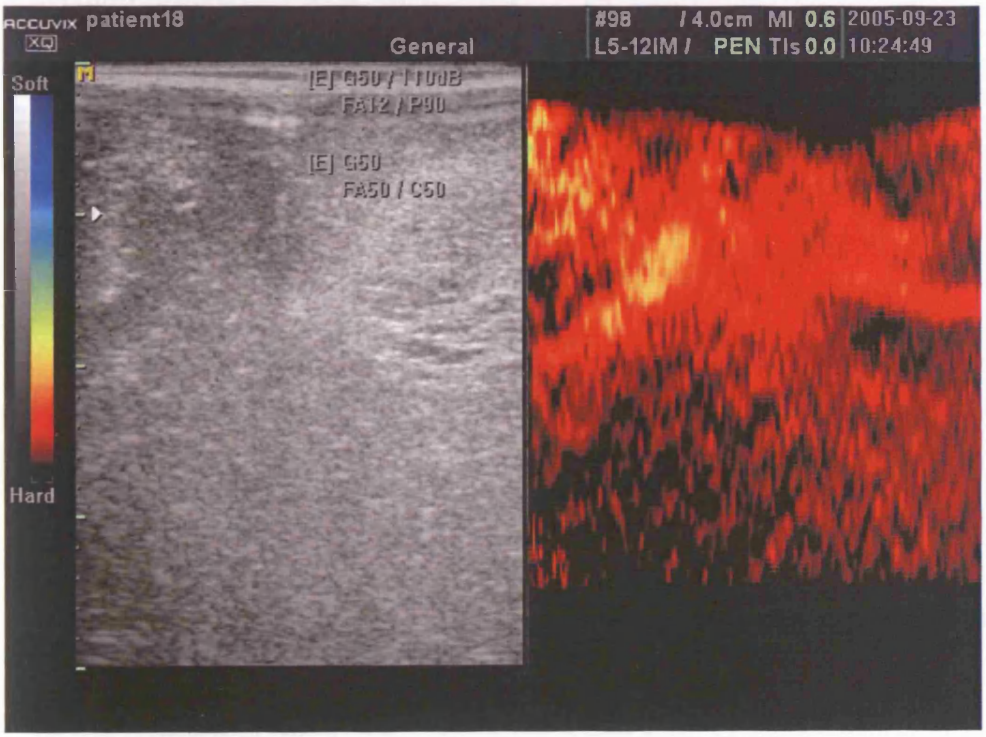

Figure 5.6 Real-time elastogram for a patient with tumour stiffness heterogeneity
The tumour is in the top right of both images

5.3.1.4 Group 4

Cystic Tumours with a Solid Component

There were 2 patients where the surgeon found cystic tumours where the wall was found to be stiffer than brain. One of these patients had elastograms that were too poor in quality to merit further study. The other had good correlation with the surgical findings (Figure 5.7).

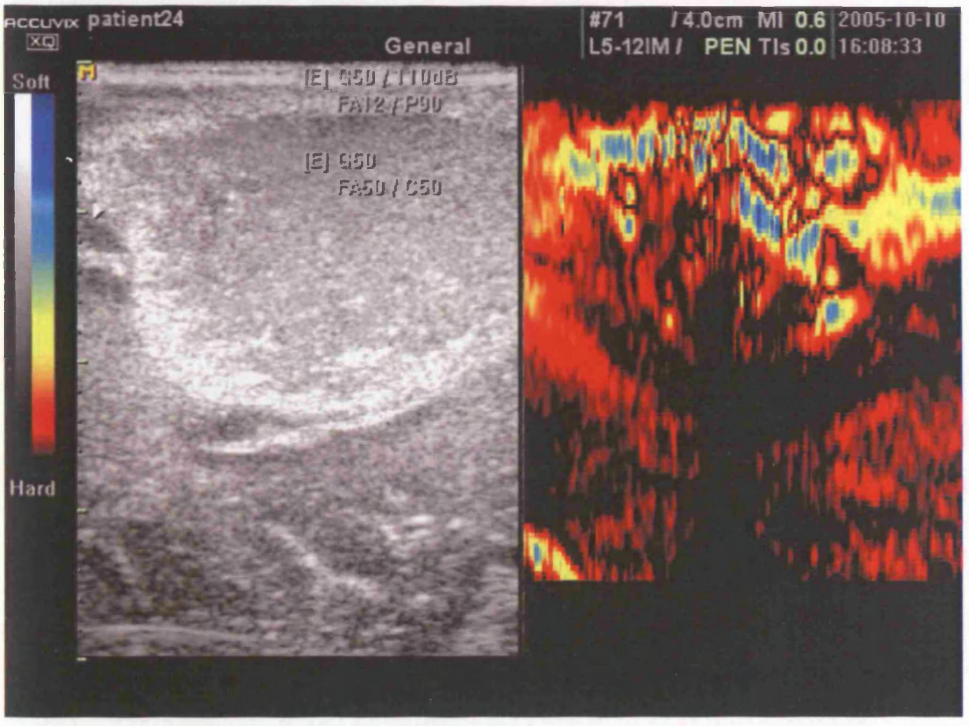

Figure 5.7 Real-time elastogram for a patient with a cystic tumour where the cyst wall was stiffer than brain

There was one patient where a biopsy was performed so the surgeon was not able to comment on mechanical properties. The elastogram suggested that the tumour was stiff with areas of stiffness heterogeneity.

Figure 5.8 shows elastograms created by 2 palpation techniques. It is obvious that the elastogram created with a fast small amplitude compression

was inferior to that created with a slower larger amplitude compression. The heterogeneity of tumour is far more obvious on the elastogram produced with a slower palpation. Also strain has propagated far deeper providing better definition at depth.

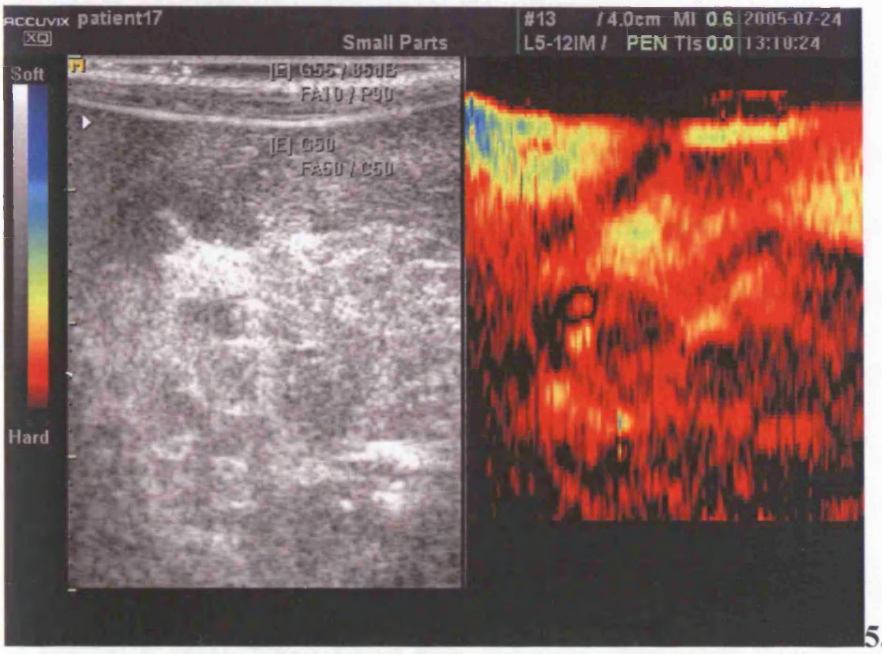

5.8a

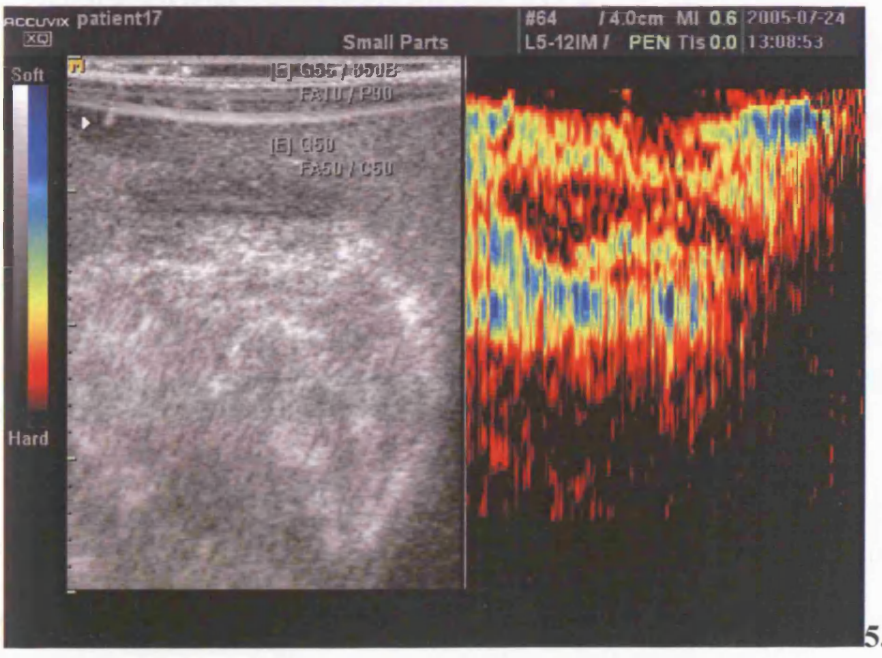

5.8b

Figure 5.8 2 Real-time elastograms demonstrating how the speed of palpation affects elastogram quality a) Slow large amplitude compression applied, b) fast small amplitude compression applied

5.4 Discussion

A number of commercial and non-commercial real-time ultrasound elastogram systems have recently been developed. This has been possible with the advent of faster computer processing and with improvements in the efficiency of ultrasound elastogram algorithms.

Konig et al (2005) used real-time ultrasound elastography to assist in biopsy of prostatic lesions. They found that sensitivity at detection of prostatic cancer increases when ultrasound elastography is used in conjunction with conventional diagnostic methods. The technique of displacement tracking (often the most computationally expensive part of the elastography process) used a phase root seeking algorithm which has been shown to be computationally more efficient (Pesavento 2000).

Itoh et al (2006) used real-time ultrasound elastography to assist in detection of breast tumours. They found that real-time ultrasound elastography had similar sensitivity and specificity at detecting breast tumours when compared to conventional B mode ultrasonography alone. Displacement tracking was performed using the combined autocorrelation method (Shiina 2002).

Lyshchik et al (2005) compared the use of real-time and off-line processed ultrasound elastography at detecting thyroid gland lesions. These results were compared to *ex vivo* mechanical testing and histology.

There has been one paper describing the use of a real-time elastography system intra-operatively during brain tumour resection (Scholz 2005). 20 patients were recruited into this study. A technique called vibrography was

used (Pesavento 2000). Unfortunately there was no comparison to surgical findings.

The study reported in this chapter demonstrates that real-time elastography scanning can accurately differentiate stiffer areas from softer areas *in vivo* during brain tumour resection.

Brain tumours appear to have quite complex stiffness characteristics. This study demonstrates the heterogeneity in stiffness. For this reason tumours have been divided into the groups as shown. This heterogeneity means that elastography would need to differentiate this stiffness heterogeneity and not just whether tumour is stiffer than surrounding brain; a method that has been adopted when using elastography in other parts of the body. However the application of this technique intra-operatively during brain tumour resection is worth pursuing and developing because it potentially provides a more objective measure compared to surgical evaluation, and provides information from regions too deep to be accessible to palpation. Hence this could potentially be an improvement in comparison to palpation.

The technique of palpation using an ultrasound probe, when performing ultrasound elastography is critical and cannot be understated. As with conventional B mode ultrasonography, the quality of elastograms is user dependent. There is a learning curve associated with application of this technique intra-operatively.

The commercial scanner used in this study is able to provide a very high frame rate of ultrasound elastograms. Such a high frame rate could be counterproductive in some respects. If an elastogram is created by averaging over a number of frames the quality of the image improves. It is important

to note that elastography relies on displacements which are obviously time dependant. In comparison to images produced using an off-line elastography system where frame averaging occurred the real-time elastograms were vastly inferior. The trade-off of waiting 1 to 2 seconds for a high quality elastogram compared to having numerous elastograms shown in near real-time of inferior quality may be worth further evaluation.

There are drawbacks in the use of an off-line system in that there is no adequate feedback at the time of data acquisition to ensure that one has interrogated the appropriate area and that the elastogram quality is adequate.

5.5 Conclusion

The studies have demonstrated that real-time ultrasound elastography using the Acuvix XQ® scanner with Elastoscan® can differentiate softer regions from stiffer regions when resecting brain tumours in real-time. Thus real-time elastography is potentially a useful clinical tool in the context of tumour neurosurgery. It is clear that the method of palpation is critical in producing good quality elastograms.

Chapter 6

In vitro testing of Slip Elastography; a novel method for visualisation and characterization of mechanical properties at the tumour tissue interface

Chapter 6

In vitro testing of Slip Elastography; a novel method for visualisation and characterization of mechanical properties at the tumour tissue interface

This chapter presents the theoretical basis of a new imaging technique called slip elastography. The technique images the spatial location of a slip boundary and measures the force required to cause slip at this interface. *In vitro* phantom experiments are then presented.

6.1 Introduction

There are a number of tumours that develop within solid organs including brain tumours, renal tumours, breast tumours, musculoskeletal tumours, skin lesions and liver tumours. An interface between tumour and normal tissue must necessarily be present. Identification of the anatomical location of this interface and evaluation of adherence between the two surfaces are important for a number of reasons.

1) Surgical Resection

Complete surgical excision is only possible with prior knowledge of the anatomical location of the tumour tissue interface. Accurate identification of the interface helps prevent incomplete resection or excessive resection of normal tissue. This is especially important when resecting brain tumours and, to a lesser extent, liver tumours, renal tumours, breast tumours musculoskeletal and skin lesions.

Surgical resection at the tissue tumour interface involves dissection of tumour away from normal tissue. Adherence of tumour to normal tissue at this interface could hinder surgical resection making complete excision difficult. Prior knowledge of the anatomical location and mechanical properties at this interface may assist the surgeon to plan for safe and complete tumour excision (Yasargil 1996).

The vascular supply for tumours connect tumour to tissue. Characterization of the mechanical properties within these areas may prevent haemorrhagic complications (Yasargil 1996).

2) Characterization of tumours and prognosis

Benign tumours tend to have a well defined interface between tumour and normal tissue with few interactions between the two. Conversely, malignant tumours are more likely to invade and adhere to normal tissue. The adherence of tumour to tissue may assist in characterization of tumour intra-operatively (Yasargil 1996).

Local recurrence is common and, in general, prognosis poor in patients with malignant tumours when compared to patients with benign tumours (see chapter 2.1). In addition complete surgical excision is often more difficult and sometimes impossible when attempting to resect malignant tumours. Partial surgical resection has been associated with a poorer prognosis and is more likely to lead to recurrence (see chapter 2.1). Thus characterization of the tissue tumour interface may be important in patient prognosis.

6.1.1 Theoretical Basis of Slip Elastography

Most imaging modalities used in clinical practice assist in identifying the anatomical location of the tumour tissue interface however there are no imaging modalities that measure mechanical properties at this interface. Conventional ultrasound elastography measures the induced normal axial strain produced following application of an axial compressive stress using the ultrasound probe. As it measures normal strain, it is limited in detection

of other mechanical properties at a tissue tumour interface such as slip or static frictional force.

The method adopted for calculating normal strain using ultrasound elastography in this thesis has been to create an axial displacement field from pre- and post-compression RF ultrasound data, and obtain the gradient in the axial direction of this displacement field (Doyley 2001). Lateral strain images have also been produced by creating lateral displacement fields from pre and post compression RF ultrasound data and obtaining the gradient in the lateral direction of the lateral displacement field (Konofagou 1998).

Equations 1 and 2 define the normal axial strain and normal lateral strain that these techniques are based on, where $\frac{\partial v}{\partial y}$ is the axial gradient (y-direction) of axial displacement, v, or normal axial strain, and $\frac{\partial u}{\partial x}$ is the lateral gradient (x-direction) of lateral displacement, u, or normal lateral strain.

$$\varepsilon_{y,y} = \frac{\partial v}{\partial y} \tag{1}$$

$$\varepsilon_{x,x} = \frac{\partial u}{\partial x} \tag{2}$$

Shear strain identifies the change of displacement with distance in a direction perpendicular to the displacement. The equation defining true shear strain in 2 dimensions that has been implemented in the context of ultrasound based elasticity imaging is;

$$\varepsilon_{x,y} = \frac{1}{2}\left(\frac{\partial u}{\partial y} + \frac{\partial v}{\partial x}\right) \qquad (3)$$

where $\varepsilon_{x,y}$ is the shear strain, $\frac{\partial u}{\partial y}$ is the axial strain of the lateral displacement (describing lateral shear, for which the term lateral shear strain will be used) and $\frac{\partial v}{\partial x}$ is the lateral strain of the axial displacement (describing axial shear, for which the term axial shear strain will be used).

An alternative method for quantifying the amount of shear is to identify the angle, θ, of the displacement vector for each area within the displacement field. The angle can be calculated by using the following equation where, u is the axial displacement and v is the lateral displacement;

$$\theta = \arctan\left(\frac{u}{v}\right) \qquad (4)$$

By spatially differentiating this angle field it is possible to identify discontinuities in the displacement direction that might be characteristic of a slip boundary.

A perceived limitation of ultrasound elastography has been the difficulty in accurately estimating normal strain in the presence of shear strain (see Chapters 4 and 5). An artefactually high strain value is often assigned to slip boundaries using conventional elastography (Konofagou 2000). One of the reasons for this high strain value is the inability of conventional elastography to differentiate shear strain from normal strain adequately. In addition, when applying axial compression to generate conventional

elastograms, it is likely that shear strain attenuates normal strain propagation making normal strain estimations, hence stiffness estimations, unreliable distant to an area where shear strain has occurred.

Assessment of all components of the two-dimensional strain tensor, namely the lateral normal strain, the axial normal strain and the shear strain may assist in data interpretation.

It is important to define slip in terms of shear strain. Slip is a type of shear strain occurring where there is contact between two surfaces. Consider two solid structures in contact over a linear surface (figure 6.1a). Take two points, one for each of the structures, equidistant from the contact surface and apply a force that would result in shear. If the distance of each of the points to the surface were reduced to nearly zero, the relative position of each of the points would determine whether slip or non slip shear occurred. For non slip shear the spatial position of the points would tend to converge to a single point on the surface of the boundary. For slip however there would be a discontinuity with 2 discrete points in different spatial positions on the surface.

There are other characteristics of slip that are commonly seen in association with slip but do not necessarily provide such an accurate description of slip and do not necessarily distinguish slip from non slip shear. One such property is the fact that slip is an all or nothing phenomenon that, if unconstrained, will (unlike elastic shear strain) continue to occur, and may be unlikely to reverse when the shear stress is removed (unless surrounding structures were to provide a restoring force). Furthermore, the magnitude of shear strain when slip occurs will be disproportionate to both the magnitude

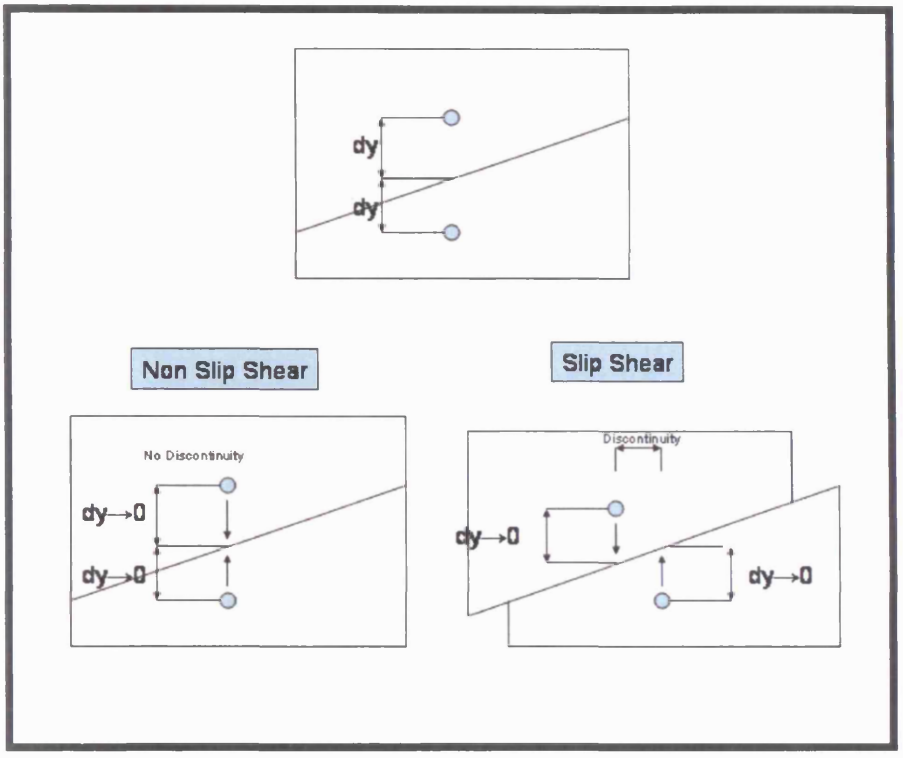

Figure 6.1a

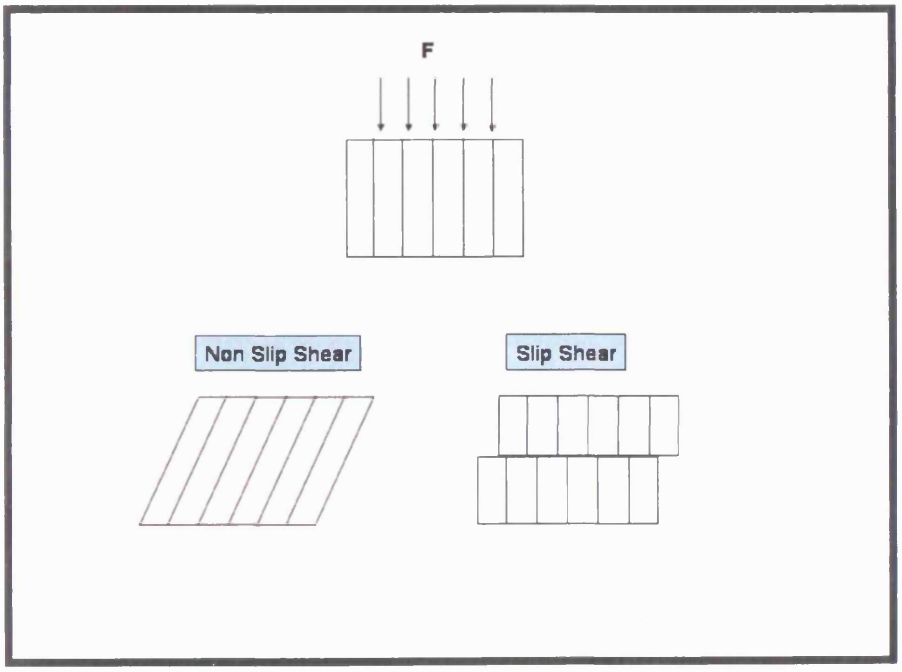

Figure 6.1b

Figure 6.1 Diagram explaining the difference between Slip and Non Slip Shear

a) As dy tends to zero slip occurs when the shearing force results in a discontinuity in the spatial position of 2 points under study whereas non slip shearing would result in convergence of these 2 points. b) The effect is shown more clearly in figure 6.1b as dy tends to 0.

of applied stress and the magnitude of induced normal strain. Thus, a method of distinguishing slip from elastic shear strain could be to identify if shear strain continues to occur and continues to rise in magnitude with increasing axial compression. This method would not be useful however if the structure of the material under study containing the slip boundary has constraints or boundary conditions. For example a tumour with a slip boundary abutting normal tissue may slip only a certain amount following application of an appropriate force as the surrounding 3 dimensional structures would prevent continued slip. In a further example, if lateral slip of a relatively soft but elastic material were to occur at its surface of contact with a relatively rigid material, due to the lateral expansion of the soft material under an axial compressive stress, then full reversal and recovery of the original conditions at the contact surface may well occur when the stress is removed.

Another property that may assist in distinguishing slip from non slip shear could be the assessment of the magnitude of induced axial strain deep to the slip boundary. Once slip has occurred the force applied to structures deep to the slip boundary would be greatly reduced as much of the force would be involved in continuation of slip. Thus the normal axial strain would markedly reduce in these deeper areas. It would be possible to use this reduction is strain as a marker of slip. There would be limitations to using this technique however. Boundary conditions and constraints could anchor deeper areas causing a greater amount of strain to be induced at depth. Nevertheless, one example where this behaviour has been observed is in elastography of superficial tissues under tensile stress applied to the skin; a

high lateral shear strain was observed at the subcutaneous fat-muscle boundary, coincident with a loss of normal lateral tensile strain in the muscle relative to that in the fat (Coutts 2006).

Slip is an important measure in the context of tumour surgery. When an incremental stress is applied to a solid organ containing tumour a point may be reached when the surface of the tumour slips over the surface of the solid organ in contact with the tumour. Thus, an imaging method for detecting slip may assist in identifying the tumour tissue interface.

In order for slip to occur, the static frictional force binding the two surfaces together must be overcome. In the example of a tumour within a solid organ, application of an axial stress at the external surface of the solid organ can produce slip of the tumour over the surface of tissue in contact with the tumour. The force required to overcome the static frictional force is related to the magnitude of stress applied to the external surface of the solid organ.

Evidence for this was observed in the present work during the first few cases studied with conventional elastography, both off-line and real-time, as reported in chapters 4 and 5. For example, figure 4.5 (p92), and the associated text, described a situation where exceptionally high strain appeared to occur at the tumour-brain interface, and little strain was generated in either tumour or brain deep to the boundary, when a large pre-compressive force was used to compress the tissue. However, the opposite was true when a small pre-compressive force was used (figure 4.7, p97), i.e. virtually no strain was generated at the interface but high strain contrast occurred on either side of it. Another example, this time using real-time elastography, was provided in figure 5.5 (p130), where the brain-tumour

interface displayed high local apparent strain when the maximum pre-compression was applied but no such strain when little or no pre-compression was applied. Examples such as this led to the hypothesis that quantification of the external stress applied to produce slip might provide a measure of the static frictional force at the slip boundary and act as a measure of adherence between the two surfaces of the slip boundary. A new technique was therefore devised and evaluated, as described in this chapter, to depict the spatial location of a slip boundary and to quantify the applied force necessary to generate slip at each location. Two new components to the ultrasound elastography system were needed to provide this capability; a device to continuously measure the force being applied to the tissue during palpation with the ultrasound probe and a strain estimator to detect, at each spatial location, when slip has occurred. At the outset of the study no knowledge existed concerning how best to detect when slip first occurs. Therefore this chapter also describes a comparative investigation of various potential measures of slip for this purpose; specifically the use of a true shear strain estimator, the two components of the true shear strain estimator (lateral shear and axial shear) and a shear strain estimator based on the spatial gradient of the direction of the displacement vector are compared. The technique developed was named slip elastography. This chapter describes its development and evaluation *in vitro*. Chapter 7 describes its evaluation *in vivo*.

6.2 Materials and Methods

6.2.1 Data Acquisition System

In order to create slip elastograms synchronized RF ultrasound data over a number of frames and the magnitude of axial force applied by the ultrasound probe for each of the RF frames were required.

The Acuson 128XP scanner (Acuson, CA, USA) with the L7 5-12MHz probe was used in all experiments. The L7 probe was housed in a purpose built Perspex holder (figure 6.2). This holder also housed 3 load cells (RDP electronics, model 31, USA) in an equilateral triangle the centre of which corresponded to the centre of the L7 probe in the axial plane. The triangular pattern of load cells was designed to provide a force vector readout that might permit a measurement to be made of the direction of the force applied to the tissue at the ultrasound probe's surface as well as its magnitude, although in the work to be described little use was made of the direction information, beyond a check that no substantial rotational or shearing stress was being applied. Nevertheless, the three load cells in this pattern enabled a more accurate and precise estimate to be obtained of this force than would have been possible with a single load cell. The 3 load cells were connected to a platform thus ensuring that force applied by holding the platform was transmitted exclusively through the 3 load cells to reach the surface of the probe. Care was taken to ensure that the probe cable was not in contact with the platform of the holder.

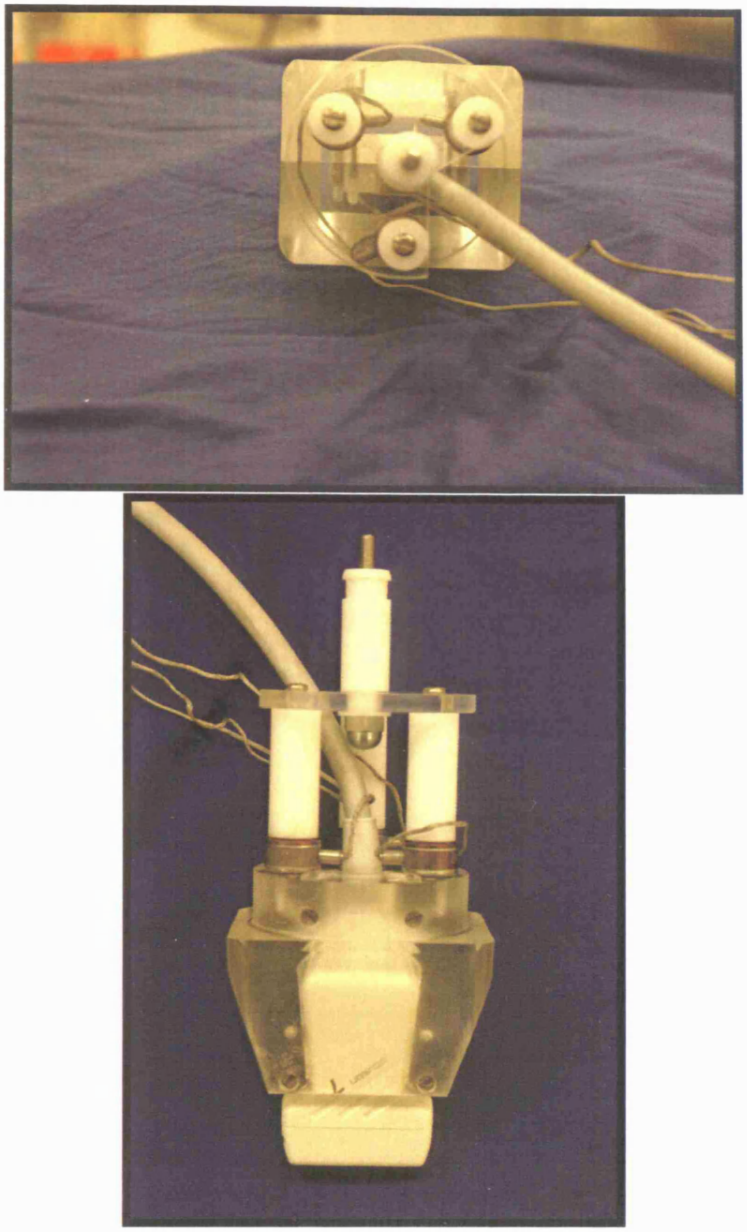

Figure 6.2 The L7 ultrasound probe with purpose-built platform housing 3 load cells forming an equilateral triangle

6.2.2 Data acquisition and Synchronization

It was necessary to synchronize values obtained from the load cells with each ultrasound frame produced.

Load cell data from the 3 load cells were digitised and transmitted from respective load cell conditioning units, using serial communications, via an RS232/485 converter, to a personal computer. Data were read in by commands to an RS232 interface card from visual basic code embedded within a Microsoft Excel™ spreadsheet, which also stored the acquired load cell data as a time sequence. This spreadsheet program also commenced and synchronized acquisition of force data from the load cells and IF echo data

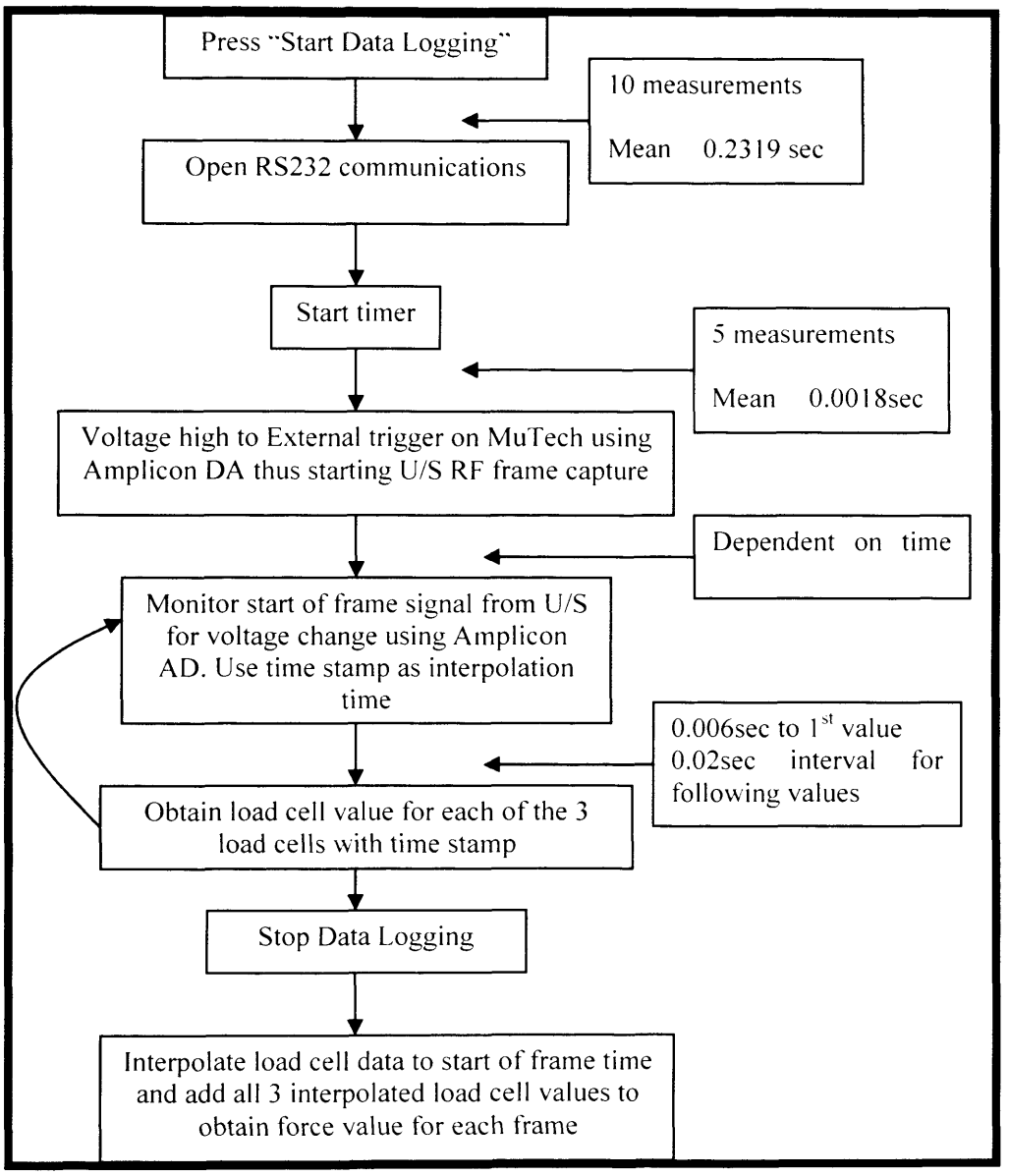

Figure 6.3 Flow chart of the data acquisition and synchronization program

The program was written in Microsoft Visual Basic within an Excel spreadsheet, showing the Stages and Timings for Synchronization of Load Cell Capture with Ultrasound RF Data Capture

from the ultrasound scanner. A schematic diagram describing the programming steps is shown in figure 6.3.

Once data logging was initiated by the spreadsheet program, the RS232 communications port opened. Ultrasound IF frame capture was then initiated. This was achieved by instructing the digital to analogue (DA) function on an Amplicon 9111 PCI card (Amplicon, UK) to send a voltage high signal thus enabling the external trigger function on the MuTech MV-1000 PCI card. The Amplicon 9111 PCI card is a 32 bit PCI card which has DA and analogue to digital (AD) capability with an AD sampling rate of 100kSamples/second and analogue voltage input and output range of ±10V. The external trigger function on the MuTech MV-1000 card, once triggered, initiated RF ultrasound data capture.

The output from the scanner contains an analogue start of frame voltage signature as well as the IF data. This analogue start of frame signal was digitized, again using the AD capability of Amplicon 9111 PCI card. The waveform characteristics of the start of frame signal were analyzed using an oscilloscope and are schematically drawn in figure 6.4. Start of frame was heralded by an increase in negative voltage of above -5V.

Once the start of frame was identified a signal was sent to each of the conditioning units. A value from each load cell was obtained and logged in the spreadsheet application with the corresponding time. The timer used was a built in windows kernel application which had a resolution that depended on the computer hardware but for the computer used was 19μs. After 3 load cell values were obtained, start of frame was detected again using the AD function on the Amplicon 9111 card before a further 3 data values could be

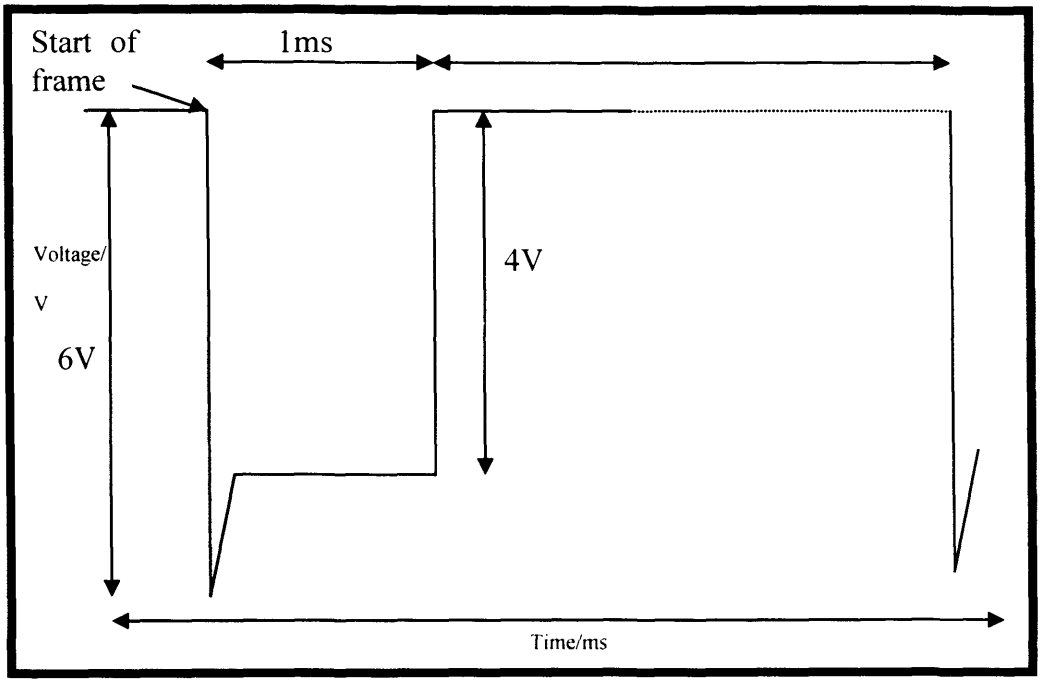

Figure 6.4 Voltage signature of the start of frame signal

recorded. This loop continued until all load cell values and echo data were obtained for the desired number of ultrasound echo frames.

The rate of frame production by the Acuson 128XP and the rate of frame capture by the MuTech MV-1000 card were measured by attaching an oscilloscope to the start of frame signal and by assessing the data log provided by the MuTech software respectively.

Time intervals for opening the communications port, triggering the external trigger on the MuTech card and initialising the AD capture on the Amplicon card were calculated. The rate of capture of 3 load cell values, one from each load cell, was calculated. The RF frame capture rate on the MuTech card was already in the data log and was cross referenced to the timings for load cell data capture.

Following data capture, a linear interpolation algorithm was used to estimate the load cell values for the exact time for each start of frame.

The force of axial compression applied for each ultrasound RF frame was calculated by summating the 3 load cell values at the appropriate time.

Force value differences between the 3 load cells were analyzed to detect any shearing or rotation of the ultrasound probe at the surface of the phantom.

6.2.3 Phantom Development

A simple phantom-based experiment was designed with four objectives: (a) to demonstrate the principle of the proposed method of slip elastography, (b) to determine whether it could reliably define the existence and the location of a slip boundary, (c) to determine whether the force measured at defined thresholds for shear strain is indeed a measure of the static frictional force between two materials at their interface, and (d) to compare the utility of the various shear strain estimators for this purpose. With these objectives in mind it was decided to use homogeneous phantoms each containing a single slip interface at an inclined plane. All phantoms were constructed in an identical manner, except that the angle of the inclined slip interface was varied, so that the force needed to initiate slip ought to have varied only according to the normal reacting force at the slip surface, the coefficient of friction being assumed not to vary from phantom to phantom.

Homogenous gelatine phantoms (16% porcine skin gelatine, type A, 175 Bloom, Sigma-Aldrich, USA) were impregnated with 1% polyethylene granules (~119μm mean diameter). The polyethylene granules acted as acoustic scatterers to augment speckle tracking.

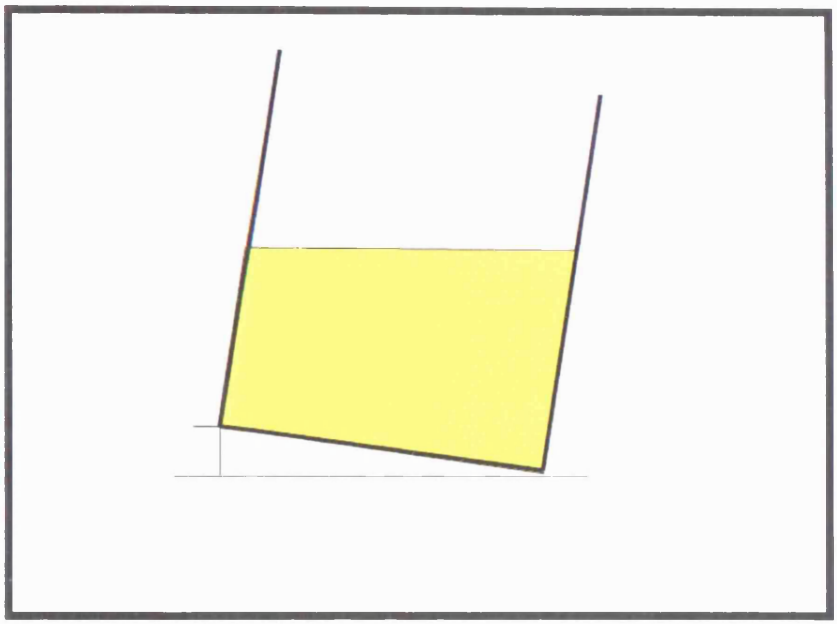

Figure 6.5 Figure showing how a slip boundary was made using gelatine phantoms

Slip boundaries were created in the following way. The gelatine mixture was allowed to set in a rectangular cast. The rectangular cast was placed with one end raised compared to the other so that an angle could be created as a result of gravity (Figure 6.5). This was repeated in an identical fashion thus producing 2 gelatine phantoms with complimentary angles of the surfaces that when in contact would form the slip boundary. The 2 gelatine phantoms were placed one on top of the other. This method was superior to cutting the gelatine block as this potentially could cause the slip boundary to be irregular. It was felt that an irregular surface could potentially lead to unaccountable errors and poor repeatability due to variation in frictional

coefficients between different phantoms. Furthermore it reduced the risk of the superior surface sitting at an angle when both blocks were placed on top of each other.

The angle of the slip boundary relative to horizontal and the mass of the upper gelatine block was measured in each of the experiments.

The two parts of the phantom were submerged in an oil bath with the sides left unconstrained. The base was constrained ensuring slip could occur only at the angled slip boundary. Oil was used to limit interaction between phantoms and water. The static frictional force between the two blocks was of a large enough magnitude in most of the experiments to prevent slip occurring prematurely, i.e. under the action of gravity only. The angle of the slip boundary was also checked on the initial calibrated ultrasound image. It was therefore important to ensure that the probe was perfectly parallel to the upper surface of the phantom, hence parallel to the base of the oil bath.

The angle of the slip boundaries for phantoms tested were 5.7^0, 7.8^0, 9.9^0, and 13.8^0. A phantom with slip boundary angle of 27.7^0 was also created. Experiments using the phantom with slip boundary angle of 27.7^0 demonstrated slip before any compressive force was applied. However, it was possible to alter the frictional force at the slip boundary such that slip did not occur by altering the method of phantom production. Gelatine has the ability to interact with itself on contact. By increasing the contact time of one block with the other and omitting the step of lubricating the surface with oil, it was possible to produce a large angle phantom that did not slip on its own weight but would ordinarily have done so given its angle prior to

axial loading. This phantom was produced to evaluate different shear strain estimators but was not used in any other analyses.

6.2.4 Application of axial compression

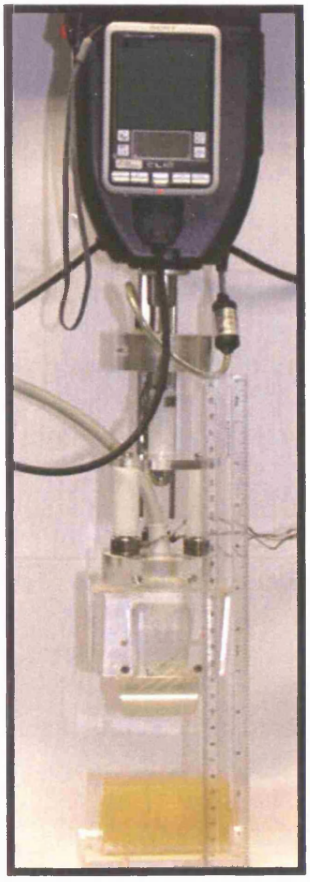

The platform of the ultrasound holder had a centrally placed attachment connected to the Inspec 2200 mechanical testing machine of area greater than the area of the superior surface of the gelatine phantom (Instron, USA) (figure 6.6). This attachment was positioned exactly in the centre of a triangle created by the 3 load cells and hence was also centred on the axis of the ultrasound probe within its holder. Axial compression was achieved using software supplied with the Inspec 2200. The rate of compression was $0.5mms^{-1}$.

Figure 6.6 The Inspec 2200 mechanical testing device with attached ultrasound probe and load cell holder

6.2.5 Obtaining Displacement images and correlation images from RF data

Programs written by Doyley, Bush, Kolen and Berry et al in Matlab® at the Institute of Cancer Research in the preceding years were used for initial data processing. A cross correlation tracking algorithm was used to produce correlation, axial displacement and lateral displacement images from ultrasound RF images. The algorithms used were based on techniques described by Doyley et al (2001). Axial and lateral displacement images were optimized for visualization by altering size of the reference window, reference window overlap and search window size. The reference window was kept small to maximize spatial resolution. The reference window overlap was 94% in the axial direction and 75% in the lateral direction. The search window size was 3 times the area on the reference window area. These variables were chosen to optimize production of displacement images with adequate correlation values.

Correlation and displacement images were subsequently used with different shear strain estimators as described below to create slip elastograms.

6.2.6 Post Processing

Post processing of shear strain images occurred in the following manner. A median filter was applied. Any areas with displacement corrected correlation values less than 0.6 were assigned a shear strain value of 0.

6.2.7 Shear Strain estimators Evaluated

Following optimization as described above, one of 4 shear strain estimators were applied to the lateral and axial displacement images. The four shear strain estimators, developed, tested and written in Matlab® by the author were, as described below;

1) A least squares axial strain estimator applied to lateral displacement data (lateral shear strain estimator).

2) A least squares lateral strain estimator applied to axial displacement data (axial shear strain estimator).

3) A true shear strain estimator (half the sum of the above 2 estimators) (equation 3).

4) A least squares axial strain estimator applied to a vector displacement field. The Arctan function was applied to the axial displacement divided by the lateral displacement for each region of interest giving an image of the angle of the displacement vector (equation 4). For slip to occur, displacement between the 2 surfaces must be occurring in opposite directions. Thus the change in angle of the displacement vector image was used as a measure of slip.

A least squares axial strain estimator was applied to the displacement vector images giving an image showing the change in angle. This strain estimator is described as a vector based shear strain estimator for the remainder of the chapter.

Shear strain images were assessed for visibility of the slip boundary and also correlation values at the slip boundary.

6.2.8 Method for measuring and imaging the force at which slip occurs; creating slip elastograms

For each ultrasound frame obtained, the force value applied by the ultrasound probe at the start of frame was measured by summating the 3 derived load cell values and interpolating to the appropriate time value.

For a given region of interest within the ultrasound plane containing a slip boundary, the force value corresponding to the ultrasound frame at which slip was first seen, was assigned. If slip was not detectable or if the correlation values were below 0.6, the force value at the very beginning of the experiment was assigned. Thus a slip elastogram was produced by assigning appropriate force values for areas where slip was detected and assigning the initial force value for all other areas within the scan plane.

A slip elastogram thus imaged the anatomical location of the slip boundary and, for each part of the slip boundary, the external axial force applied to overcome the frictional force of the slip boundary. The frictional force values were calibrated in Newtons and were depicted by the colour-scale to the right of the slip elastogram image.

Slip elastograms were created in all 5 phantom experiments with slip boundary angles of 5.7^0, 7.8^0, 9.9^0, 13.8^0 and 27.7^0. A number of these images are demonstrated in the results section. It was not possible to evaluate slip at less acute angles than 5.7^0. This was because at shallower angles the compressor compressed the phantom without producing any slip. It was not possible to create phantoms with a slip boundary greater than

13.8^0 without slip occurring spontaneously due to the weight of the gelatine phantom unless the phantom was altered in a manner described in 6.2.3.

The spatial position and characteristics of the slip boundary were identified on the B mode image and compared to the spatial position and characteristics of the slip boundary representation on the slip elastogram.

6.2.9 Distinguishing Slip from Non Slip Shear

The presence of shear in isolation was not adequate to define slip, as slip is a specific type of shear occurring between 2 surfaces. As mentioned in the introduction non slip shear occurs when the internal structural relationships of the area in question do not change whereas slip occurs when discontinuity between spatial positions of points on either side of the boundary is present.

All experiments were designed to detect this discontinuity that characterises slip. Hence, for all 4 shear strain estimators the kernel size used with the least squares strain estimator for shear strain estimation was as small as possible i.e. 2. The kernel size determined the number of values over which the gradient was to be calculated. Larger kernels resulted in smoothing at the slip boundary and, as we know, the slip boundary is in fact a discrete line in 2 dimensions, and so has no width.

Despite the settings mentioned above, the imaged appearance of the slip boundary, in all experiments, did not occupy a discrete line. The reason for

this was evident on the B mode image where the slip boundary was depicted as an area far larger than the actual size expected. This was due to the innate increased echogenicity of surfaces at slip boundaries. This led to the addition of further constraints when defining slip experimentally. It was hypothesized that non slip shear would be self limiting, even if continued stress were applied, as the internal structural relationships cannot be disrupted. Thus, another property distinguishing slip from non slip shear that was measurable, was the continuation of shear strain with continued compression. The constraint distinguishing slip from non slip shear was that shear was required to be present within the same region of interest over a number of contiguous ultrasound frames. The main assumption made for the experimental setup was that slip only occurred at the slip boundary created and not within any other part of the gelatine blocks. The number of frames over which shear was occurring in order to define slip was varied between 1, 4, 7 and 10 frames. Slip elastograms produced were compared for optimal visualization of the slip boundary with minimal non slip shear artefact.

A further constraint was on the value of shear above which slip was presumed to occur. When a material is undergoing non slip shearing the shear modulus would increase in a predictable fashion. At the point at which slip begins to occur the value of shear strain would rise above and beyond what would be expected based on the shear modulus of the material. Hence graphs of shear strain against force applied by the ultrasound probe were produced to identify the point at which slip occurred. These graphs should clearly demonstrate the point at which slip occurs. These graphs are described in the following sections in greater detail.

6.2.10 Comparison of Shear strain estimators using elastogram images

Slip elastograms obtained using the 4 shear strain estimators were compared. This was to provide comparisons in the quality of images produced and the ability of the shear strain estimator to detect slip. Each shear strain estimator for each angle of slip was compared.

6.2.11 Comparison of Shear strain estimators using cumulative graph data

The force at which slip occurred was calculated, for the chosen region of interest, by plotting a graph of the axial force applied by the ultrasound probe, for each ultrasound frame, against the calculated shear strain value for each pixel within the region of interest containing the slip boundary. The regions of interest all comprised the slip boundary seen on the ultrasound images. For this analysis, assumptions made included; 1) slip occurred throughout the slip boundary within the region of interest at the same time, and, 2) slip was an all or nothing phenomenon.

The axial force at which the maximum shear strain value rose above background was taken as the axial force at which slip occurred for that particular region of interest. This point was compared for different shear

strain estimators and also compared to visual assessment of the B mode movie to identify the first frame at which slip was visible.

6.2.12 Reproducibility of Experiment for each angle of Slip

For a given angle of slip boundary, the experiment was repeated on 10 occasions by resetting the experimental conditions where the gelatine phantoms were resting on each other. The same gelatine phantom was used for each of the 10 experiments at the same angle. The different shear strain estimator was used and graphs, as described in chapter 6.2.11, were produced. The force values were plotted against the experiment number to see if repeat experiments on the same phantom would provide reproducible results. The mean and range were also noted.

This was repeated for phantom experiments with slip boundary angles of 5.7^0, 7.8^0, 9.9^0 and 13.8^0 to the horizontal and for all 4 different shear strain estimators tested. It was hypothesised that the applied force to the surface and the coefficient of friction at the slip boundary would be identical between different phantoms if the experimental setup was identical. Thus the coefficient of friction was calculated for all four shear strain estimators.

6.2.13 Comparison of the sensitivity of different Shear Strain Estimators at detecting Shear

The shear strain threshold for the detection of onset of slip needed to be determined prior to slip elastogram generation, and it was hypothesized that this value might be different for the 4 strain estimators due to differences in their sensitivity. Also, the angle of the slip boundary may have an impact on this aspect of performance. A more sensitive shear strain estimator would identify slip, within a region of interest containing a slip boundary, at lower axial force values applied to the slip boundary, when compared to a less sensitive shear strain estimator. It would also be desirable if there were no angular dependence of the performance of the shear strain estimator.

The sensitivity was compared using identical regions of interest containing a slip boundary and identical axial and lateral displacement data.

Comparison between different angles of slip boundary required knowledge of forces applied to the slip boundary that may change as a result of differences in the experimental setup. It was assumed that the only forces of significance acting on the slip boundary were axially applied forces. The forces measured were the gravitational force applied by the upper gelatine block of the phantom and the force applied by the ultrasound probe. The following equation was applied to measure the axial force applied at the slip boundary.

$$Fa=Fg + Fp \qquad (5)$$

Fa was the axial force applied at the slip boundary, Fg was the force applied by the upper gelatine block due to gravity and Fp was the axial force applied by the probe.

The gravitational force applied by the upper block was calculated by measuring the mass of the block and multiplying by acceleration due to gravity (g) or $9.8ms^{-2}$.

The force versus shear graphs, and force versus subjective B-mode movie observations, were analysed to determine the force at which slip occurred, for the chosen region of interest, as described previously.

The experiment was repeated for 4 different angles of slip boundary (not using the phantom with slip boundary angle of 27.7^0); the minimum number that would enable preliminary comparative graphs. A graph of angle of slip boundary against axial force required to produce slip for all 4 shear strain estimators was plotted.

6.2.14 Frictional Force Quantification and Reproducibility of experimental setup between different Angles

Although the gelatine phantoms were created in a similar manner and exposed to equivalent experimental conditions it was very difficult to reproduce mechanical properties at the slip boundary. However, the data

obtained was adequate to evaluate the force required to overcome the static frictional force at the slip boundary.

The mass of the blocks had been measured prior to each experiment hence the force required to produce slip at the boundary could be calculated. The force applied along the slip boundary causing slip was calculated using the following equation;

$$F_{slip}=Fa \times \sin\theta \qquad (6)$$

If this is measured at the threshold of shear strain that defines onset of slip, then F_{slip} is the force required to produce slip, and is therefore equal to the frictional force, where θ is the angle at the slip boundary relative to the horizontal. Using the above equation it was possible to measure the frictional force over the whole slip boundary.

It was hypothesized that the frictional force over the whole slip boundary should not change regardless of the phantom used as experimental conditions were similar. The disparity in values for frictional force over the whole slip boundary would give an indication of the robustness of the experimental setup.

The phantom with slip boundary angle 27.7^0 was excluded from this analysis as it was purposely designed to contain a more adherent slip boundary.

6.3 Results

6.3.1 Data synchronization

The frame rate produced by the Acuson 128XP at a scan depth of 50mm was 16 frames per second. The frame acquisition rate of the MuTech MV-1000 PCI card in external trigger mode at the same scan depth was 8 frames per second.

Figure 6.3 shows the steps taken for data acquisition with timings for individual steps. It took 0.02 seconds to obtain a load cell value or 0.06 seconds for a set of 3 load cell values thus a potential maximum of 16 complete sets of load cell values per second could be obtained.

A complete set of load cell values were sampled for each ultrasound RF frame captured as confirmed by cross-referencing the MuTech card data log of time intervals between each RF frame with load cell time intervals.

The difference in force values between 3 individual load cell values obtained at any time during the experiment, for any of the experiments demonstrated negligible rotational or torsional force being applied.

6.3.2 Examples of Displacement, Correlation and Shear Strain Images

Figure 6.7 shows a B mode ultrasound image with corresponding axial displacement image, lateral displacement image, correlation image and true

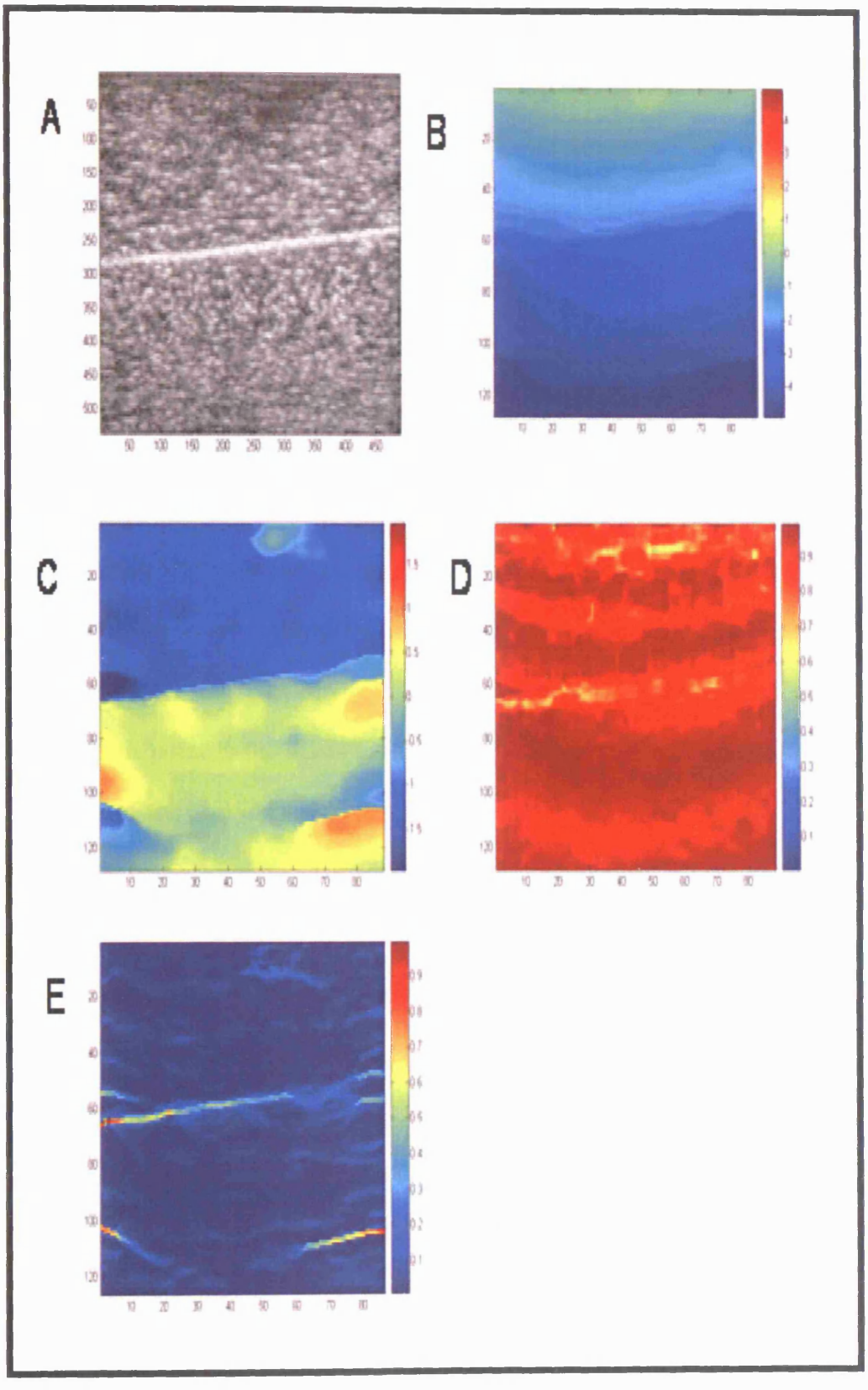

Figure 6.7 a) B mode Image, b) Axial Strain Image, c) Lateral Strain Image, d) Correlation Image and e) True shear strain image for phantom experiment with slip boundary angle of 7.8^0

shear strain image for one of the phantom experiments with slip boundary angle of 7.8^0 taken at a time when slip was occurring. The shear strain image was taken at a time when slip was demonstrable on the B mode movie. For all experiments, slip boundaries were visible on shear strain images when demonstrable on B mode movies.

There appeared to be some de-correlation in the vicinity of the slip boundary compared to the surrounding however displacement tracking was still possible in all cases.

Figure 6.8 shows a B mode image and 2 slip elastograms created a using phantom with slip boundary angle of 13.8^0. The slip elastogram shown in figure 6.8b was created using frames 1 to 15 and figure 6.8c was created using frames 1 to 30. These images (and others in figures 6.9 and 6.10) are shown at this point in the thesis to illustrate the appearance and some of the properties of the slip elastograms, even though the graphs of force versus shear strain that lead to the criterion for defining when slip has occurred are shown later in this chapter. For the moment the reader is kindly requested to make the assumption that a clear definition exists for a threshold shear strain at which slip is deemed to have occurred. The slip elastograms demonstrate the spatial position and the force required to initiate slip at the slip boundary (the static frictional force). The colour-scale to the right of the image was a measure of the external axial applied force at the moment that slip was deemed to have first occurred, calibrated in Newtons. Hence, for figure 6.8b, the magnitude of external axial force required to produce slip at the slip boundary was about 1.8N, which may be seen by cross referencing the

colour of the slip boundary with the colour axis on the right side of the slip elastogram.

The slip boundary was demonstrable on both slip elastograms and its spatial position correlated well with the spatial position of the slip boundary as seen on the B mode image.

The B mode image demonstrates a straight line for the slip boundary however the representation of the slip boundary in figure 6.8b does not. The slip elastogram contains discontinuities in the area representing the slip boundary. Different force values at which slip was identified are represented along the slip boundary.

Figure 6.8c used more ultrasound frames, allowing slip to be detected at points on the boundary that appeared to remain adherent in figure 6.8b. The slip boundary was thicker than seen in the B mode image or in figure 6.8b. Furthermore, a gradient in force values at which slip occurred was demonstrated with lower force values further away from the ultrasound probe. This trend was observed for all angles of slip boundary and for all shear strain estimators tested.

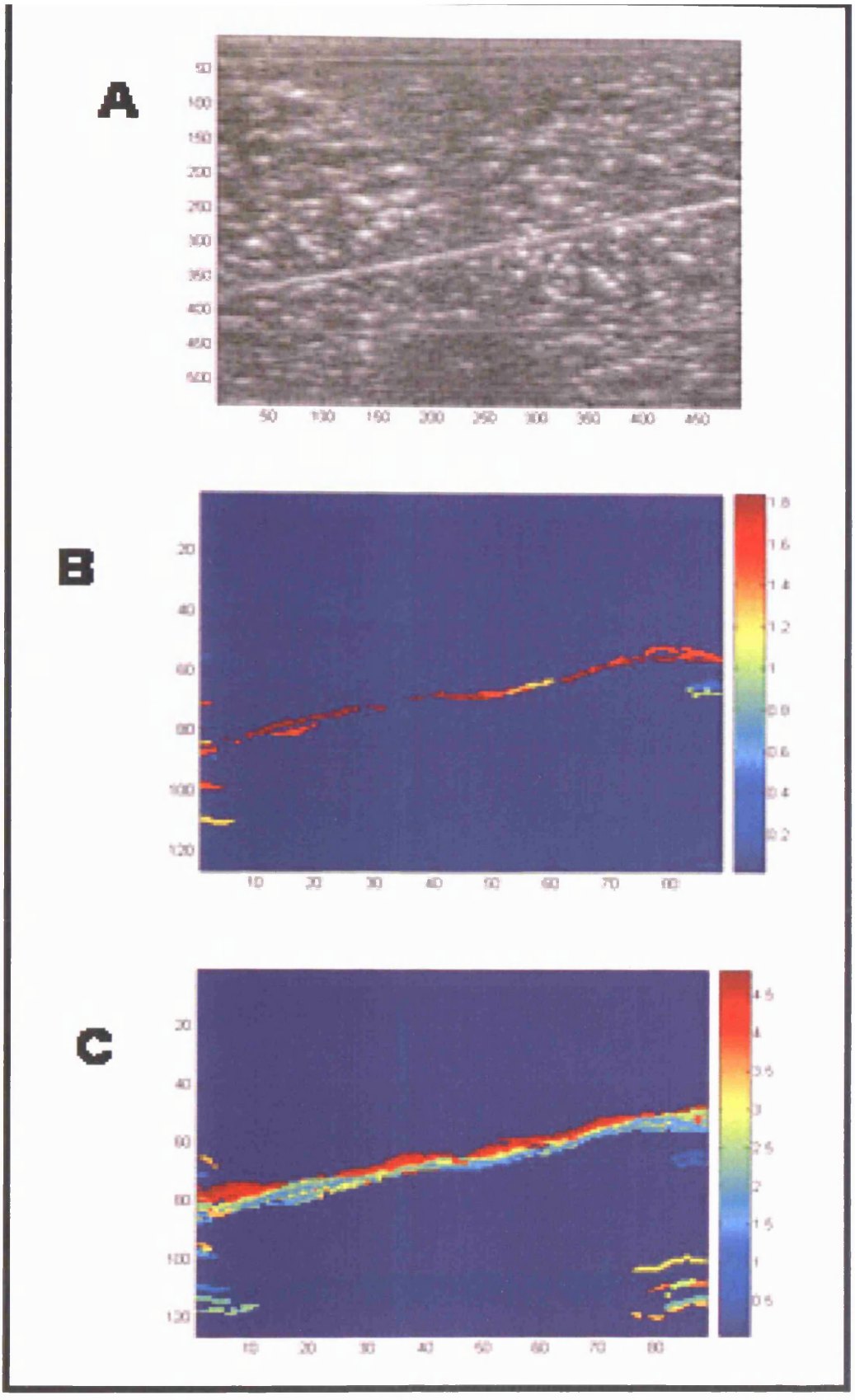

Figure 6.8 B-mode image and 2 slip elastograms created from a phantom with a slip boundary angle of 13.8°
See text for explanations.

6.3.3 Distinguishing Slip from Non Slip Shear

Data were analyzed using the axial strain estimator applied to a lateral displacement field at a slip boundary angle of 13.8^0. Figure 6.9 shows 4 slip elastograms produced by altering the number of frames over which shear was required to have been present above a pre-defined threshold prior to assigning slip for that area. The numbers of frames chosen were 1, 4, 7 and 10. As the number of frames was increased the presence of non slip shear became less apparent.

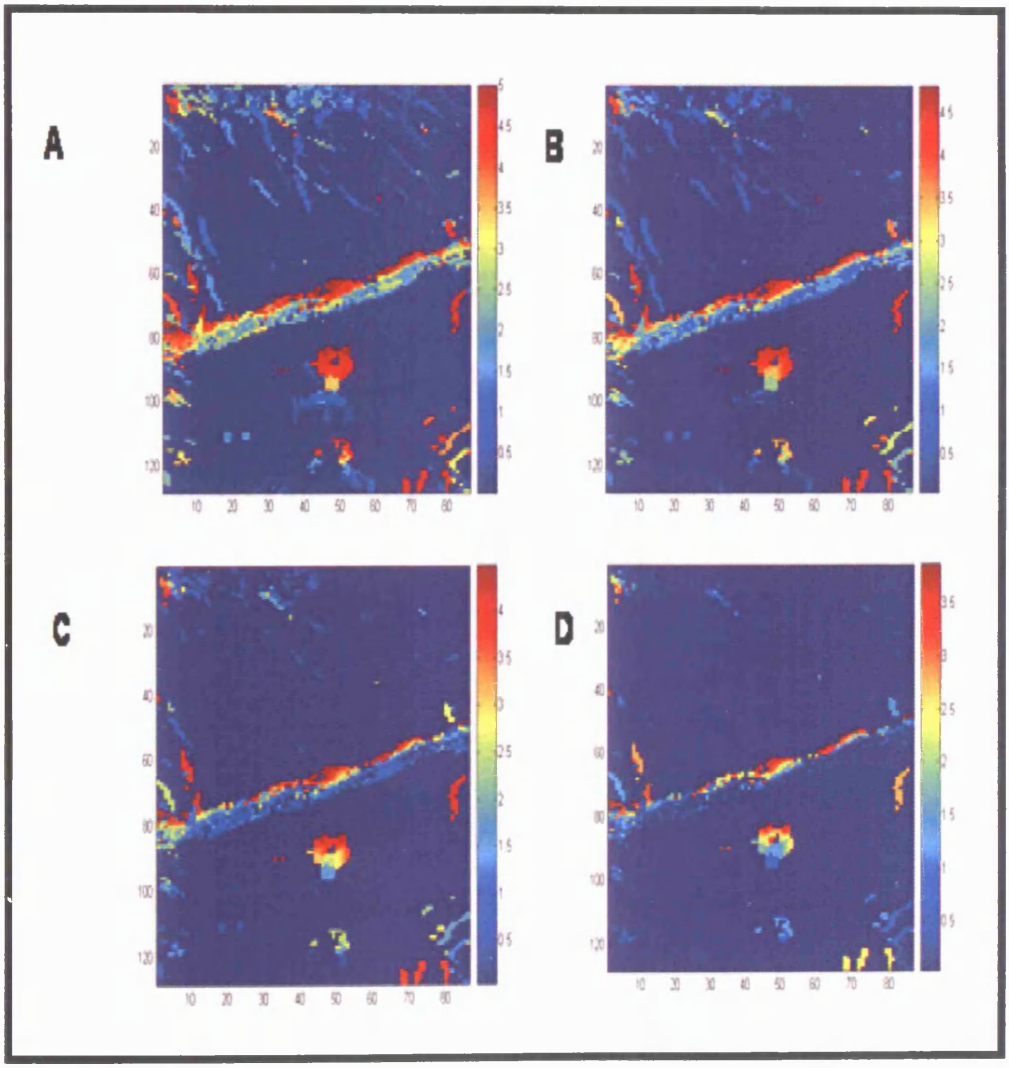

Figure 6.9 4 slip elastograms produced by altering the number of frames over which shear was required to be present

a) 1frame, b) 4 frames, c) 7 frames, d) 10 frames

6.3.4 Comparison of strain estimators using slip elastogram images

Slip boundaries were demonstrable using all 4 shear strain estimators at all angles of slip boundary.

Figure 6.10 shows slip elastograms produced from phantoms with slip boundary angles of 5.7^0, 13.8^0 and 27.7^0 using the 4 shear strain estimators tested.

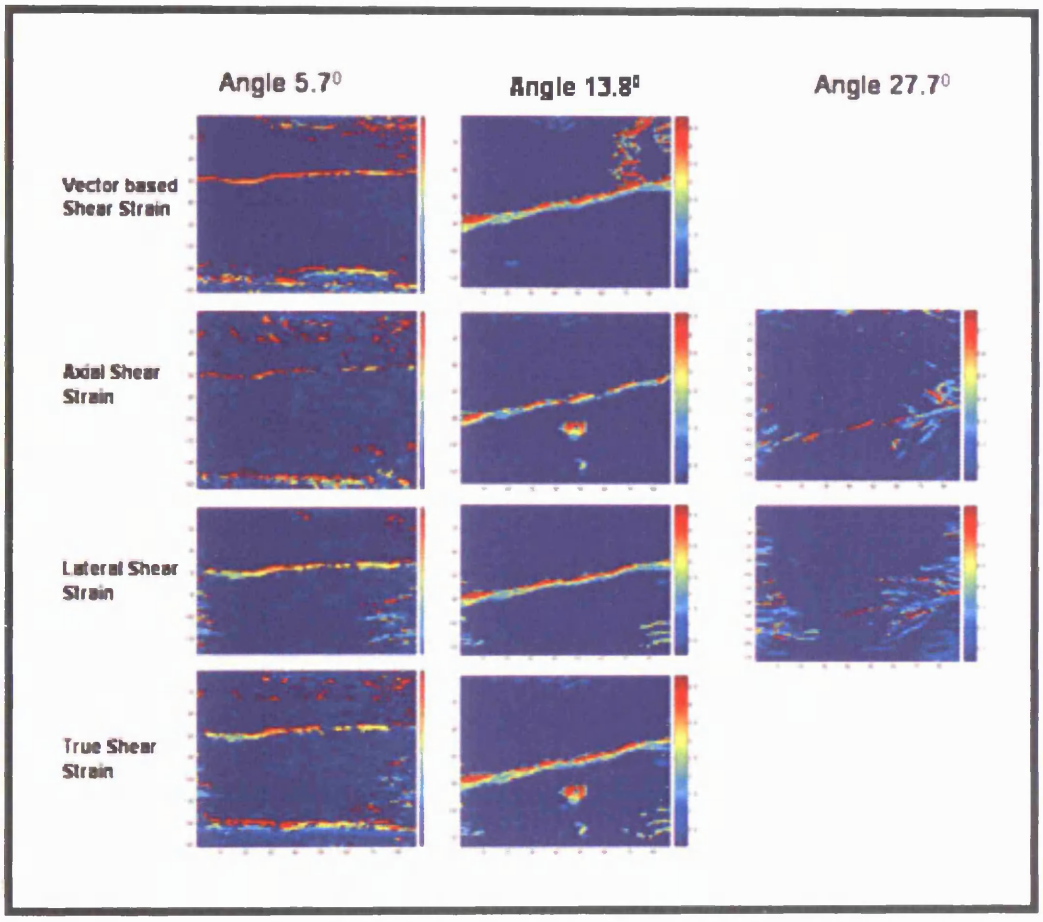

Figure 6.10 Slip elastograms produced from phantoms with slip boundary angles of 5.7^0, 13.8^0 and 27.7^0 using the 4 shear strain estimators tested.

See text for descriptions. The vector based shear strain and true shear strain estimators were not shown with angle of phantom 27.7^0 as these 2 estimators have no angular dependence.

When comparing the lateral strain estimator applied to an axial displacement field (axial shear strain) with the axial strain estimator applied to a lateral displacement field (lateral shear strain) the angle of the slip boundary had an effect on the performance. At very shallow angles, using axial shear strain, the slip elastogram demonstrated discontinuities in the slip boundary. The slip boundary was more evident using lateral shear strain.

At steeper angles performance in terms of slip boundary identification was equivalent when comparing both shear strain estimators mentioned above. At steeper angles still, the axial shear strain estimator was more sensitive at detecting slip compared to the lateral shear strain estimator.

The true shear strain estimator and the vector based shear strain estimator performance at detecting slip boundaries also improved at steeper angles.

Non slip shearing artefact was present on slip elastograms when using all four shear strain estimators. The vector based shear strain estimator had the least non slip shear artefact followed by the axial shear strain estimator.

The true shear strain estimator had the greatest amount of artefact.

The lateral shear strain estimator consistently contained horizontal lines of shear strain artefact originating from the sides of the image.

6.3.5 Comparison of different Shear Strain Estimators at detecting Shear using cumulative graph data

All 4 shear strain estimators were able to detect shear. Figure 6.11 shows 4 graphs representing the 4 different shear strain estimators tested. A region of interest was chosen from within the displacement field that contained the slip boundary. The dimensions of the rectangular region of interest were 60 x 40 pixels. The shear strain values for each of these pixels for each ultrasound frame were plotted as shown. Graphs where no slip boundary was present contained a background of shearing artefact with no point at which the shear strain value rose disproportionately compared to the applied force.

The initial flat section, where maximum shear strain values were small and did not rise with increasing force, characterise the period when the axial compressive stress was not large enough to overcome the static frictional force at the slip boundary and represent noise in the estimation of shear strain.

Local shear caused by slip occurred once the force applied at the slip boundary was greater than the static frictional force at the slip boundary.

This was represented on the graphs by an increase in the magnitude of shear strain with increasing force. The threshold force value at which slip was judged to initially occur could be evaluated using these plots. The threshold force value was defined as the point at which the shear strain value was 3

standard deviations above background for more than 2 consecutive ultrasound frames.

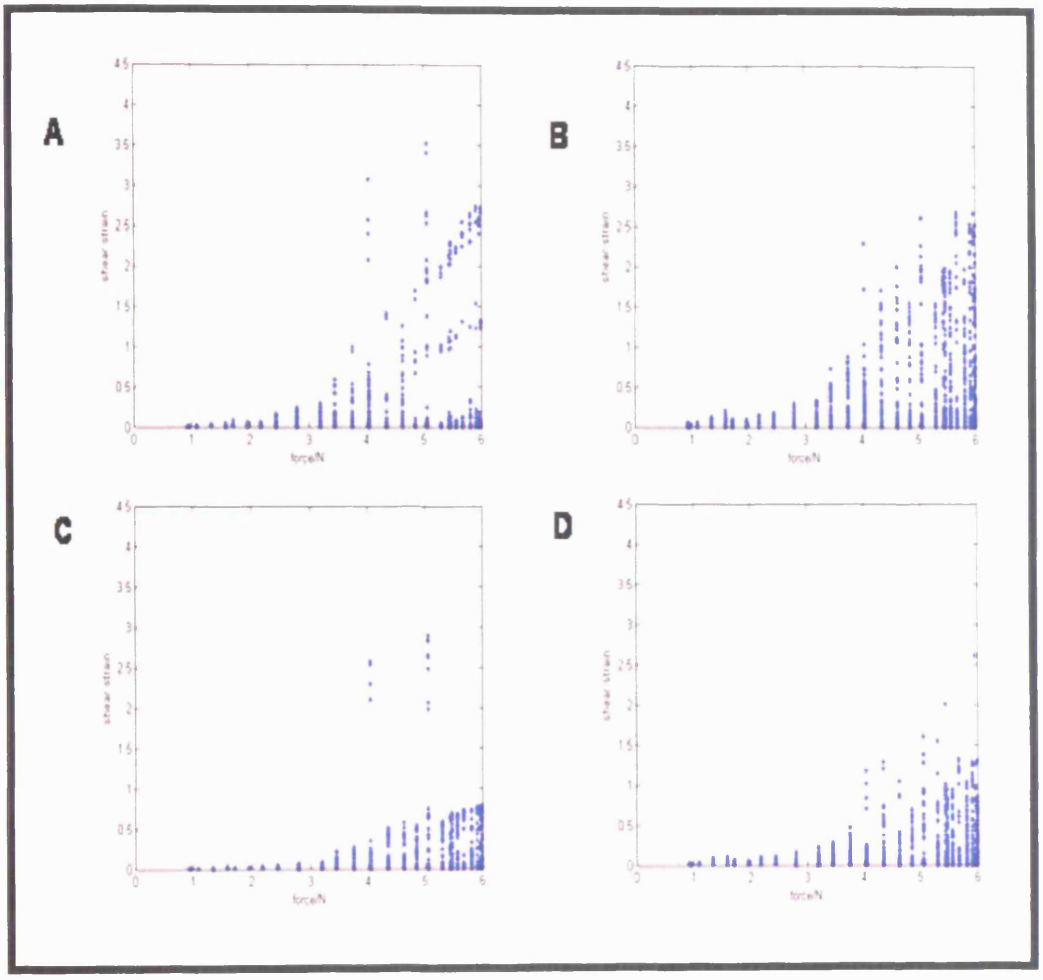

Figure 6.11 Graphs representing the 4 different shear strain estimators tested for phantom with slip boundary angle of 7.8°.

Shear strain was plotted against force. a) Axial shear Strain, b) lateral shear strain, c) vector based shear strain, d) true shear strain

6.3.6 Reproducibility of experimental setup for different Angles of Slip

Figure 6.12 shows the axial force applied by at the slip boundary in order to produce slip (using equation 5) as detected using the 4 different shear strain estimators for each of the 10 experiments, for each angle. Note that some

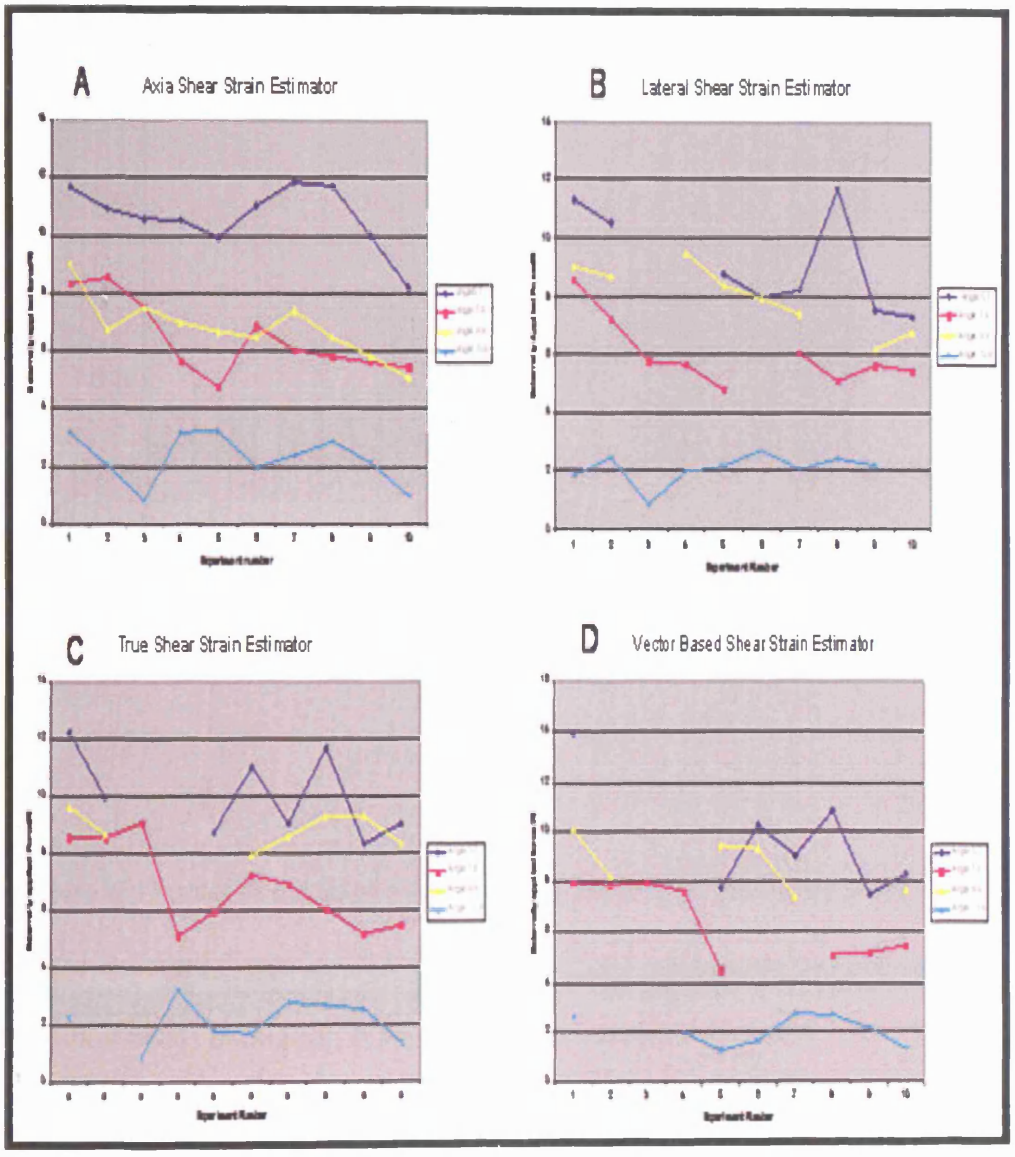

Figure 6.12 Graph of externally applied force applied against experiment number for each of the four angles of slip boundary for each strain estimator tested

a) Axial shear strain estimator, b) lateral shear strain estimator, c) True shear strain estimator, d) vector based shear strain estimator
The y axis is a plot of the externally applied force required to initiate slip and the x axis plots the experiment number. The blue traces represent the angle 5.7^0, purple 7.8^0, yellow 9.9^0 and light blue 13.8^0 of slip boundary.

data were missing where the graphs did not demonstrate a distinct point at which slip was demonstrated. Figure 6.13 demonstrates a graph of one of these excluded experiments.

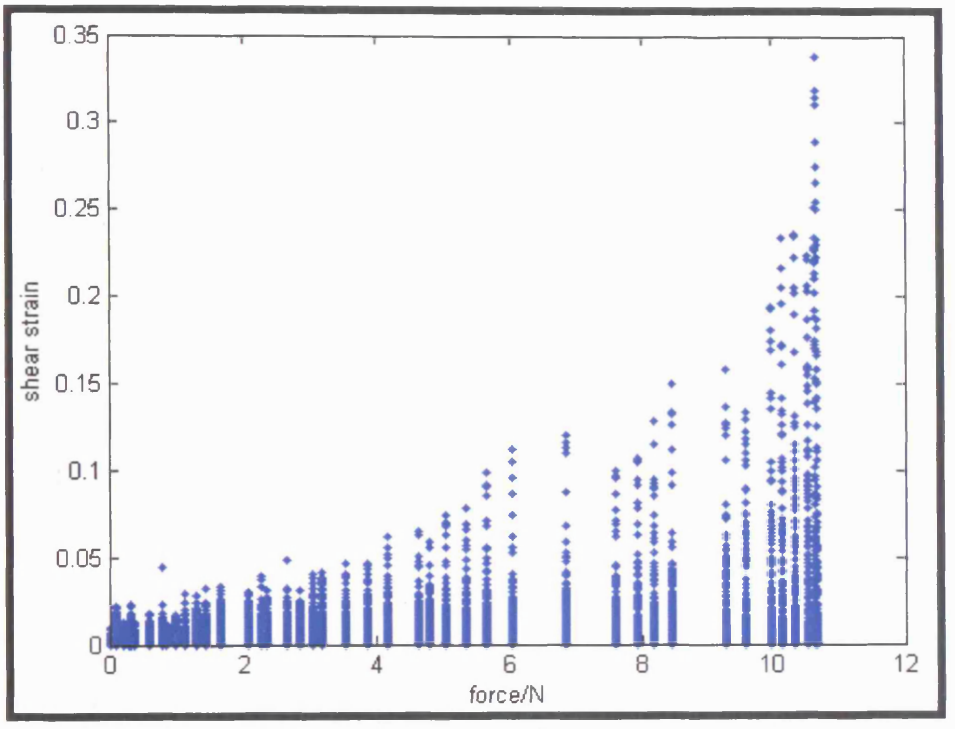

Figure 6.13 Graph showing an experiment not demonstrating an obvious point at which slip could be said to have started

Figure 6.12 also demonstrates that there was both consistency and overlap in the externally applied force between different angles of slip. This is also demonstrated in figure 6.14 where the mean value and the standard deviation error bars over the 10 or less experiments (as indicated in figure 6.12) are shown for each angle of slip and for each shear strain estimator. There was a trend whereby, as expected, the externally applied force

required to initiate slip was greater when the angle of the slip boundary was reduced.

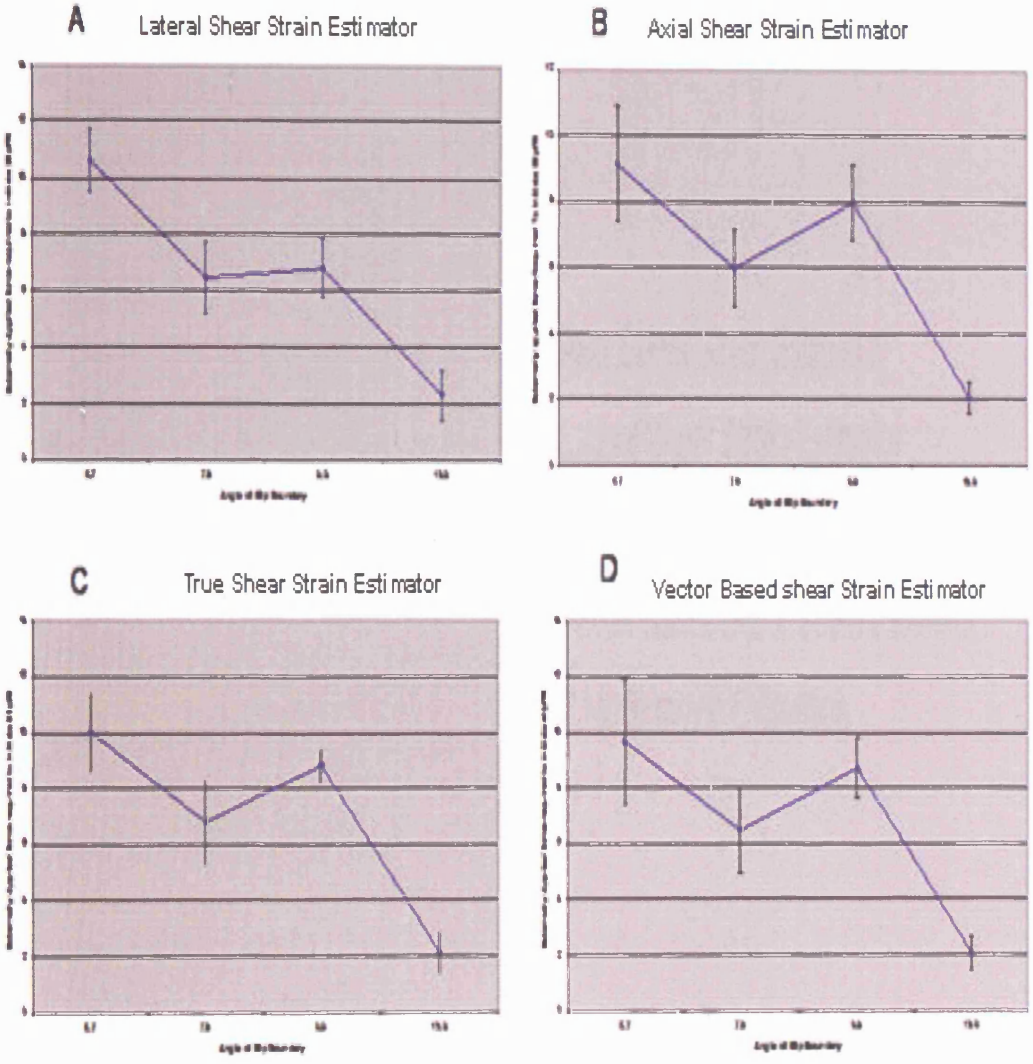

Figure 6.14 Graphs demonstrating the mean and standard deviation error bars for each of the angles of slip for each shear strain estimator tested

a) Axial shear strain estimator, b) lateral shear strain estimator, c) True shear strain estimator, d) vector based shear strain estimator
The y axis plots the mean value of the externally applied force required to initiate slip for the 10 experiments (or less) and the x axis plots the angle of slip boundary

6.3.7 Comparison of the sensitivity of different Shear Strain Estimators at detecting Shear

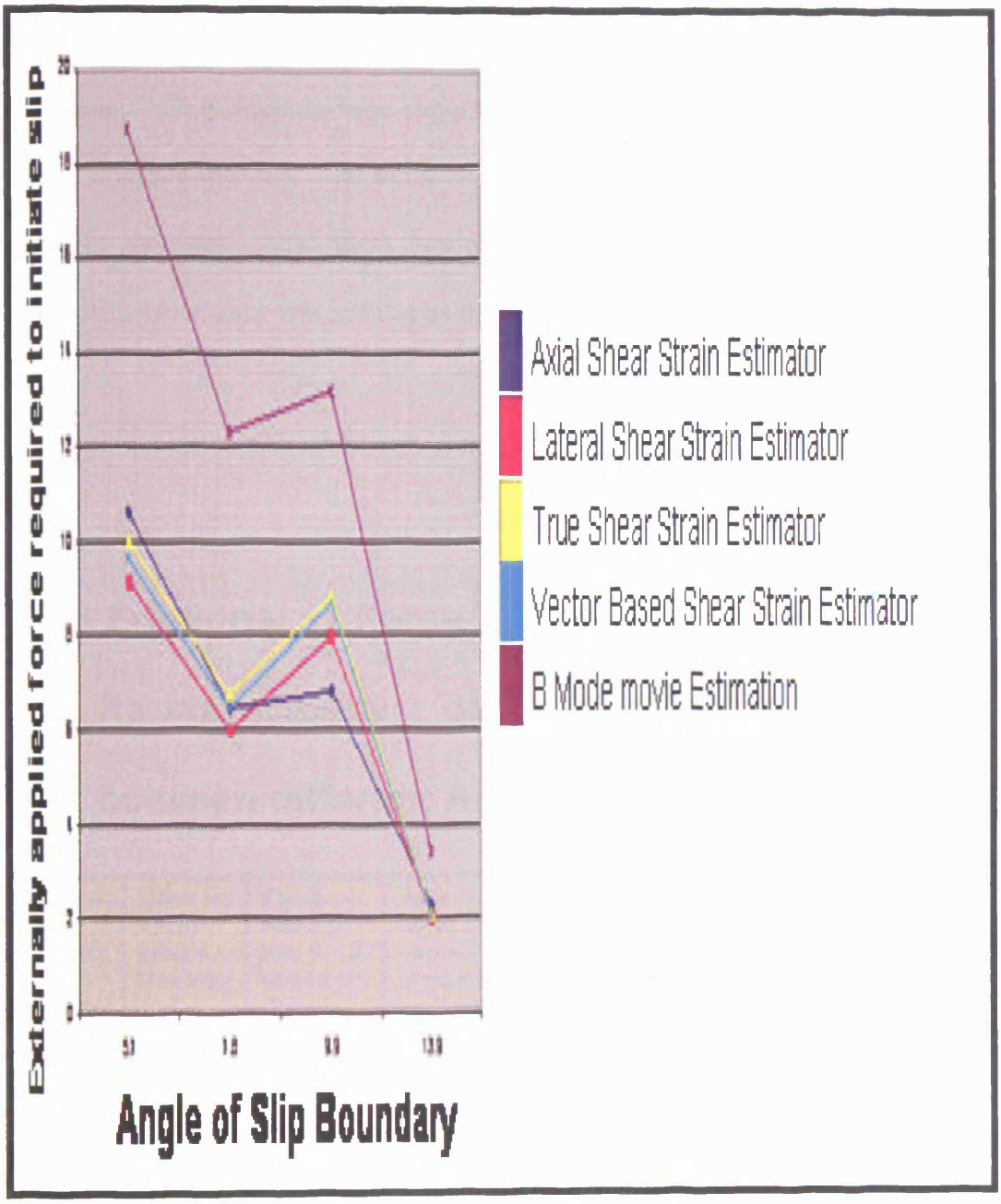

Figure 6.15 Graph comparing different shear strain estimators and visualization of the B mode movie at detecting slip

The y axis plots the externally applied force required to initiate slip

Figure 6.15 shows a graph of the mean value for axial force applied at the slip boundary when slip was initially detected, using equation 5, for the 10 experiments against the angle of the slip boundary, for all 4 shear strain estimators. It also shows when slip was identified following analysis of the B mode movie.

All shear strain estimators were superior to visual inspection of the B mode movie at detecting slip. The axial shear strain estimator was slightly less sensitive than the lateral shear strain estimator at shallow angles of slip however performance was similar as the angle became more acute.

6.3.8 Frictional Force Quantification and Reproducibility of experimental setup between different Angles

Angle of Slip boundary	Mass of upper gelatine Block/kg	Force applied due to Gravity/N (Fg)	Axial force applied by ultrasound probe/N (Fp)	Axial Force applied at Slip Boundary/N (Fa)	Frictional Force at slip boundary/N (F_{slip})	Coefficient of Friction
5.7	0.0924	0.906	9.9606	10.8666	1.0793	0.100
7.8	0.0923	0.905	8.8340	9.7390	1.3217	0.137
9.9	0.0924	0.906	7.0783	7.9843	1.3727	0.1750
13.8	0.0967	0.948	2.2515	3.1995	0.7631	0.246

Table 6.1 Table showing frictional force calculations at different slip boundary angles

Table 6.1 shows the mass and axial force applied for experiments performed for each of the angles tested. Note this measurement was not performed on data from the phantom with slip boundary angle of 27.7^0. The table shows values obtained using the true shear strain estimator only. It contains mean values for the calculated static frictional force at the slip boundary for experiments conducted on phantoms with slip boundaries at different angles. The values for the static frictional force were similar except for the phantom with angle 13.8^0. This implied that the experimental setup was, on the whole, reproducible. The coefficient of friction given in the table was calculated dividing frictional force calculated by the cosine of the angle and by the axial applied force required to first initiate slip.

Note when calculating the force applied due to gravity g was $9.8ms^{-2}$. The axial force applied at a slip boundary was the sum of the force due to gravity and the axial force applied by the ultrasound probe. The force applied in the line of the slip boundary was calculated using the equation $F_{slip}=Fa \times \sin\theta$.

6.4 Discussion

Imaging mechanical properties of tissue is a relatively new field despite the fact that qualitative assessments of these properties underlie so many aspects of clinical practice. Ultrasound elasticity imaging techniques are beginning to have an impact on clinical practice (see chapter 2). There are numerous mechanical properties that can be imaged with an ultrasound based system that may potentially be useful in clinical practice. One such application has been presented.

A method for imaging slip and quantifying the external force required to produce slip within an ultrasound scan plane using techniques based on conventional ultrasound elastography has been developed. The primary difference between slip elastography and conventional elastography is that a criterion for the onset of slip is assessed and the applied force required to create this condition at each point in the field of view is displayed as an image. In the present work the criterion for onset of slip used was the threshold level of shear strain that needed to be reached and maintained for a set number of ultrasound frames. Conventional elastography, on the other hand, simply displays an image of normal axial strain.

Shear strain has been measured within an ultrasound field based on the technique of conventional ultrasound elastography (Konofagou 2000, Konofagou & Ophir 2000, Thitaikumar 2005, Righetti 2005, Thitaikumar 2006) however this is the first time a quantitative measure of the external axial force required to produce slip, which is related to the static frictional force at the slip boundary, has been applied in conjunction with shear elastography. It is important to note that the majority of these studies were

performed independently and were occurring concurrently with the work described in this thesis. It has been suggested that the magnitude of shear strain and its width may provide a quantitative measure of the bonding strength at an interface (Thitaikumar 2006). This was based on a finite element analysis simulation study. The studies performed in 2000 were based on simulation experiments and no studies except the current study described have gone as far as attempting to quantify adherence between two surfaces.

A critical aspect of the system design was to synchronize the measurement of slip with the measurement of externally applied force. It is asserted that the system described provides adequate synchronization however the system described can be improved by removing the requirement to interpolate data produced from the 3 load cells. This may be achieved by using a 6 axis force transducer or by parallel processing of the 3 load cell data streams using a synchronization signal from the start of frame signal. Data acquisition is at an adequate rate for use in an *in vivo* setting.

Four different shear strain estimators were tested against visual inspection at detecting slip. It was found that, when using only one or other of the components of true shear strain (the lateral shear stain or the axial shear strain), the angle of the slip boundary had an effect on detecting slip. This was less of a factor when using the true shear strain estimator or the vector based shear strain estimators.

There are 2 factors that are important to consider. The first is that theoretically, axial compression of a shallow angled slip boundary producing slip would result in a larger magnitude of lateral displacement

compared to axial displacement. Thus, assuming axial displacement tracking has equivalent precision to lateral tracking, tracking with a lateral displacement estimator would be more accurate compared to an axial displacement estimator. One would therefore expect the lateral shear strain estimator to be more sensitive at detecting slip at very shallow angles compared to an axial shear strain estimator. These two shear strain estimators would have equal sensitivities at detecting slip if the angle of the slip boundary was 45^0. At angles greater than 45^0, the axial shear strain estimator should be more sensitive at detecting slip compared to the lateral shear strain estimator. However, and this is the second point, precision of displacement estimation in the lateral direction is at least 6 times worse than in the axial direction (Thitaikumar 2006b). This difference is because the rate of fluctuation in the RF echo signal laterally is determined by the ultrasound beam width, whereas in the axial direction it is determined by the wavelength (Bilgen 2000). Thus, one would expect the axial displacement field to have superior displacement tracking precision compared to the lateral displacement field.

The lateral shear strain estimator was more sensitive at detecting slip at very shallow angles compared to the axial shear strain estimator. At an angle of 13.2^0 the two shear strain estimators had equivalent sensitivity at detecting slip. At a slip boundary angle of 27.7^0, the axial shear strain estimator outperformed the lateral shear strain estimator at detecting the slip boundary. These findings are compatible with the theoretical prediction in an idealised system combined with the inherent limitations of the displacement tracking using RF ultrasound echoes.

The true shear strain estimator and the vector based shear strain estimator did not have as great an angular dependence on performance at detecting slip because of the method by which strain was calculated. The true shear strain estimator, however, did suffer in terms of non slip shearing artefact as it combined non shear artefact created by both of its components. The vector based shear strain estimator had the least shear strain artefact.

It was important to define slip as a subset of shear strain. It is reasonable to believe that the assumption that slip occurred exclusively at the slip boundary created was true. Certainly inspection of the gelatine phantoms and the B mode movies did not demonstrate any areas where 2 surfaces were in contact other than at the slip boundary. Non slip shear strain is likely to be an artefact that will be difficult to remove completely because of its similarities to slip. With the system described it has not been possible to differentiate slip from non slip shear exclusively utilising the definition of slip mentioned in the introduction. This was due to the echogenicity at the interface between two surfaces. Improvements in signal processing and ultrasound probe design may assist in utilising the definition that addresses the discontinuity of the internal structure when slip occurs as opposed to the self limiting nature of non slip shear strain.

It has been possible to distinguish slip from non slip shear strain by altering the number of frames over which slip must occur. This approach has been shown to reduce non slip shear strain artefact. The self limiting nature of non shear slip that has been highlighted for improving image quality is dependant on the boundary conditions and constraints applied to the material under study whereas an algorithm for detecting discontinuity could

potentially be used in any situation where slip occurs if resolution is high enough.

It was possible to detect slip in areas where two surfaces were in contact once the static frictional force of the two surfaces was overcome using slip elastography. The technique was able to quantify the external axial force required to produce slip at the slip boundary. This force measurement is potentially a useful indirect measure of adherence between the two surfaces comprising the slip boundary. Quantification of the externally applied force may be potentially useful clinically despite the measure suffering from not being truly quantitative. This measure would provide a better indication of the frictional force at a slip boundary when compared to the use of shear elastography in isolation. For example, consider two patients with tumours in a solid organ. If an external force of 1N is required to produce slip at the tissue tumour interface for patient 1 but a force of 10N is required to produce slip for patient 2 the clinician is likely to infer that the tumour in the patient 2 is more adherent to tissue than the first patient. This process is not truly quantitative but may be an improvement compared to the subjective assessment made by the clinician without imaging. If a shear elastogram were used in isolation there would be no reference value for which the clinician could make such a comparative assessment. Obviously absolute quantification would be ideal but not possible without a measure of the mass applied to the slip boundary and an analysis of constraints applied to the slip boundary in all 3 dimensions. These measurements are difficult to quantify in controlled environments not to mention *in vivo*.

When the force due to gravity, or weight, applied at the slip boundary was also taken into account, a more accurate measurement of the frictional force at the slip boundary was possible. This technique may be useful for *in vitro* mechanical testing.

The phantom design was thus chosen so that constraint issues could be ignored and the mass applied to the slip boundary could easily be measured. This enabled assessment of the repeatability of the experimental setup. A circular inclusion within a phantom would suffer from constraints and quantification of the gravitational force acting on the slip boundary would be difficult to measure.

On the whole, slip boundaries created in individual experiments had similar static frictional force values with the exception of the phantom with slip boundary angle 13.9^0.

It was interesting to see differences in the images as a result of altering the number of frames containing shear that were used to create the slip elastogram. When relatively few frames were included it was possible to visualise the heterogeneity of force required to produce slip within different parts of the slip boundary. This was probably due to the differences in adherence of different parts of the slip boundary.

The representation of the slip boundary on slip elastograms increased in area as more frames were added to create the slip elastogram. This was due to the change in spatial position of the slip boundary with continued axial compression. As axial compression occurs the slip boundary gets closer to the ultrasound probe's surface. On a B mode movie this can be visualised as the slip boundary moving upwards. Slip elastograms are produced by

cumulatively processing a number of ultrasound frames. Thus, the area depicting slip corresponded to the change in spatial position seen on the B mode movie associated with axial compression. This also accounts for the gradient of axial compressive forces applied seen at the slip boundary. Compression producing a change in axial position of the slip boundary is also the reason why the slip boundary, when using few ultrasound frames containing slip, was not a perfect straight line.

It is likely that slip elastography could be utilised in a clinical setting however the results would need to be interpreted with due caution. Furthermore, the force applied would need to be large enough to produce slip but not so large that damage occurs at the surface of the solid organ. The constraints *in vivo* compared to *in vitro* are also very different. In this experiment once slip occurred it was an all or nothing event and the upper gelatine block slid off the lower block. *In vivo* however this would not happen. In fact, one would expect the object to spring back to its original position following compression, as a result of constraints from surrounding tissues and structures.

Despite these drawbacks it is potentially useful as a semi-quantitative tool that could provide the clinician with mechanical property information that was previously unavailable and subjectively interpreted.

6.5 Conclusion

A new imaging technique called slip elastography has been developed. It is based on conventional ultrasound elastography but measures the shear strain as opposed to normal strain. The technique has been developed to distinguish slip from non shear slip. The most appropriate shear strain estimator to use is either one based on true shear strain or one based on a vector based shear strain estimation. The next chapter describes the implementation of slip elastography *in vivo* to assist during brain tumour resection.

Chapter 7

Slip Elastography to determine the adherence of tumour to brain during brain tumour resection; pilot study

Chapter 7

Slip Elastography to determine the adherence of tumour to brain during brain tumour resection; pilot study

This chapter describes the use of slip elastography intra-operatively during brain tumour resection. The technique was performed on 22 patients.

7.1 Introduction

As discussed in chapter 2 and chapter 6 it is potentially useful to the surgeon to have prior knowledge of the mechanical properties at the brain tumour interface. Of specific importance are the anatomical location of the interface and the adherence of tumour to brain at that interface. This may reduce the risk of intra-operative complications and may improve prognosis.

Conventional ultrasound elastography had limitations when used intra-operatively during brain tumour resection especially when performed in the presence of slip boundaries (Chakraborty 2006). Conventional normal axial strain elastography aims to display an image related to tissue stiffness, but regions of high shear at slip boundaries can generate a high normal strain artefact, which may be interpreted as indicating very soft tissue when in fact it is due to a tissue discontinuity. Shear elastography should help to resolve such misinterpretations. Thus slip elastography was developed to identify and isolate the shear strain component of the strain tensor.

When an incremental stress is applied to a solid organ containing tumour a point may be reached, if the tissues of the organ and tumour are well demarcated (such as when the tumour possesses a capsule), when the surface of the solid organ slips over the tumour with which it is in contact with. Thus, an imaging method for detecting slip may assist in identifying the tumour tissue interface and in assessing the degree to which the two tissues are mechanically continuous.

For the case where there is indeed good separation between tumour tissue and surrounding organ tissue, in order for slip to occur, the static frictional force binding the two surfaces together must be overcome. In the example

of a brain tumour, application of an axial stress at the external surface of the solid organ can produce slip of the tumour over the surface of tissue in contact with the tumour. The force required to overcome the static frictional force is related to, amongst other things, the magnitude of stress applied to the external surface of the solid organ. Quantification of the external stress applied to produce slip may provide, in part, a measure of the static frictional force at the slip boundary and act as a measure of adherence between the two surfaces of the slip boundary.

Chapter 6 has detailed the theory and *in vitro* experiments underlying slip elastography as a method for identifying the anatomical location of a slip boundary and measuring adherence between 2 surfaces.

This chapter describes a preliminary clinical feasibility study where the technique of slip elastography was applied *in vivo* prior to brain tumour resection. The ability of slip elastography to identify the spatial location of the brain tumour interface and the adherence of tumour to brain was thus evaluated. Slip elastogram findings were compared to surgical findings.

7.2 Methods

Approval from the Local Research Ethics Committee was obtained. Patient recruitment was from the Neurosurgical Department at the host institution. Twenty two patients who were due to undergo craniotomy for excision of

brain tumour were recruited for this study. Inclusion criteria into this study were patients undergoing craniotomy and debulking of presumed brain tumour and the patient's ability to provide informed consent. All consecutive cases that fulfilled these criteria were included. Intrinsic and extrinsic tumours were included. These were the same patients used in the clinical studies described in chapters 4 and 5. Data were captured intra-operatively and analysis, including elastogram generation, was performed by the author retrospectively using computing facilities at the Institute of Cancer Research Physics Department.

The Acuson 128XP ultrasound scanner was used with the 7.5MHz L7 ultrasound probe.

The ultrasound probe was housed in a purpose built Perspex holder (figure 6.2, p149). This holder also housed 3 load cells (RDP electronics, model 31, USA) in an equilateral triangle the centre of which corresponded to the centre of the ultrasound probe in the axial plane. The 3 load cells were connected to a platform thus ensuring that force applied by holding the platform was transmitted exclusively through the 3 load cells to reach the surface of the probe. Care was taken to ensure that the probe cable was not in contact with the platform of the holder.

The ultrasound probe and holder with all wires were housed in a sterile ultrasound sheath (Mana-Tech, England) with a camera cover to eliminate the risk contamination of the operative site.

For extrinsic tumours data were obtained prior to dural opening and for intrinsic tumours following dural opening.

Following craniotomy, data were obtained for slip elastogram production using the following method. A freehand ultrasound elastography technique was adopted for data capture (Doyley 2002). This meant that compression was applied using the ultrasound probe by the operator and not by a mechanical device. This reduced complexity of the experimental setup and most likely reduced the time taken to perform all the necessary experiments. All experiments were performed by neurosurgeons with training in slip elastography data capture. Initiation of data capture coincided with initiation of compression. The probe and probe holder were held from its platform in two hands. No part of the operator or any of the wires and cables were in contact with the lower portion of the probe holder so any force applied by the operator was transmitted through the 3 load cells exclusively. The amplitude of compression applied, in order to avoid any damage, was determined by the operator. The time taken for one compression cycle was approximately two seconds. Care was taken by visual observation of the real-time ultrasound image during all acquisitions to minimize lateral and elevational transducer displacements. A slow steady gradually increasing compressive force was applied over about one second resulting in brain displacement of no more that 5mm. The cycle was completed by gradually removing the probe and holder from the surface.

Data collected included IF ultrasound data from the ultrasound machine and force values from each of the 3 load cells. For a given ultrasound frame the cumulative force applied through the 3 load cells was measured. Thus accurate synchronization of data capture from the ultrasound machine and

from the load cells was required. Details of how synchronization was achieved can be found in chapter 6.

Slip elastograms were produced the using equipment and software described in chapter 6.

Slip elastograms were produced and analysed in the 22 patients. These findings were compared to surgical findings in the following manner.

7.2.1 Comparison of surgical findings to slip elastogram findings

Surgical findings on tumour brain adherence were documented by the surgeon without knowledge of the results of slip elastography. The surgeon was asked the following questions;

1) Was the tumor encased with no demonstrable plane of cleavage?
2) Was the tumour adherent to brain but a plane of cleavage could be identified?
3) Did the tumour have an obvious slip boundary?

Additional comments on whether slip was observed within the tumour or whether the brain showed evidence of slip were also noted.

The adherence of tumour to brain was evaluated on slip elastograms by asking similar questions. Only the author evaluated the slip elastograms and this was performed in a blinded manner to the surgical findings.

Specifically, the elastograms in combination with the B mode ultrasound images were analyzed to determine whether slip could be identified. If slip was identified the next stage was to evaluate whether there was evidence of a confluent slip boundary. Finally the externally applied axial force required to produce slip was measured using the slip elastogram and associated colour-scale.

7.3 Results

No adverse events occurred to any of the patients as a result of any of these interventions. Table 7.1 summarizes surgical and slip elastogram findings on tumour brain adherence for all 22 patients.

There was one patient where a biopsy was performed so the surgeon was unable to evaluate adherence of tumour to brain. This patient had an intrinsic tumour that appeared to have a slip boundary that was adherent to the surrounding brain requiring 4N of axial external force to initiate slip.

Another patient had slip elastography performed after an intrinsic glioma was macroscopically resected. No slip boundary was identifiable on the slip elastogram.

Of the remaining 20 patients, 14 patients had intrinsic tumours, one patient had an arachnoid cyst and 5 patients had extrinsic tumours. Of the 15 patients with intrinsic space occupying lesions, 4 had cystic lesions where a

Patient Number	Diagnosis	Surgical slip Score	Slip Elastogram Score at interface	Force for slip	Correlation between surgical and slip elastogam findings	Comments
3	Parietal GBM	No slip boundary seen	Slip boundary seen but not confluent	0.6N	No	
4	Parietal Gliosarcoma	No slip boundary detected	No Slip boundary seen	N/A	Yes	
5	Parietal Convexity Meningioma	Obvious slip boundary	Obvious confluent slip boundary	1.7N	Yes	
6	Posterior frontal metastasis	No slip boundary detected	No slip boundary seen	N/A	Yes	
7	Frontal GBM, large fluid cyst, little tumour seen	No slip boundary	No slip boundary seen	N/A	Yes	Slip seen in normal brain where cyst would potentially expand into at 3.5N
8	Parafalcine meningioma	Obvious slip boundary	Obvious confluent slip boundary	0.15N	Yes	
9	Recurrent frontal GBM	Tumour adherent but plane found	Slip boundary with differing adherence	2N	Yes	
10	CP angle Meningioma	Obvious slip boundary	Obvious confluent slip boundary	3.5N	Yes	Slip of brain over tentorial edge seen at 6N
11	Parafalcine GBM	No slip boundary	No slip boundary	N/A	Yes	
12	Intraventricular GBM	No slip boundary	No slip boundary	N/A	Yes	Slip seen within the tumour
13	frontoparietal GBM, post op	No slip boundary	No slip boundary	N/A	Yes	
14	Frontal GBM (biopsy only)	N/A	Obvious confluent slip boundary	4N	N/A	
15	Temporal low grade intrinsic glioma	No slip boundary	No slip boundary	N/A	Yes	
16	Frontal arachnoid cyst, normal brain	No slip boundary	No slip boundary	N/A	Yes	
17	Parietal GBM	No slip boundary	No slip boundary	N/A	Yes	
18	Frontal low grade glioma	No slip boundary	No slip boundary	N/A	Yes	
19	Sphenoid ridge meningioma	Obvious slip boundary	Obvious confluent slip boundary	2.8N	Yes	
20	Occipital cystic GBM	No slip boundary	No slip boundary	N/A	Yes	Non confluent lip seen in normal brain 2.5N
21	CP angle acoustic neuroma	Obvious slip boundary	Obvious slip boundary	0.5N	Yes	
22	Parietofrontal GBM	No slip boundary	No slip boundary	N/A	Yes	
23	Occipital cystic GBM	No slip boundary	No slip boundary	N/A	Yes	
24	Occipital Cystic GBM	No slip boundary	No slip boundary	N/A	Yes	

Table 7.1 Surgical and slip elastogram findings on tumour brain adherence for all 22 patients

GBM stands for Glioblastoma multiforme

brain tumour interface along the cyst wall could not be identified macroscopically. One patient had a predominantly cystic tumour where the cyst was lined with tumour.

Figure 7.1 shows a B mode image with the corresponding slip elastogram for a patient with a convexity meningioma (patient 5). The surgeon stated that tumour did not adhere to underlying brain. The slip elastogram demonstrates the spatial position and the force required to initiate slip at the slip boundary (the static frictional force). The colour-scale to the right of the image was a measure of the external axial force applied to produce slip, calibrated in Newtons. Hence, for figure 7.1b, the magnitude of external axial force required to produce slip was about 1.7N and was obtained by cross-referencing the colour of the slip boundary with the colour axis on the right side of the slip elastogram. The spatial location of the slip boundary on the slip elastogram correlated well with the presumed spatial position of the brain tumour interface on the B mode image and, in a number of cases with the co-registered MRI using neuro-navigation as described in chapter 4.

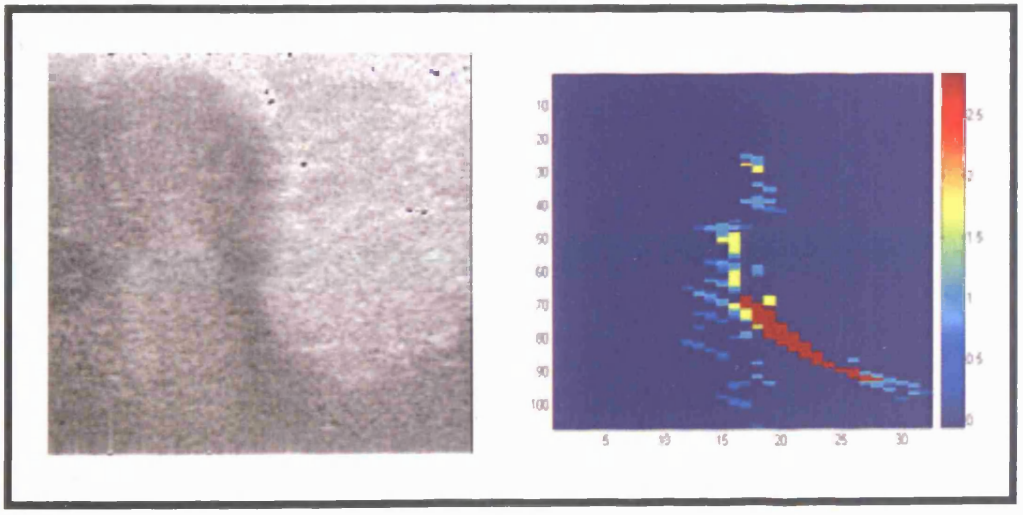

Figure 7.1 a) B mode image and b) Slip elastogram for patient with an obvious slip boundary between tumour and brain (patient 5)

Figure 7.2 shows a B mode image with the corresponding slip elastogram for a patient with a recurrent frontal glioblastoma multiforme. The surgeon felt that the tumour was adherent to brain but a plane of cleavage was identifiable. The slip elastogram demonstrated focal areas where slip was present and the force required to produce slip was about 3N.

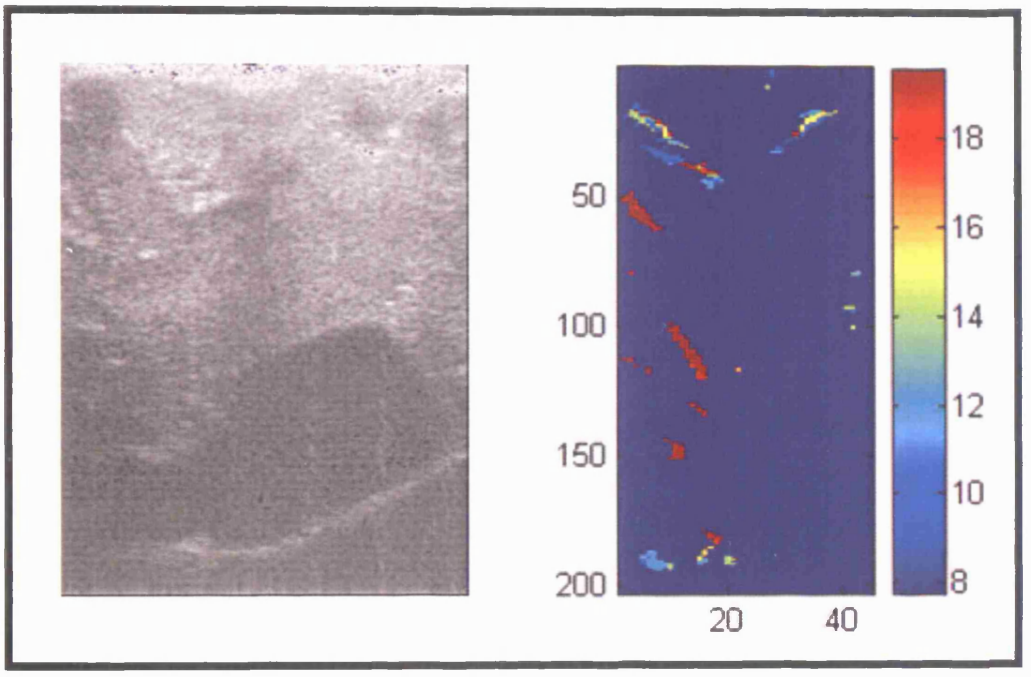

Figure 7.2 a) B mode image and b) Slip elastogram for patient with tumour that was adherent to brain but where a cleavage plane was identifiable

Figure 7.3 shows a B mode image with corresponding slip elastogram for a patient with a glioblastoma multiforme of the left parietal lobe. The surgeon stated that the tumour was encased in brain and no slip boundary was evident. The slip elastogram demonstrated no evidence of slip.

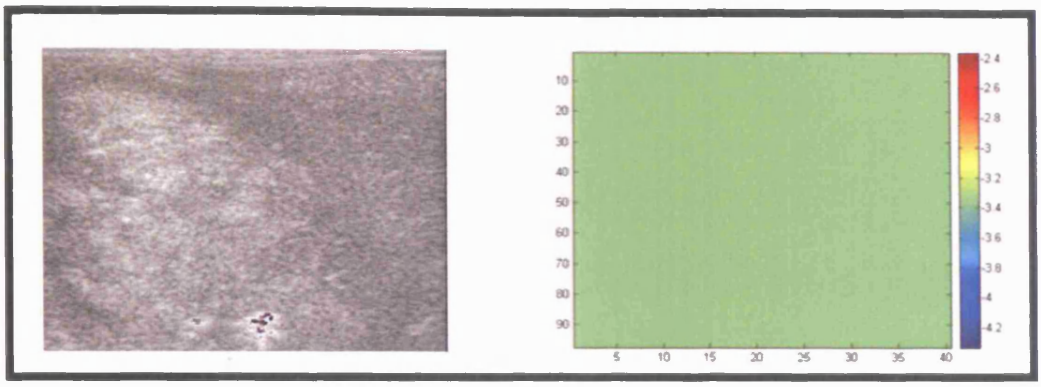

Figure 7.3 a) B mode image and b) Slip elastogram in patient where no slip boundary was evident

Table 7.1 demonstrates that there was good correlation between the surgical findings on stiffness and the slip elastogram findings in 19 of the 21 cases where a comparison was made. It is interesting to note that all patients with extrinsic tumours had minimal adherence of tumour to brain. It was encouraging to note that the slip elastogram findings correlated with the surgical findings.

There were 10 patients with predominantly solid intrinsic tumours and one with a cystic tumour where the cyst wall was macroscopically lined with tumour. In these 11 cases tumour was found to be adherent to brain or encased within the brain substance. Slip elastogram findings corroborated with surgical findings in 9 of the 11 cases.

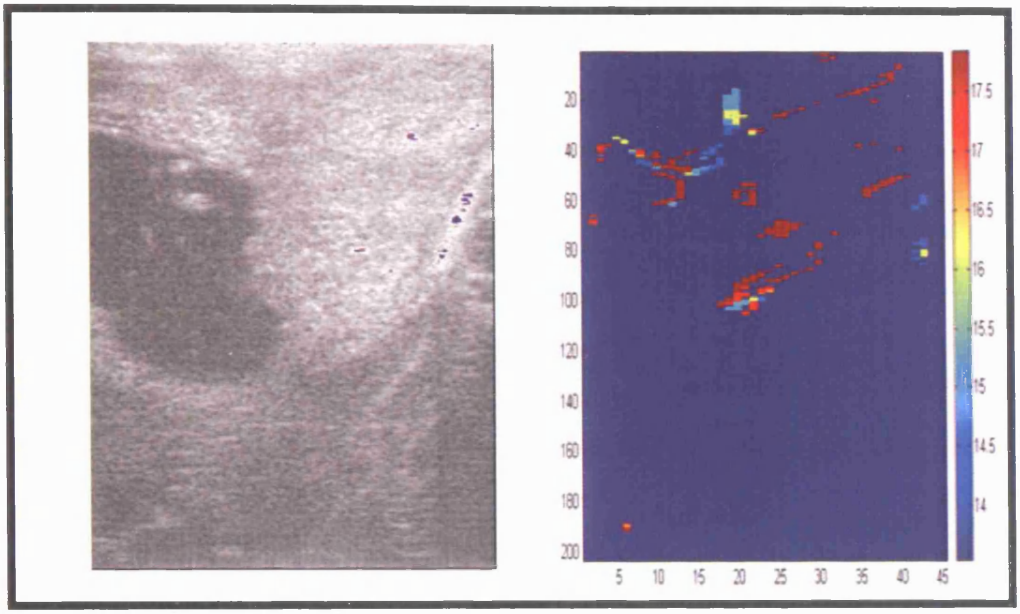

Figure 7.4 B mode image and slip elastogram in patient where slip boundary was noted in normal brain tissue

For the 4 patients with cystic space occupying lesions where there was no macroscopic evidence of tumour over the cyst wall, no slip was seen. It was interesting to note the findings in patient 7. Patient 7 had a frontal glioblastoma with a very large cyst. The cyst wall was not felt to be infiltrated with tumour macroscopically. The slip elastogram demonstrates that slip was evident in the surrounding brain substance (figure 7.4). It is likely that the cyst would expand in these areas where slip was identified taking the path of least resistance to expand.

7.4 Discussion

Safe and complete macroscopic excision with maximal sparing of normal tissue is usually the surgeons aim when attempting to resect brain tumours (Weingart 2004).

Safe tumour resection is mainly dependent on the surgeon's skill and judgement. There are a few pre-operative and intra-operative investigations that may prevent complications and ensure safe tumour resection such as preoperative angiography (Choi 2000) or intra-operative facial nerve stimulation (Sampath 2004).

Specifically, with regard to brain tumour resection, prior knowledge of the anatomical location and mechanical properties at the brain tumour interface may assist the surgeon in planning his resection strategy.

Imaging mechanical properties of tissue is a relatively new field despite the fact that qualitative assessments of these properties underlie so many aspects of clinical practice.

Conventional ultrasound elastography of the brain and brain tumours has been evaluated by three research groups, including the work reported in earlier chapters of this thesis. The aim of work reported in chapters 4 and 5 was to determine whether ultrasound elastography was able to discriminate tumour from brain in terms of stiffness. The findings suggested that the presence of slip boundaries limited the utility of ultrasound elastography at differentiating stiffer tissue from softer tissue, unless great care was taken to minimise loss of stiffness contrast by not applying much force during palpation. This concept has been taken further in the present chapter by suggesting that the mechanical properties at the boundary between brain and

tumour are more important than the relative stiffness of brain compared to tumour. Thus slip elastography was developed specifically to assist in identifying mechanical properties and spatial position at the brain tumour interface.

The technique of palpation was a very important consideration. Safety was of paramount importance thus only neurosurgeons with prior training in elastography performed any of the experiments. It was important to ensure that the magnitude of compression was not too great both for safety reasons and for data acquisition. If compression was performed too quickly and with too large an amplitude there would be the risk of sparse data capture compromising slip elastogram generation. Conversely too small an amplitude of external compression may have resulted in no slip occurring at all as the static frictional force was not overcome.

Data acquisition was found to be optimal using parameters mentioned in the methods section. A possible future improvement on the safety aspect would be to add an alarm whenever the magnitude of compression exceeds a certain value.

The force values that are shown in the slip elastograms are not a truly quantitative measure of the static frictional force at the slip boundary for a number of reasons. These include;

1) Boundary Conditions and constraints

2) The orientation of the slip boundary relative to the externally applied force

3) The weight of the tissue acting at the slip boundary.

7.4.1 Boundary Conditions and constraints

If one were to apply a compressive force to an object on a slope it would slip off the slope as there are no constraints preventing slip. Consider part of the brain that has been compressed. Once the compressive force has been removed and slip has occurred at depth the surrounding brain parenchyma constrains the region preventing continued slip. Furthermore the mechanical properties at the edges of the compressed area are unknown. Thus the material is said to have unknown boundary conditions and substantial constraints. These parameters are currently impossible to quantify *in vivo* within the brain and so the forces acting on any slip boundary would be impossible to quantify.

Consider a block of elastic background gel containing a spherical or cylindrical simulated stiff tumour separated from the background by a slip boundary, the background gel will flow and slip around the tumour during compression but because it is elastic it will reverse this process when the compressive force is removed. Similar, seemingly reversible events were seen to occur *in vivo*.

7.4.2 The orientation of the slip boundary relative to the externally applied force

An important limitation of this technique has to do with the orientation of the slip boundary relative to the direction of the externally applied

compressive force. If one were to compress in a situation where the slip boundary was perpendicular to the compressive force, slip would not occur. As the angle of the slip boundary edged towards 90^0 then maximal slip would occur. This means that the orientation of the slip boundary relative to the angle the force is being applied has a large effect on the magnitude of force required to produce slip, much like the inclined plane experiment carried out in chapter 6.

.

7.4.3 The weight of the tissue acting at the slip boundary

Another unknown force acting on the slip boundary would be the force due to gravity. Tissue above the slip boundary would have a mass exerting a force onto the slip boundary. It is not possible to accurately quantify this mass *in vivo*.

Despite these limitations the author believes that the force value provided has great utility. This technique provides the surgeon with a force value that produces slip at depth. This acts as an estimate of the force he will require to develop the plane of cleavage at the brain tumour interface. He will also have an idea of where tumour is particularly adherent to brain. This information would otherwise only have been available to him at the time of development of the cleavage plane.

Many of the problems described above may be overcome by using techniques such as radiation force (Nightingale 2002) to create displacement within the scan plane by applying a high intensity ultrasound wave focusing on a specified area to produce focused compression at depth. As shown by Melodelima et al (2006) this method may be used to create strain images, and compares to conventional elastography where strain is created by propagation of external applied compression, usually using the ultrasound probe, to deeper tissues. If the wave were focused at or around the brain tumour interface internal slip could potentially be generated. Furthermore one may be able to increase the force applied (tissue heat permitting) to greater values than would be considered safe using conventional external axial compression as this would be a highly focused pushing beam.

It was encouraging to observe such a good correlation between surgical findings and slip elastogram findings.

For patients with cystic lesions and no macroscopic evidence of tumour around the cyst lining it was encouraging to note that no slip was observed except within the brain substance in one of the patients. Slip within the brain substance was also easily identifiable on the B mode movie. This suggests that cyst would have expanded in the direction the slip boundaries were identified.

As was expected extrinsic tumours were less adherent to brain compared to intrinsic tumours. Patient 6 had a frontal metastasis resected. This was the only patient with a metastasis in this series. Metastatic deposits commonly contain a solid tumour mass without intervening brain tissue. These tumours tend to be well demarcated compared to the surrounding oedematous brain.

A gliotic pseudocapsule surrounds the tumour. A well demarked plane of cleavage is usually evident (Lang 2004). Tumour is usually moderately adherent to brain. This description reflects the slip elastogram findings where slip was evident in some areas following compression of approximately 2.5N.

8 out of 10 patients with primary gliomas that were predominantly solid had the tumour encased within the brain substance. This is to be expected as primary gliomas invade as well as cause space occupation, thus the brain tumour interface would be more difficult to define.

One of the important issues to mention is that all data analysis was performed retrospectively. None of the images had any bearing on patient management. Based on this study it should be technically feasible to develop a near real-time slip elastogram system in the near future.

7.5 Conclusion

This study has shown that slip elastography is able to identify the anatomical location of a slip boundary and measure a derivative of the frictional force acting at the boundary *in vivo* during brain tumour resection. It is possible that with further development slip elastography may act as an intra-operative adjunct during tumour resection to ensure safe and complete macroscopic resection.

Chapter 8

Discussion

8.1 Introduction

The purpose of this project was to evaluate the use of ultrasound elastography intra-operatively during brain tumour resection. At the beginning of the project there were no published reports relating to this subject. Since then there have been two groups that have reported on its use to assist in brain tumour resection (Sellbeck 2005, Scholz 2006). The work reported in this thesis began without knowledge of the other groups and conducted independently of them.

This project stands alone as an original contribution that may help in the intra-operative detection of brain tumours. This chapter will discuss why this is the case.

The decision to develop slip elastography was based on a specific lack of information expressed by a number of neurosurgeons when resecting brain tumours. To date this is the only mechanical imaging technique that has been developed and investigated for use in the pre-operative planning of resection of brain tumours. This chapter will discuss how this technique may enhance tumour resection.

8.2 The use of ultrasound elastography intra-operatively during brain tumour resection

As outlined in chapter 2 there is now reasonably compelling evidence that brain tumours should be resected. There is evidence that gross total tumour resection confers a survival advantage to the patient when compared to partial resection of malignant gliomas however this evidence is based on a number of controlled studies, all of which may be prone to selection bias. The current practice of most neurosurgeons involves complete macroscopic excision where appropriate and feasible.

Within this thesis it has been hypothesized that tumour has different stiffness characteristics in contrast to normal brain, and that this difference in stiffness can be detected using ultrasound elastography. At the start of this project there were no *in vivo* published data looking at the stiffness of tumour compared to brain. As mentioned earlier there are now two published series relating to this topic, in addition to the work reported here. Our series provides the only data where any comparative study has been performed. Stiffness of tumour and brain using the surgeon's evaluation of stiffness of tumour and brain were compared to the ultrasound elastogram findings in all cases. Furthermore, in a number of cases tissue was mechanically tested to provide a more objective measure of stiffness. Although the surgical evaluation is a subjective assessment, it is appropriate and important to utilize this as a reference for comparison since it represents

current practice. It is important to note that the surgeon exclusively uses this assessment of stiffness in combination with visual inspection to determine whether to resect tissue or not in the majority of cases. Intra-operative scanning of any kind is not widely used at present and intra-operative mechanical imaging methods are non-existent in routine surgery.

It is unfortunate that it was not possible to obtain more tumour and brain samples for mechanical testing. However, the results presented here demonstrate that tumour and brain in the experimental conditions described exhibit a highly non linear stress strain relationship. It would be difficult, given this constraint to compare the stress strain relationship between tissue samples i.e. it would be difficult to ascertain a quantitative value that determines which sample is stiffer. Furthermore, it is not known whether measurement from an *ex vivo* sample is representative of the mechanical properties *in vivo*. Thus mechanical testing *ex vivo* was not utilized as a gold standard. Further studies aiming to characterize the stress strain relationship are likely to enable *ex vivo* mechanical testing to become the gold standard at measurement of stiffness. Technical constraints such as the most appropriate mechanical testing methods to be used when testing small irregularly cut samples of soft tissue would also need to be addressed. The effect of removal of blood supply and how this affects stiffness would also need to be addressed. This work was outside of the scope of this thesis.

This thesis is the first to describe mechanical properties of brain and brain tumour in humans.

The results demonstrate that ultrasound elastography can image relative stiffness of components within a scan plane intra-operatively during brain

tumour resection. This is the first study to demonstrate this. An extremely important point that is not widely discussed in the literature is that tumours are not invariably stiffer that normal tissue. This study has demonstrated the extent of tumour stiffness heterogeneity in the context of brain tumours. Yet many of the other clinical applications of ultrasound elastography discussed in chapter 1 have assumed that tumour is stiffer than surrounding tissue. The results presented in this thesis clearly demonstrate that, in the case of brain tumours, this is not the case. There is a definite and important requirement for this type of comparative data in the context of other applications of ultrasound elastography. Otherwise there may well be a reduction in sensitivity and specificity of ultrasound elastography when aimed at detecting tumour and discriminating tumour type.

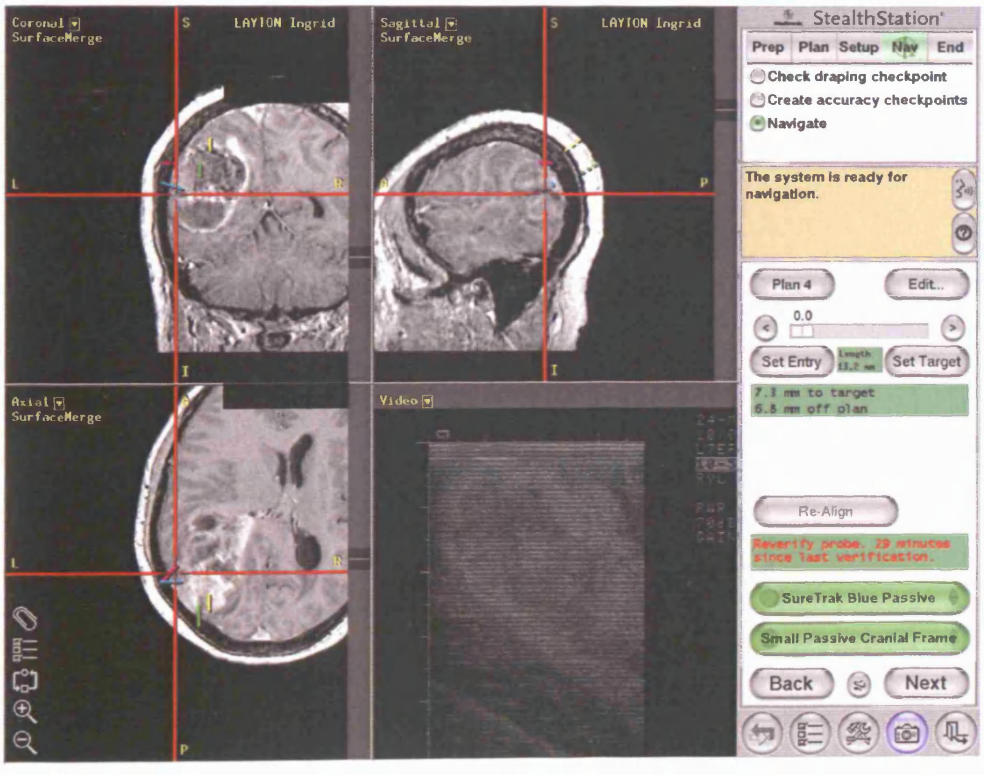

Figure 8.1 StealthStation™ screenshot of patient 4 demonstrating how the tumour heterogeneity seen on MRI is likely to be related to stiffness heterogeneity

The MRI appearances of many tumours demonstrate heterogeneity within tumour (figure 8.1).

It is interesting to note that the stiffness of brain tumours is extremely heterogeneous even within a tumour. For intrinsic tumours this is intuitively correct as one of the hallmarks of high grade gliomas is necrosis. Necrosis is the macroscopic consequence of cell death. Thus the structural integrity of the tissue is damaged. This is likely to have a profound effect on stiffness. Our studies corroborate with this assertion. The MRI appearances may reflect this tumour stiffness heterogeneity.

Many tumours, intrinsic and extrinsic, undergo heterotopic calcification. Calcified areas are subjectively stiffer than normal tissue, however the process does not usually occur homogeneously throughout the tumour thus leading to areas of different stiffness within the tumour. This effect was seen in patient 1. Tumour stiffness heterogeneity in contrast to brain stiffness homogeneity may be an alternative approach to identify the brain tumour interface using ultrasound elastography.

This study demonstrates that it is incorrect to assume that brain tumours are stiffer than normal brain. Thus it does put into question the utility of ultrasound elastography intra-operatively prior to brain tumour resection. In addition there are a number of imaging modalities that assist in directing the surgeon to the brain tumour interface prior to commencing tumour resection. These include neuro-navigation, and intra-operative imaging such as intra-operative ultrasound, CT and MRI. The findings in this thesis were that intra-operative ultrasound was superior to conventional ultrasound elastography at its current stage of development, at demarcating the brain

tumour interface. In this small study, using the technique described, given the current technical constraints, ultrasound elastography was not as useful as other imaging techniques at detecting the brain tumour interface.

However there are a number of factors that may improve the performance of ultrasound elastography at detection of the brain tumour interface prior to tumour resection.

Ultrasound elastography is a growing field with technical advances occurring continuously. Currently, the image quality of the elastograms is poor when compared to other imaging modalities such as MRI or CT, which have had many decades of technical development to reach their current state of maturity. This will improve with improving technologies.

An exciting development is radiation force elastography where an acoustic impulse is used to create a strain at depth. There is no requirement for an externally applied stress. This technique could counter many of the artifacts seen using conventional ultrasound elastography. For example, stress dissipation as a result of slip boundaries would no longer occur as the strain could be generated beyond the slip boundary. Stress concentration that often occurs surrounding a very stiff inclusion could also be reduced by this technique. Figure 8.2 shows an elastogram produced in the paper by Melodelima et al (2006) using radiation force elastography.

This technique could have important advantages in the context of tumour neurosurgery. Compression of brain would no longer be required. Adherence of tumour to brain would no longer have an effect on the elastograms produced and the presence of fluid cysts would no longer have

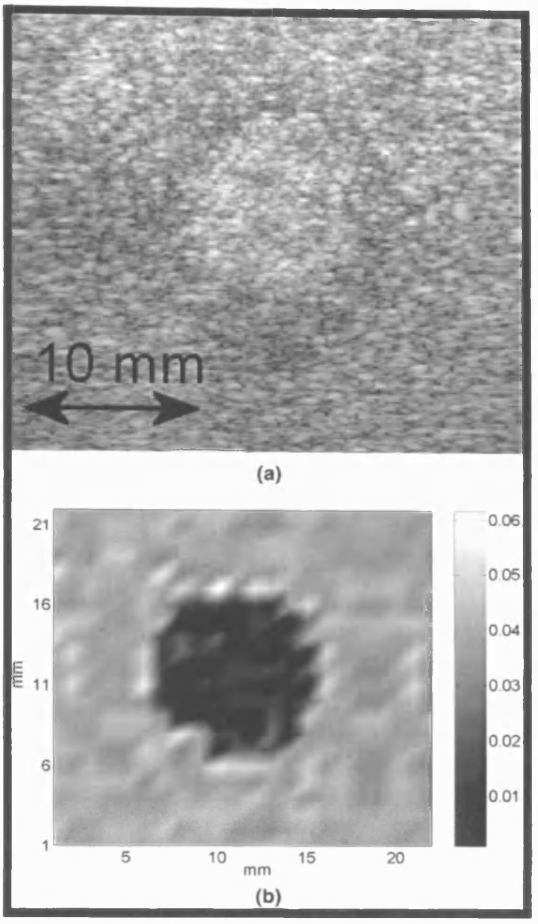

Figure 8.2 B mode image and radiation force elastogram
(reproduced with permission of the authors from MelodeLima et al, 2006)

an effect on the elastogram quality deep to the cyst. Work is in progress to develop a system that could potentially be used intra-operatively.

There is a great deal of interest in multimodality image fusion. Ultrasound is among the most cost effective intra-operative methods for imaging. Its utilization has not been universal as image interpretation can be difficult and the image is not usually referenced to anatomical landmarks. Fusion with historically acquired MRI as demonstrated in this thesis overcomes some of these problems. However brain shift and tissue removal limit the accuracy of the MRI. There are a number of groups that are attempting to alter the MRI using real-time ultrasound data. This type of technology would preclude the requirement for expensive intra-operative scanners such as

MRI. The use of ultrasound elastography intra-operatively would have to be proven to be clinically useful before being applied to this kind of multimodality fusion imaging technique.

The intra-operative use of ultrasound elastography following tumour resection may well be an important application of ultrasound elastography. In this thesis one patient had ultrasound elastography performed following tumour resection. Currently there are few methods for confirming completeness of tumour resection intra-operatively. Yet there is evidence to suggest that partial tumour resection confers a poorer prognosis to the patient (see chapter 2).

Many surgeons biopsy the margins and obtain a frozen section (Folkerth 1994) however this can be time consuming and the whole of the resection margin cannot be assessed. Intra-operative MRI gives excellent image quality (Nimsky 2004) but is not widely available. Intra-operative B mode ultrasonography is difficult to interpret following tumour resection and so is not reliable (Keles 2003). The difference in tumour stiffness compared to brain may be a physical property that can be visualized using ultrasound elastography following tumour resection to assess extent of tumour resection intra-operatively.

The results from chapter 5 demonstrate that certain algorithms can be implemented with adequate speed to produce real-time ultrasound elastograms. The algorithm used to produce real-time elastograms using the Medison™ scanner was not known. This aspect of the thesis demonstrated that it is feasible to perform ultrasound elastography intra-operatively during

brain tumour resection producing images that could be potentially clinically useful. This illustrates the level of technical development of the technique.

The images produced using the real-time elastogram algorithm provided similar information to images produced using off-line processing. The main difference was that the off-line processed algorithm was more flexible and provided superior image resolution. This tradeoff in image quality will be the determinant of the utility of the technique in clinical practice.

A freehand ultrasound elastography palpation technique was used in all experiments. The consequence of excessive force applied to the surface of the brain, in contrast to other parts of the body, are potentially catastrophic. The other two groups presenting the use of ultrasound elastography intra-operatively during brain tumour resection used different methods for application of a strain. The freehand technique used here has been shown to be safe in the hands of neurosurgeons. It is far simpler that other techniques requiring low amplitude compression. This makes this technique far more attractive to the neurosurgeon. In the future it may be possible to produce elastograms without application of external axial compression using the technique of radiation force elastography.

An important point is whether the implementation of ultrasound elastography intra-operatively during brain tumour resection improves completeness of resection of brain tumours and whether this makes brain tumour resection safer. Based on the results from chapter 4 and 5 it is not possible to draw conclusions on this point as the sample size was too small. We can conclude that ultrasound elastography is able to distinguish tissue of different stiffness confirming part of the hypothesis. This part of the thesis

also revealed the heterogeneity within tumours in terms of stiffness. This property of tumour stiffness heterogeneity may be exploited by ultrasound elastography to assist in differentiating tumour from brain.

The first part of the hypothesis that relative tumour stiffness can be imaged using ultrasound elasticity imaging techniques intra-operatively during brain tumour resection has been proven.

8.3 The use of slip elastography intra-operatively during brain tumour resection

Slip elastography was conceived following the analysis of results obtained using ultrasound elastography intra-operatively during brain tumour resection in patients 1 and 2. It must be appreciated that the surgeon will almost always find the tumour once craniotomy has been performed. Thus ultrasound elastography would have no role in pre-resection anatomical identification unless its image quality in terms of tissue contrast and resolution outperforms echography, and makes the images easier to interpret, more like MRI. The presence of tumour stiffness heterogeneity is also not a physical property that is particularly clinically useful to the surgeon prior to resection as the surgeon is likely to resect the tumour

irrespective of the stiffness. Most other uses of ultrasound elastography have concentrated on the stiffness differences as a diagnostic investigation. When used intra-operatively during brain tumour resection diagnosis is of secondary importance at the time of operation. Identification of the brain tumour interface is the critical property to assess where ultrasound elastography may be useful.

Slip elastography was thus developed specifically to identify the anatomical location and mechanical properties of the brain tumour interface. It was felt that this information could potentially assist the surgeon in avoiding complications and assist when attempting complete macroscopic excision.

The results have demonstrated, both *in vitro* and *in vivo*, that slip elastography can identify the anatomical location and the adherence between the two surfaces of a slip boundary. It remains to be seen whether this is a clinically useful technique.

Chapter 6 discusses the development of the system for creating slip elastograms from its theoretical basis to the testing of the system *in vitro*. It was not possible to implement directly the definition of slip into the system as the resolution was too poor. Thus modifications were made to help discriminate slip from non slip shear. The problem lies in the resolution of RF data at the slip boundary. A surface will reflect acoustic signals creating the appearance of a larger slip boundary. This problem is not easy to rectify using an ultrasound-based system.

It is important to note that slip elastography is only a semi-quantitative measure of adherence at a slip boundary. Other forces acting at the slip boundary include gravity. In order to incorporate the effect of gravity,

knowledge of the mass acting at the slip boundary would be required. The system has been based on a two dimensional unconstrained model of slip. However all biological materials where this technique is likely to be used will have tissue elasticity and peripheral constraints in the same image plane as well as in the elevational plane. These constraints are much more difficult to quantify accurately. Despite these problems the magnitude of externally applied force that is required to produce slip is potentially a useful semi-quantitative measure of adherence at the slip boundary. A finite element analysis incorporating measurable constraints could be developed but the results are unlikely to provide accurate data *in vivo* as there would be too many unknown parameters.

The slip elastography system was applied intra-operatively during brain tumour surgery on 22 patients as described in chapter 7. The results demonstrate that the anatomical location of a slip boundary can be visualized and that the adherence at that boundary can be measured semi-quantitatively.

A drawback of the current system is the image quality. Furthermore images can only be produced off-line following a great deal of processing. Thus, as the technique stands it is not possible to obtain clinically useful information. As has been demonstrated with conventional ultrasound elastography however, there is likely to be an evolution resulting in improved image quality, faster data processing and perhaps even a different method of excitation to produce slip. This will be subject to the success of future studies.

The method of palpation, potentially, may cause damage to underlying brain if too great a force is applied. It would be preferable if this was not the case. A technique based on radiation force elastography where tissue is pushed at a specific depth, and deep to the focus of the pushing impulse slip is detected, could potentially be developed to counter this problem. The magnitude of the radiation force required to produce slip could then be used to provide a semi quantitative measure of the adherence.

There is no objective measure of adherence between tumour and brain. Thus, it was necessary to obtain the opinion of the surgeon, however subjective, on the adherence of tumour to brain.

Slip elastography was able to identify the anatomical location of the brain tumour interface and provide a semi quantitative measure of adherence between tumour and brain at this interface. Thus the second part of the hypothesis that adherence of tumour to brain can be imaged using ultrasound elasticity imaging techniques intra-operatively during brain tumour resection has been proven.

8.4 The contribution made by this work

The thesis has critically analyzed the mechanical properties of brain and tumour and used a number of techniques to image them.

It has been shown that tumour stiffness can be imaged using ultrasound elastography. The stiffness of tumour has been shown to be very heterogeneous. It has been shown that the real-time elastography system used is appropriate for clinical use during tumour resective surgery.

Slip elastography has been developed from theory, *in vitro* experimentation to *in vivo* testing. The results demonstrate that slip elastography can identify the anatomical location of a slip boundary within an ultrasound plane and provide a semi-quantitative measure of adherence at that slip boundary. Slip elastography was able to identify slip boundaries and measure adherence *in vivo* at the brain tumour interface prior to tumour removal.

8.5 Future work

This thesis opens up a number of avenues for continued research into the subject of mechanical imaging applied to neurosurgery. Important hurdles need to be overcome before this type of technique becomes clinically useful. Image quality appears to be one of the major obstacles at present. The off-line processed elastograms, the real-time elastograms and the slip elastograms were generally inadequate for clinical practice currently. Image quality will improve with continued development. Certainly the images produced using radiation force elastography look very promising. It would be of value to develop a radiation force elastography system that is able to

perform ultrasound elastography and slip elastography and is handheld. This would be a considerable technical challenge however.

It would be mandatory to develop a real-time or near real-time slip elastography system for the technique to prove its clinical utility. This should be achievable by using faster computing hardware and/or more efficient displacement tracking algorithms.

There is a huge void of information on the biomechanical properties of the brain and tumour. Yet many techniques such as finite element analysis modelling of brain tumours and mechanical imaging are reliant of this type of data. It would be important to step back and develop more cohesive generalizations on the biomechanical properties of brain and brain tumours based on experimental mechanical testing. Only then would the true nature of the images produced be appreciated.

Ultrasound elastography may well have clinical utility at evaluating post resection tumour residual. Slip elastography, on the other hand, may have clinical utility during the planning part of tumour resection.

Some centres are beginning to develop three dimensional elastography (Lindop 2006). The development of three dimensional elastography would potentially have two major advantages. In the short term this three dimensional displacement tracking could be utilized to enhance two dimensional ultrasound elastography. Out of plane motion could thus be accounted for and incorporated into the algorithm to minimise decorrelation. This would be useful in the context of slip elastography as slip is likely to occur in an out of plane direction. In the longer term three dimensional

ultrasound elastography could provide volumetric maps of tumour based on stiffness differences.

The ultimate vision would be of a real-time multimodality system. This would be based on radiation force elastography. It would provide three dimensional mechanical imaging data. It would incorporate three dimensional stiffness measurements using ultrasound elastography and slip boundary anatomical and semi quantitative adherence measurements using three dimensional slip elastography.

The ultrasound images would provide three dimensional data in the form of multiple slices so as to improve image interpretability thus precluding the requirement for intra-operative MRI.

8.6 Concluding remarks

This thesis has described the use of ultrasound elastography to image stiffness differences within an ultrasound plane intra-operatively during brain tumour resection.

It has also described the development of slip elastography from theory, *in vitro* testing to *in vivo* testing to detect the anatomical location of slip boundaries and to measure adherence at the slip boundary.

Both parts of the hypothesis, that brain tumour heterogeneity and adherence of tumour to brain can be imaged using ultrasound elasticity imaging techniques intra-operatively during brain tumour resection, have been proven.

Chapter 9

References

Chapter 9

References

1) Albert FK, Forsting M, Sartor K, Adams H-P, Kunze S. Early postoperative magnetic resonance imaging after resection of malignant glioma: objective evaluation of residual tumour and its influence on regrowth and prognosis. Neurosurgery 1994; 34: 45-61.

2) Alvernia JE, Sindou MP. Preoperative neuroimaging findings as a predictor of the surgical plane of cleavage: prospective study of 100 consecutive cases of intracranial meningioma. Journal of Neurosurgery 2004; 100: 422-430.

3) Bamber J, Hasan P, Cook-Martin G, Bush N (1988) Parametric imaging of tissue shear and flow using B-scan decorrelation rate. J Ultrasound Med; 7(No.10 Suppl.):S135.

4) Bamber JC, Barbone PE, Bush NL, Cosgrove DO, Doyely MM, Fuechsel FG et al. Progress in freehand elastography of the breast. IEICE Trans Inf & Syst 2002; E85D(1): 5-14.

5) Bamber, J.C. and Daft, C. Adaptive filtering for reduction of speckle in pulse-echo images. Ultrasonics 1986; 24: 41-44.

6) Barnett GH. Surgical Navigation for Brain tumours, in Winn RH (Ed): Youmanns Neurological Surgery (5th Ed). Philadelphia, Saunders, 2004, 941-949.

7) Bilgen M. Dynamics of errors in 3D motion estimation and implications for strain-tensor imaging in acoustic elastography. Phys. Med. Biol. 2000; 45: 1565-1578.

8) Bilston LE, Liu Z, Phan-Thien N. Linear viscoelastic properties of bovine brain tissue in shear. Biorheology 1997; 34(6): 377-385.

9) Carter TJ, Sermesant M, Cash DM, Barratt DC, Tanner C, Hawkes DJ. Application of soft tissue modelling to image-guided surgery. Med Eng Phys. 2005; 27(10):893-909.

10) Chacko AG, Kumar NKS, Chacko G, Athyal R, Rajshekhar V. Intra-operative ultrasound in determining the extent of resection of parenchymal brain tumours – a comparative study with computed tomography and histopathology. Acta Neurochirurgica 2003; 145: 743-748.

11) Chakraborty A, Bamber JC, Berry G, Bush N, Dorward NL. Intra-operative ultrasound elastography and registered magnetic resonance imaging of brain tumours; a feasibility study. In: Proceedings of the 3rd

International Conference on the ultrasonic measurement and imaging of tissue elasticity. Lake Windemere, UK, 2004; 1:57.

12) Chakraborty A, Berry G, Bamber J, Dorward N. Intra-operative ultrasound elastography and registered magnetic resonance imaging of brain tumour; a feasibility study. Ultrasound 2006; 14(1): 43-49.

13) Choi IS, Tantivatana J. Neuroendovascular management of intracranial and spinal tumours. Neurosurgery Clinics of North America 2000; 11(1): 167-185.

14) Coutts L, Bamber J, Miller N, Mortimer P. Ultrasound elastography of the skin and subcutis under surface extensive loading. Ultrasound 2006; 14(3): 161-166.

15) Coats B, Margulies SS. Material properties of porcine parietal cortex. J Biomech. 2006;39(13):2521-5.

16) Demuth T, Berens ME. Molecular mechanisms of glioma cell migration and invasion. Journal of Neuro-oncology 2004; 70(2): 217-228.

17) Devaux BC, O'Fallon JR, Kelly PJ Resection, biopsy, and survival in malignant glial neoplasms. A retrospective study of clinical parameters, therapy, and outcome. J Neurosurg. 1993 May;78(5):767-75.

18) Dickinson RJ, Hill CR. Measurement of soft tissue motion using correlation between A-scans. Ultrasound in medicine and biology 1982; 8: 263-271.

19) Dorward NL, Alberti O, Palmer JD, Kitchen ND, Thomas DGT. Accuracy of true frameless stereotaxy: *in vivo* measurement and phantom studies. Journal of Neurosurgery 1999; 90: 160-168.

20) Dorward NL, Alberti O, Velani B, Gerritsen FA, Harkness WFJ, Kitchen ND et al. Postimaging brain distortion: magnitude, correlates and impact on neuro-navigation. Journal of Neurosurgery 1998; 88: 656-662.

21) Doyley MM, Bamber JC, Fuechsel F, Bush NL. A freehand elastographic approach for clinical breast imaging; system development and performance evaluation. Ultrasound Med Biol 2001;27:1347-1357.

22) Estes, M.S. and McElhaney J.H., Response of Brain Tissue of Compressive Loading, ASME Paper No. 70-BHF-13, 1970.

23) Galford, J.E. and McElhaney, J.H., A Viscoelastic Study of Scalp, Brain and Dura. J. Biomech., 1970, 3, 211-221

24) Garra BS, Cespedes IE, Ophir J, Spratt SR, Zuurbier RA, Magnant CM et al. Elastography of breast lesions: Initial Clinical Results. Radiology 1997; 202: 79-86.

25) Gronningsaeter A, Kleven A, Ommedal S, Aarseth TE, Lie T, Lindseth F et al. SonoWand, an ultrasound-based Neuro-navigation system. Neurosurgery 2000; 47(6): 1373-1379.

26) Hamhaber U, Sack I, Papazoglou S, Rump J, Klatt D, Braun J. Three-dimensional analysis of shear wave propagation observed by *in vivo* Magnetic resonance imaging of the brain. Acta Biomaterialia 200; 3(1): 127-137.

27) Hiltawsky KM, Kruger M, Starke C, Heuser L, Ermert H, Jensen A. Freehand ultrasound elastography of breast lesions: clinical results. Ultrasound in medicine and biology 2001; 27: 1461-1469.

28) Itoh A, Ueno E, Tohno E, Kamma H, Takahashi H, Shiina T et al. Breast Disease: clinical application of US Elastography for diagnosis. Radiology 2006; 239(2): 341-350.

29) Jeremic B, Grujicic D, Antunovic V, Djuric L, Stojanovic M, Shibamoto Y. Influence of extent of surgery and tumor location on treatment outcome of patients with glioblastoma multiforme treated with combined modality approach. J Neurooncol. 1994;21(2):177-85.

30) Kallel F, Ophir J. A least squares strain estimator for elastography. Ultrasound Imaging 1997; 19(3): 195-208.

31) Kehler U, Arnold H, Muller H. Long term follow-up of infratentorial pilocytic astrocytoma.Neurosurgical Review 1990; 13(4):, 315-320.

32) Keles EG, Anderson B, Berger MS. The effect of extent of resection on time to tumour progression and survival in patients with glioblastoma multiforme of the cerebral hemisphere. Surgical Neurology 1999; 52: 371-379.

33) Keles EG, Lamborn KR, Berger MS. Low-grade hemispheric gliomas in adults: a critical review of resection as a factor influencing outcome. Journal of Neurosurgery 2001; 95: 735-745.

34) Keles GE, Chang EF, Lamborn KR, Tihan T, Chang CJ, Chang SM, Berger MS. Volumetric extent of resection and residual contrast enhancement on initial surgery as predictors of outcome in adult patients with hemispheric anaplastic astrocytoma. J Neurosurg. 2006 Jul;105(1):34-40.

35) Keles GE, Labmorn KR, Berger MS. Coregistration accuracy and detection of brain shift using intraoperative sononavigation during resection of hemispheric tumours. Neurosurgery 2003; 53(3): 556-562.

36) Kelly PJ, Hunt C. The limited value of cytoreductive surgery in elderly patients with malignant gliomas. Neurosurgery. 1994 Jan;34(1):62-6.

37) Konig K, Scheipers U, Pesavento A, Lorenz A, Ermert H, Senge T. Initial experiences with real-time elastography guided biopsies of the prostate. Journal of Urology 2005; 174(1): 115-117.

38) Konofagou E, Harrigan T, Ophir J. Shear strain estimation and lesion mobility assessment in elastography. Ultrasonics 2000; 38: 400-404.

39) Konofagou E, Ophir J. A new elastographic method for estimation and imaging of lateral displacements, lateral strains, corrected axial strains and Poisson's Ratios in Tissues. Ultrasound Med Biol 1998; 24(8): 1183-1199.

40) Konofagou E, Ophir J. Precision estimation and imaging of normal and shear components of the 3D strain tensor in Elastography. Phys. Med. Biol. 2000; 45: 1553-1563.

41) Kreth FW, Berlis A, Spiropoulou V, Faist M, Scheremet R, Rossner R, Volk B, Ostertag CB. The role of tumor resection in the treatment of glioblastoma multiforme in adults. Cancer. 1999 Nov 15;86(10):2117-23.

42) Kreth FW, Warnke PC, Scheremet R, Ostertag CB. Surgical resection and radiation therapy versus biopsy and radiation therapy in the treatment of glioblastoma multiforme. J Neurosurg. 1993 May;78(5):762-6.

43) Krouskop TA, Wheeler TM, Kallel F, Garra BS, Hall T. Elastic moduli of breast and prostate tissues under compression. Ultrasonic Imaging. 1998 Oct;20(4):260-74.

44) Kyriacou SK, Mohamed A, Miller K, Neff S. Brain mechanics for neurosurgery: modelling issues. Biomech Model Mechanobiol. 2002; 1(2):151-64.

45) Lacroix M, Abi-Said D, Fourney DR, Gokaslan ZL, Shi W, DeMonte F et al. A multivariate analysis of 416 patients with glioblastoma multiforme: prognosis, extent of resection and survival. Journal of Neurosurgery 2001; 95(2): 190-198.

46) Lang FF, Chang EL, Abi-Said D et al. Metastatic Brain tumours, in Winn RH (Ed): Youmanns Neurological Surgery (5th Ed). Philadelphia, Saunders, 2004, 1077-1097.

47) Laws ER, Parney IF, Huang W, Anderson F, Morris AM, Ashre A et al. Survival following surgery and prognostic factors for recently diagnosed malignant glioma: data from the glioma outcomes project. Journal of neurosurgery 2003; 99: 467-473.

48) Leighton C, Fisher B, Bauman G, Depiero S, Stitt L, Macdonald D et al. Supratentorial low-grade glioma in Adults: an analysis of prognostic factors

and timing of radiation. Journal of clinical Oncology 1997; 15(4): 1294-1301.

49) Lerner R, Huang S, Parker K. Sonoelasticity images derived from ultrasound signals in mechanically vibrated tissues. Ultrasound in medicine and biology 1990; 16: 231-239.

50) Lindop JE, Treece GM, Gee AH, Prager RW. 3D elastography using freehand ultrasound. Ultrasound Med Biol. 2006 Apr;32(4):529-45.

51) Lyshchik A, Higashi T, Asato R, Tanaka S, Ito J, Mai JJ et al. Thyroid gland tumor diagnosis at US elastography. Radiology 2005; 237(1): 202-211.

52) Makuuchi M, Torzilli G, Machi J. History of intra-operative ultrasound. Ultrasound in Medicine and Biology 1998; 24(9):1229-1242.

53) McCracken PJ, Manduca A, Felmlee J, Ehman RL. Mechanical transient-based magnetic resonance elastography. Magn Reson Med. 2005;53(3):628-39.

54) Melodilima D, Bamber JC, Duck FA, Shipley JA, Xu L. Elastography for breast cancer diagnosis using radiation force: System development and performance evaluation. Ultrasound in medicine and biology 2006; 32(3): 387-396.

55) Melodilima D, Bamber J, Berry G, Bush N, Duck F, Shipley J, Xu L. Transient radiation force elastography: a preliminary comparison with surface palpation elastography. In: Proceedings of the 5th International Conference on the ultrasonic measurement and imaging of tissue elasticity. Utah, USA, 2006; 1:57.

56) Mikkelsen T, Enam SA, Roseblum ML. Invasion in malignant glioma. . in Winn RH (Ed): Youmanns Neurological Surgery (5th Ed). Philadelphia, Saunders, 2004, 757-770.

57) Muthupillai R, Ehman RL. Magnetic resonance elastography. Nature medicine 1996; 2(5): 601-603

58) Nightingale K, Soo MS, Nightingale R, Trahey G. Acoustic radiation force impulse imaging; in vivo demonstration of clinical feasibility. Ultrasound in medicine and biology. 2002; 28(2): 227-235.

59) Nimsky C, Fujita A, Ganslandt O, von Keller B, Fahlbusch R. Volumetric assessment of glioma removal by intra-operative high-field magnetic resonance imaging. Neurosurgery 2004; 55(2): 358-370.

60) Nimsky C, Ganslandt O, Cerny S, Hastreiter P, Greiner G, Fahlbusch R. Quantification of, visualization of, and compensation for brain shift using intraoperative magnetic resonance imaging. Neurosurgery 2000; 47(5): 1070-1079.

61) Nitta T, Sato K. Prognostic implications of the extent of surgical resection in patients with intracranial malignant gliomas. Cancer. 1995 Jun 1;75(11):2727-31.

62) Ophir J, Cespedes I, Ponnekanti H, Yazdi Y, Li X. Elastography: a quantitative method for imaging the elasticity of biological tissues. Ultrason Imaging 1991; Apr;13(2):111-34

63) Pena A, Bolton MD, Whitehouse H, Pickard JD. Effects of brain ventricular shape on periventricular biomechanics: a finite-element analysis. Neurosurgery. 1999; 45(1):107-16.

64) Pesavento A, Lorenz A, Siebers S, Ermert H. New real-time strain imaging concepts using diagnostic ultrasound. Physics in medicine and biology 2000; 45: 1423-1435.

65) Pesavento A, Perrey C, Krueger M, Ermert H. A time efficient and accurate strain estimation concept for ultrasonic elastography using iterative phase zero estimation. IEEE transactions Ferroelectr. Freq. control 1999;46: 1057-1067.

66) Prange MT, Margulies SS. Regional, directional and age-dependent of the brain undergoing large deformation. Journal of biomechanical engineering 2002; 124(2): 244-252.

67) Quigley MR, Maroon J. The relationship between survival and the extent of the resection in patients with supratentorial malignant gliomas. Neurosurgery 1991; 29(3): 385-388.

68) Quinn M, Babb P, Brock A, Kirby L, Jones J. Cancer Trends in England and Wales 1950-1999. Studies on Medical and Population Subjects No. 66. Office for national Statistics. Crown Copyright 2001.

69) Ribalta T, Fuller GN. Brain tumours: an overview of histopathological classification. in Winn RH (Ed): Youmanns Neurological Surgery (5th Ed). Philadelphia, Saunders, 2004, 661-672.

70) Righetti R, Kumar TA, Srinivasan S, Ophir J, Krouskop TA. Novel strain elastographic techniques. 4th international conference on the ultrasonic measurement and imaging of tissue elasticity. Lake Travis, USA, 2005.

71) Rouviere O, Yin M, Dresner MA, Rossman PJ, Burgart LJ, Fidler JL, Ehman RL. MR Elastography of the liver: preliminary results. Radiology 2006; 240(2): 440-448.

72) Sahay, K.B., Mehrotra, R., Sachdeva, U. and Banerji, A.K., Elastomechanical Characterization of Brain Tissues. J. Biomechanics. 1992, 25, 319-326.

73) Sampath P, Long DM. Acoustic neuroma, in Winn RH (Ed): Youmanns Neurological Surgery (5th Ed). Philadelphia, Saunders, 2004, 1147-1168.

74) Scholz M, Fricke B, Monnings P, Brendel B, Schmieder K, Siebers S, von During M, Ermert H, Harders A. Vibrography: first experimental results in swine brains. Minim Invasive Neurosurg. 2004 Apr;47(2):79-85.

75) Scholz M, Noack V, Pechlivanis I, Engelhardt M, Fricke B, Linstedt U et al. Vibrography during tumour neurosurgery. Journal of ultrasound in medicine 2005; 24: 985-992.

76) Selbekk T, Bang J, Unsgaard G. Strain processing of intraoperative ultrasound images of brain tumours: initial results. Ultrasound in medicine and biology 2005; 31(1): 45-51.

77) Shiina T, Nitta N, Ueno E, Bamber JC, Real-time tissue elasticity imaging using the combined autocorrelation method. Journal of Medical Ultrasonics 2002; 29: 119-128.

78) Shinoura N, Takahashi M, Yamada R. Accurate characterization of the main trunk of the anterior cerebral artery by means of intraoperative sononavigation with Doppler sonography: implications for brain tumor surgery. J Ultrasound Med. 2005 Nov;24(11):1527-32.

79) Simon C, VanBaren P, Ebbini ES. Two-dimensional temperature estimation using diagnostic ultrasound. IEEE Transactions on ultrasonics, ferroelectrics and frequency control 1998; 45: 1088-1099.

80) Simpson JR, Horton J, Scott C, Curran WJ, Rubin P, Fischbach J et al. Influence of location and extent of surgical resection on survival of patients with glioblastoma multiforme: results of three consecutive Radiation Therapy Oncology Group (RTOG) clinical trials. Int J Radiat Oncol Biol Phys. 1993 May 20:26(2):239-44.

81) Sinkus R, Tanter M, Xydeas T, Catheline S, Bercoff J, Fink M. Viscoelastic shear properties of *in vivo* breast lesions measured by MR elastography. Magnetic resonance imaging 2005; 23: 159-165.

82) Souchon R, Rouviere O, Gelet A, Detti V, Srinivasan S, Ophir J et al. Visualization of HIFU lesions using elastography of the human prostate *in vivo*: preliminary results. Ultrasound in medicine and biology 2003; 29(7): 1007-1015.

83) Svennson WE, Amiras DG, Shousha S, Rattansingh A, Chopra D, Sinnett HD et al. Elasticity imaging of 67 cancers and 167 benign breast lesions shows that it could halve biopsy rates of benign lesions. In: Proceedings of the 4th International Conference on the ultrasonic measurement and imaging of tissue elasticity. Austin, Texas, USA, 2005; 1:87.

84) Thitaikumar A, Ophir J, Krouskop TA, Garra BS. Interface bonding strength in axial-shear strain elastography. 5th international conference on the ultrasonic measurement and imaging of tissue elasticity. Snowbird, Utah, USA 2006.

85) Thitaikumar TA, Ophir J, Krouskop TA. Comparison between axial elastograms of a connected and disconnected inclusion in homogeneous background: Simulation study. 4th international conference on the ultrasonic measurement and imaging of tissue elasticity, Lake Travis, USA, 2005.

86) Thitaikumar TA, Righetti R, Krouskop TA, Ophir J. Resolution of axial shear strain elastography. Physics in medicine and biology; 51: 5245-5257.

87) Toms SA, Ferson DZ, Sawaya R. Basic surgical techniques in the resection of malignant gliomas. Journal of Neuro-oncology 1999; 42: 215-226.

88) Tristam M, Barbosa DC, Cosgrove DO, Bamber JC, Hill CR. Application of Fourier analysis to clinical study of patterns of tissue movement. Ultrasound in medicine and biology 1988; 14: 695-707.

89) Van Den Hauwe L, Parizel PM, Martin JJ, Cras P, De Deyn P, De Schepper AMA. Postmortem MRI of the brain with neuropathological correlation. Neuroradiology 1995; 37: 343-349.

90) Van Velthoven. Intraoperative ultrasound imaging: comparison of pathomorphological findings in US versus CT, MRI and intraoperative findings. Acta Neurochirurgica Supplement 2003; 85: 95-99.

91) Velardi F, Fraternali F, Angelillo M. Anisotropic constitutive equations and experimental tensile behavior of brain tissue. Biomech Model Mechanobiol. 2006; 5(1): 53-61.

92) Vuorinen V, Hinkka S, Farkkila, LaaskelainenJ. Debulking or biopsy of malignant glioma in elderly people-a randomised study. Acta Neurochirurgica 2003; 145: 5-10.

93) Walker MD, Green SB, Byar DP, Alexander E, Batzdorf U, Brooks WH et al. Randomized comparisons of radiotherapy and nitrosureas for the treatment of malignant glioma after surgery. The new England journal of medicine 1980; 303(23): 1323-1329.

94) Weingart J, Brem H. Basic principles of cranial surgery for brain tumours. P899-907. In Youmann's Neurological Surgery 5th Edition. Ed RH Winn. 2004 Elsevier, Philadelphia, USA.

95) Whittle IR, Basu N, Grant R, Walker M, Gregor A. Management of patients aged >60 years with malignant glioma: good clinical status and radiotherapy determine outcome. Br J Neurosurg. 2002 Aug;16(4):343-7.

96) Yasargil G. Microneurosurgery Volume IVB Microneurosurgery of CNS tumours. Chapter 4. Strategies, tactics and techniques. P69-91. Thieme medical publishers New York, USA.